Author Manuscript

Author Manuscript

Author Manuscript

Author Manuscript

HHS Public Access

Author manuscript

Ocul Surf. Author manuscript; available in PMC 2020 July 01.

Published in final edited form as:

Ocul Surf. 2019 July ; 17(3): 589–614. doi:10.1016/j.jtos.2019.03.010.

Neutrophil Extracellular Traps (NETs) contribute to Pathological Changes of ocular Graft-vs.-Host Disease (oGVHD) Dry Eye: Implications for novel Biomarkers and Therapeutic Strategies

Seungwon An[1,#], **Ilangovan Raju**[1,#], **Bayasgalan Surenkhuu**[1], **Ji-Eun Kwon**[1], **Shilpa Gulati**[1], **Muge Karaman**[2], **Anubhav Pradeep**[1], **Satyabrata Sinha**[3], **Christine Mun**[1], **Sandeep Jain**[1,*]

[1]Cornea Translational Biology Laboratory, Department of Ophthalmology and Visual Sciences, University of Illinois at Chicago, Chicago, IL 60612

[2]Department of Bioengineering, University of Illinois at Chicago, Chicago, IL 60612

[3]Cole Eye Institute, Cleveland Clinic, Cleveland, Ohio 44195

Abstract

Purpose: To investigate the role of neutrophil extracellular traps (NETs) and NET-associated proteins in the pathogenesis of oGVHD and whether dismantling of NETs with heparin reduces those changes.

Methods: Ocular surface washings from oGVHD patients and healthy subjects were analyzed. Isolated peripheral blood human neutrophils were stimulated to generate NETs and heparinized NETs. We performed *in vitro* experiments using cell lines (corneal epithelial, conjunctival fibroblast, meibomian gland (MG) epithelial and T cells), and *in vivo* experiments using murine models, and compared the effects of NETs, heparinized NETs, NET-associated proteins and neutralizing antibodies to NET-associated proteins.

Results: Neutrophils, exfoliated epithelial cells, NETs and NET-associated proteins (extracellular DNA, Neutrophil Elastase, Myeloperoxidase, Oncostatin M (OSM), Neutrophil gelatinase-associated lipocalin (NGAL) and LIGHT/TNFSF14) are present in ocular surface washings (OSW) and mucocellular aggregates (MCA). Eyes with high number of neutrophils in OSW have more severe signs and symptoms of oGVHD. NETs (and OSM) cause epitheliopathy in murine corneas. NETs (and LIGHT/TNFSF14) increase proliferation of T cells. NETs (and NGAL) inhibit proliferation and differentiation of MG epithelial cells. NETs enhance proliferation and myofibroblast transformation of conjunctival fibroblasts. Sub-anticoagulant dose Heparin (100 IU/mL) dismantles NETs and reduces epithelial, fibroblast, T cell and MG cell changes induced by NETs.

[*]Corresponding author: Sandeep Jain, jains@uic.edu Telephone: 312-996-4476; Fax: 312-413-7063.
[#]Equal contribution

Conflict of Interest:
Sandeep Jain, MD: Consultant, Ocugen, Inc; Stock Ownership, Advaite, LLC; Patent application

Publisher's Disclaimer: This is a PDF file of an unedited manuscript that has been accepted for publication. As a service to our customers we are providing this early version of the manuscript. The manuscript will undergo copyediting, typesetting, and review of the resulting proof before it is published in its final citable form. Please note that during the production process errors may be discovered which could affect the content, and all legal disclaimers that apply to the journal pertain.

Author Manuscript Author Manuscript Author Manuscript Author Manuscript

Conclusion: NETs and NET-associated proteins contribute to the pathological changes of oGVHD (corneal epitheliopathy, conjunctival cicatrization, ocular surface inflammation and meibomian gland disease). Our data points to the potential of NET-associated proteins (OSM or LIGHT/TNFSF14) to serve as biomarkers and NET-dismantling biologics (heparin eye drops) as treatment for oGVHD.

Keywords

NETs; ocular GVHD; Dry Eye; Heparin; Biomarkers

Introduction

Chronic graft-versus-host disease (GVHD) is a complication occurring in 30 to 70% of patients following allogeneic hematopoietic stem cell transplantation (HSCT).[1] The immunopathophysiology of chronic GVHD is complex,[2] and involves both adaptive and innate immune pathways that initiate and perpetuate fibrosis in multiple organ systems.[1–3] Chronic ocular GVHD (oGVHD) occurs in approximately 50% patients after HSCT, with observed incidences ranging from 33% to 89.5%.[4–8] On average, the clinical presentation of oGVHD occurs 9 months after HSCT, however, disease may present as soon as 7 months or as late as 18 months following transplantation.[6,9] Ocular GVHD is a 'distinctive' manifestation of chronic GVHD, that is, oGVHD is not considered sufficient in isolation to establish an unequivocal diagnosis of systemic chronic GVHD.[1]

Ocular GVHD is a severe ocular surface disease with signs and symptoms resembling those seen in immunologic disorders such as Sjogren's syndrome.[4,10–13] Ocular GVHD presents as a combination of clinical signs and symptoms, some of them unique, that include: (i) symptoms of ocular discomfort[14] (pain/sore eyes, photophobia and burning sensation). Ocular pain scores reported by oGVHD patients are comparable in magnitude to those reported by patients with ocular chemical burns, and pain can severely impact their quality of life.[14] After bone marrow transplantation, 60% patients are unable to work.[15] (ii) tear deficiency and its consequences (corneal and conjunctival epitheliopathy); (iii) Eyelid disease (Meibomian gland atrophy,[16–19] Lid margin telangiectasia and keratinization); (iv) ocular surface cicatrization[20, 21] (conjunctival subepithelial fibrosis, fornix foreshortening and symblepheron formation); (v) Superior limbic keratoconjunctivitis (SLK)[22]; and (vi) active ocular surface inflammation (mucocellular aggregates, tear fluid debris and ocular redness). It is important that oGVHD is not viewed as solely a form of tear deficient dry eye as this over-simplified understanding fosters inadequate treatment of this disabling condition. Recognizing that oGVHD has sufficiently different pathophysiology and management than dry eye disease, the FDA recently allowed orphan drug designation for developing therapies that specifically treat ocular GVHD.

New onset ocular sicca (after HSCT) documented by low Schirmer's test with a mean value of ≤ 5 mm at 5 minutes or a new onset keratoconjunctivitis sicca by slit lamp exam with mean Schirmer's test values of 6 to 10 mm is sufficient to diagnose oGVHD for the purpose of treatment[1,23]. If baseline evaluations are not available to determine whether signs are 'new onset', the International Chronic Ocular GVHD Consensus Group diagnostic criteria

Author Manuscript Author Manuscript Author Manuscript Author Manuscript

can be used to diagnose oGVHD [24, 25]. Four subjective and objective variables are measured and scored: OSDI, Schirmer's score without anesthesia, corneal staining, and conjunctival injection. In a majority of patients, oGVHD follows systemic GVHD, however, it can also precede or develop independently of systemic disease in a minority of patients.[9] New onset or progressive ocular GVHD is generally not regarded as an indication for systemic immunosuppression therapy, therefore, the mainstay of ocular therapy is topical lubricant and antiinflammatory eye drops. To date there are no FDA-approved drugs to treat oGVHD, therefore, it represents an unmet medical need.

The pathophysiology of the oGVHD involves inflammation and fibrosis resulting from dysregulated innate and adaptive immunity. While the contribution of antigen presenting cells and T cells (adaptive immune system) in the pathophysiology of the oGVHD are relatively well established [26], the role of neutrophils (innate immune system) is still being explored. It is well recognized that neutrophils are the first lines of defense against infection and are closely involved in the initiation of inflammatory responses. [27] However, accumulating data shows that neutrophils also have important biological functions in both innate and adaptive immunities, far beyond cytotoxicity against pathogens. [28] The importance of neutrophils in the pathogenesis of autoimmune rheumatic diseases, such as systemic lupus erythematosus[29] and rheumatoid arthritis[30], is being increasingly recognized. [31] A proinflammatory role for neutrophils in the pathogenesis of systemic GVHD has been described for acute but not chronic GVHD.[32–34] Neutrophils contribute to inflammatory innate immune responses that facilitate and enhance adaptive donor T cell immune responses stimulated by recipient alloantigens, and may amplify tissue damage caused by conditioning regimens. In contrast to systemic GVHD where neutrophil role has been described only in acute disease, the presence and role of neutrophils has been described in 'chronic' oGVHD. In a pre-clinical murine model of chronic oGVHD, neutrophils form a significant component of the intracorneal infiltrate.[35] Marked abundance of neutrophil elastase has been reported in tears of chronic oGVHD patients,[36] which is indirect evidence of neutrophilic activity. Neutrophils have been found in impression cytology specimens from the ocular surfaces of patients with chronic oGVHD.[37] The number of neutrophils at the upper palpebral conjunctiva in chronic oGVHD patients show moderate positive correlation with the clinical manifestations and inflammatory status of the ocular surface.[37] Neutrophils may act as a biomarker for monitoring disease activity, progressive fibrosis, and response to therapy in other ocular cicatrizing diseases as well, such as ocular mucous membrane pemphigoid (oMMP).[38] In oMMP, eyes with high number of conjunctival neutrophils have greater degrees of conjunctival fibrosis compared to those without neutrophils.

Our laboratory was the first to discover that numerous neutrophils are present on the ocular surfaces of severe tear-deficient dry eye disease patients (Sjogren's syndrome, chronic oGVHD, non-Sjogren's DED and ocular cicatricial pemphigoid) and to observe that these neutrophils release nuclear chromatin complexes as a type of biologic "spider's web".[39,40] These extracellular DNA (eDNA) webs are termed neutrophil extracellular traps (NETs). [41,42] NETs/eDNA accumulate on the ocular surface of DED patients either because of increased formation (due to hyperosmolarity)[43] and/or reduced clearance (due to tear deficiency and consequent nuclease deficiency).[39] Our data suggests that eDNA production and clearance mechanisms are dysregulated in tear deficient dry eyes. Abnormal regulation

Author Manuscript Author Manuscript Author Manuscript Author Manuscript

of NETs (excessive formation of NETs (NETosis) and deficient nucleases) has been suggested to play a role in other inflammatory conditions as well (e.g. in the pathogenesis of dermatomyositis and polymyositis).[44] Elevated levels of NETs or their biomarkers are associated with several autoimmune diseases.[45,46] We hypothesize that excessive accumulation NETs and NET-associated proteins over the ocular surface contributes to development of ocular GVHD. Here we perform complementary *in vitro* and *in vivo* experiments to provide evidence that NETs can produce the pathological changes characteristic of chronic ocular GVHD. We also provide a method to dismantle NETs that may have therapeutic potential.

Materials and methods

Study approval was obtained from the Institutional Review Board of the University of Illinois at Chicago (UIC). Informed consent was obtained from all participants after the nature and possible consequences of the study were explained. Research was conducted in accordance with the tenets of the Declaration of Helsinki. Ocular GVHD diagnosis was based on the Chronic Ocular GVHD consensus scoring algorithm.[24] The parameters for diagnosis included: (i) symptoms of ocular discomfort as measured by the Ocular Surface Disease Index (OSDI) score. The OSDI is a questionnaire that provides assessment of the symptoms of ocular irritation consistent with dry eye disease and their impact on vision-related functioning. The overall OSDI score defined the ocular surface as normal (0–12 points) or as having mild (13–22 points), moderate (23–32 points), or severe (33–100 points) disease[47–49] (ii) Tear secretion as measured by Schirmer I test (without anesthesia over 5 minutes). Schirmer I measurement ≤ 5 mm/5min is considered severe tear fluid deficiency; (iii) Corneal staining score as measured by Lissamine Green dye staining using National Eye Institute (NEI) grading scale.[50] The dye (5 μL of 1% solution) was applied to each eye and a slit lamp was used to observe corneal staining (16X magnification, high illumination with a diffuser). The NEI scale relies on a chart that divides the cornea into five sections and assigns a value from 0 (absent) to 3 (severe) to each section, based on the density of punctate keratitis, for a maximum of 15 points; and (iv) conjunctival injection measured using the validated bulbar redness (VBR) grading scale. VBR has 10 reference images with increasing bulbar redness. The scale starts at grade 10 and has 10-point steps between reference images (score of minimum 10 to maximum 100).[51] Patients diagnosed with definite oGVHD (score of ≥8 without systemic GVHD and ≥6 with systemic GVHD) were enrolled in the study. Healthy patients were age-matched volunteers without history of DED. Matrix metalloproteinase 9 (MMP-9) test was performed using the InflammaDry kit (RPS Diagnostics, Sarasota, FL). A negative test was scored as 0. A positive test was scored as 1.0 (faint positive), 2.0 (positive) or 3.0 (strong positive). Tear fluid osmolarity was measured using the TearLab Osmolarity Test (TearLab, San Diego, CA) according to the manufacturer's instructions and exact measurements (in mOsm/L units) were used for analysis. Bulbar redness (BR) and noninvasive tear breakup time (NITBUT) was measured using Keratograph 5M (Oculus, Inc., Arlington, WA) and the instrument-derived automated measurements were used for analyses.[52] During bulbar redness measurement, the image of exposed bulbar conjunctiva is scanned and analyzed by Keratograph 5M (R-scan), and the system generates the BR score automatically using a scale of 0.0–4.0 in 0.1 steps, based on

Author Manuscript Author Manuscript Author Manuscript Author Manuscript

the area percentage ratio between blood vessels (red) and the rest of the scanned bulbar conjunctiva (white).[53] Noninvasive tear breakup time (NITBUT) is the time (in seconds) it takes for distortions to appear in the image of concentric Placido rings that are reflected on the patient's cornea by the Keratograph. Two types of NITBUT are measured by the Keratograph 5M: (i) NITBUT-first is the time at which the first distortion of Placido rings occurs; and (ii) NITBUT-average is the average time of first breakup incidents in different locations in a corneal diameter of 8 mm. We also recorded the 'stare time' which is displayed on the Keratograph screen as the time between blinks, that is, the duration of time the patient was able to keep the eyes open without blinking. Meibomian Gland imaging was performed using LipiView II Ocular Surface Interferometer (TearScience, Morrisville, NC). Meibomian gland dropout was graded using a 0 to 4 scale based on the area of Meibomian gland loss (0, 0%; 1, <25%; 2, 25%–50%; 3, 51%–75%; and 4, >75%). The score was recorded as "meiboscale" for each eye.[54,55] Lipid layer thickness (LLT) was an instrument-derived automated measurement (scale 0–100 nanometers).

Ocular surface washings (OSW) collection and analysis:

At the slit lamp, 50 μL of artificial tears (Preservative Free Refresh Optive Sensitive, Allergan, Irvine, CA) was instilled into the inferior fornix of the eye with a pipette (Eppendorf North America, Hauppauge, NY) while using fingers to support the bottom and top eyelid to keep the eye open and the patient was instructed to perform ductions in all directions. After approximately 1 minute, OSW were collected from the inferior fornix with 10 μL glass microcapillary tubes (Microcaps®, Drummond Scientific, Broomall, PA) and transferred to PCR tubes at 4°C and transported to the laboratory for analysis. The eDNA concentration in 2 μL OSW was measured using the Qubit® 3.0 Fluorometer (Life Technologies, Eugene, OR, #Q33216) and the Qubit® dsDNA High Sensitivity Assay Kits (Life Technologies, Eugene, OR, #Q32854) according to the manufacturer's instructions. The value of eDNA was expressed as mean ± standard error of the mean (SEM, μg/mL). For eDNA size analysis, OSW were placed in a 96-well assay plate, and loaded into the FEMTO pulse (Advanced Analytical Technologies, Inc, Iowa). The size of eDNA was analyzed by Prosize software. For Live/dead cell analysis in OSW, Acridine orange/propidium iodide staining was performed and loaded into a Cellometer® cell-counting chamber (Nexcelom Bioscience, Lawrence, MA, #SD100). The number of live and dead cells were counted and cell viability calculated. For protein measurement, 2 μL of OSW was mixed with 2 μL normal saline and 2 μL of this solution was applied to the Direct Detect Assay-free card (Millipore Corporation, Billerica, MA) and read using the Direct Detect Infrared Spectrometer. The Spectrometer measures the amount of proteins in the solution with a protein calibration curve devised using serial dilutions of Bovine Serum Albumin (7% BSA, SRM 927e, National Institute of Standards & Technology, Gaithersburg, MD) in 1:1 solution of Refresh Optive and normal saline. Protein amount (mg/mL) was determined after correcting for dilution. A 1:1 solution of Refresh Optive and normal saline was used as a reference (blank).

Staining of OSW and mucocellular aggregates (MCA):

An EZ single Cytofunnel (Thermo Scientific, Kalamazoo, MI) was assembled with a cytoslide (Thermo Scientific) and10 μL of OSW was loaded into the assembled Cytofunnel.

Author Manuscript Author Manuscript Author Manuscript Author Manuscript

In order to achieve a monolayer of cell deposition on the cytoslide, the sample was centrifuged using Cytospin 4 (Thermo Scientific). After centrifugation, the slide was air dried for 5 min and then fixed with a 4% paraformaldehyde (PFA) solution for 20 min, and stored in 1X PBS at 4°C for further staining. MCA were collected from patients' eyes using sterile jeweler's forceps and transferred to a PCR tube containing Refresh Optive, and stored in an ice box at 4˚C. Fresh MCA samples were embedded in Tissue-Tek® OCT compound (Sakura Finetek, Torrance, CA, #4583) and flash frozen. Frozen sections were cut at 10 μm thickness using cryostat (Thermo Scientific, CryoStar NX50), air dried, then fixed with 4% PFA for 20 min. Immunofluorescent staining: The OSW and MCA samples were permeabilized with 0.025% Triton X-100 (Fisher Scientific, #BP151–100), and blocked with freshly prepared 10% Donkey serum with 1% Bovine Serum Albumin (Gemini Bio-Products, #700–100P) for 2 hours. After blocking, the following primary antibodies were applied, and left overnight at 4˚C: mouse monoclonal anti-human neutrophil elastase (NE) (1:100, Dako, Clone NP57, #M0752);[56,57] rabbit polyclonal to histone H3 (1:100, citrulline R2+R8+R17, 1:100, Abcam, #ab5103);[58,59] rabbit polyclonal Keratin-14 (1:1000, BioLegend, #905301, Covance #PRB-155P);[60,61] rabbit polyclonal anti-human Myeloperoxidase (MPO) (1:100, Abcam, #ab45977);[62,63] rabbit monoclonal anti-human CD3 (1:100, Abcam, #ab16669);[64,65] rabbit polyclonal anti-Oncostatin M (LifeSpan Biosciences, #LS-C104796); rabbit polyclonal NGAL (1:100, Abcam, #ab63929);[66,67] and rabbit polyclonal LIGHT/TNFSF14 (1:100, LifeSpan Biosciences, #LS-C118682). Isotype controls were used as negative controls. The specificities of the primary antibodies used in these experiments have previously been validated.[39, 56–67] Slides were then washed gently on a shaker three times for 10 min each with 1X PBS. After washing, the slides were incubated at room temperature for 1 hour with the following secondary antibodies (diluted 1:1000 in 1% BSA solution in 1X PBS): Alexa Fluor 594 Donkey anti-mouse IgG (Jackson ImmunoResearch Lab, #715–585-150); Alexa Fluor 488 Goat anti-rabbit IgG (Jackson ImmunoResearch Lab, #111–546-003); Alexa Fluor 488 Donkey anti-rabbit IgG (Jackson ImmunoResearch Lab, #711–546-152). Slides were washed twice with 1X PBS for 10 min each, air dried, and counterstained with ProLong™ Gold antifade reagent with DAPI (Invitrogen, #P36931). Images were captured using a Zeiss LSM 710 confocal microscope at 100X magnification and analyzed with the Zeiss LSM Image Software. Sytox Green staining: OSW and MCA were stained on a chamber glass slide (Millipore, #PEZGS0416) with a mixture of 1 μM Sytox Green stain and Hoechst 33342 stain (1:2000, FisherScientific, Pittsburgh, PA, #33342) diluted in 1X PBS, and immediately imaged with a Zeiss Axiocam 506 fluorescence microscope under 20X magnification. Hematoxylin and Eosin (H&E) Staining: Slides with OSW and MCA were stained with hematoxylin (H-3401; Vector Labs, Burlingame, CA), rinsed in acidified ethanol, dipped in bluing solution, and counterstained with eosin (Thermo Scientific, Waltham, MA). Slides were examined using an upright Axioscope 100 microscope (Carl Zeiss Meditec GmbH, Hamburg, Germany), imaged under 100X mag using a Zeiss MRc color camera, and analyzed using Zeiss Axiovision.

Experimental NETosis:

Peripheral blood was collected from patients via venipuncture in vacutainer tubes containing sodium heparin (BD Biosciences). Neutrophils were isolated by immunomagnetic depletion

Author Manuscript Author Manuscript Author Manuscript Author Manuscript

of non-target cells using MACSxpress beads (MACSxpress neutrophil isolation kit, Miltenyi Biotech). The residual erythrocytes were removed using MACSxpress erythrocyte depletion kit (Miltenyi Biotec). Isolated neutrophils were resuspended in serum free phenol red free RPMI-1640 medium (GIBCO). The purity of neutrophils was evaluated by flow cytometry using CD15-PE (Clone: VIMC6; Miltenyi Biotec) and CD16-APC (clone: VEP13; Miltenyi Biotec) antibodies. Isolated Neutrophils (0.5×10^6 cells/well in a 24-well plate, Falcon) were stimulated with 1 nM PMA for 8 hours at 37°C in a tissue culture incubator supplied with 5% CO_2 in order to generate NETs. After 8 hours, NETs were detached by shaking at 500 rpm for 5 min with a microplate shaker ("NETs" condition). In a parallel experiment, unstimulated neutrophils were incubated at 37°C in RPMI medium for 8 hours as a control ("No NETs" condition). RPMI medium alone served as an additional control ("RPMI" condition). The supernatant from all conditions was collected with a sterile 1 mL pipette and filtered through a 1 μm PES membrane filter (Millipore, #SLH033RS) to remove cells and cellular debris. After measuring eDNA concentration (μg/mL) using Qubit 3.0 Fluorometer, all specimen were aliquoted, and stored at −80°C for further assays.

Cytokine abundance in OSW and NETs:

The amount of cytokines in OSW from patients (Healthy, none oGVHD, and definite oGVHD) and supernatant of experimental NETosis conditions (NETs, No NETs, RPMI conditions) were measured using bead-based immunoassays in FLEXMAP 3D system (Luminex, Millipore). Sample volumes of 5 μL of OSW or 25 μL of various experimental NETosis conditions were loaded into a 96-well assay plate. Analytes were selected from following Milliplex human cytokine kits: (i) Human Cytokine/Chemokine Panel I (Cat. No. HCYTOMAG-60K); (ii) Human Sepsis Panel 3 (Cat. No. HSP3MAG-63K); and (iii) Human CVD Panel 1 (Cat. No. HCVD1MAG-67K). Assay was performed according to the manufacturer's instructions. The data was analyzed by MILLIPLEX® Analyst 5.1 software. The absolute concentrations of the samples were determined by construction of a standard curve for each anylate. The results were expressed as mean ± SEM (pg/mL).

Dismantling NETs:

Human neutrophils (0.5×10^6 cells/mL) or MCA were plated on a chamber glass slide (Millipore), and stimulated with 1 nM PMA for 8 hours at 37°C. A separate group of human neutrophils was plated on another chamber glass slide, and stimulated with 1 nM PMA for 7 hours at 37°C and then heparin (100 IU/mL) for 1 hour at 37°C. Both were stained with a mixture of 1 μM Sytox Green stain and Hoechst 33342 stain (1:2000, FisherScientific, Pittsburgh, PA) diluted in 1X PBS, and immediately imaged with a Zeiss Axiocam 506 fluorescence microscope under 20X magnification.

Assay for NET protein-associated DNA fragments for intact NETs:

Using the cell death Detection ELISA kit (Roche, IN) the following steps were completed over three days, as described in previous papers.[68] On the first day, a 96-well ELISA microplate was coated with either MPO antibodies (1:2,000, Abcam, Ab9535) to measure MPO-DNA complexes or NE (1:2,000, Dako, M0752) antibodies to measure NE-DNA complexes, and incubated overnight at 4°C. On the second day, this plate was washed three times with a washing buffer, according to the manufacturer's instructions, and 100 μL of

Author Manuscript Author Manuscript Author Manuscript Author Manuscript

blocking solution was added in each well for 2 hours at room temperature. The ELISA microplate was washed three times with the washing buffer. 100 μL of human NETs and 100 μL of OSW (10 μL + 90 μL of RPMI) were added to separate wells on the same plate, and incubated for 5 min at room temperature. After incubation, 1 μL of DNase I (Thermo Fisher, #EN0525) was added to each well for 15 min at room temperature. DNA digestion was stopped by adding 1 μL of 0.5 M EDTA (Thermo Fisher, #R1021), and followed by overnight incubation at 4°C. On the third day, the ELISA microplate was washed three times with a washing buffer, and a secondary anti–DNA-POD (HRP-conjugated anti-DNA Ab, 1:1000; Roche, #1154467501, IN, USA) was added in each well for 2 hours at room temperature. After three more washes, 100 μL of ABTS substrate (Roche, #1154467501) was added to each well and incubated for 5 min at room temperature. Optical density for each well was measured at a wavelength of 405 nm.

Kinetic NETosis assay:

NETosis was quantified from freshly isolated human neutrophils using a Sytox Green plate reader assay, as described in previous papers.[69,70] Using a robotic pipetting system, epMotion5075 (Eppendorf North America, Hauppauge, NY, USA), 20,000 cells per well were seeded in a 384-well black, flat, clear-bottom plate (Corning, #3762). The same robotic pipetting system was used to then add 1 μM Sytox Green, a cell impermeable nucleic acid stain, to each well. The plate was split up into 3 groups with 6 wells per group: (i) human neutrophils with 1 nM PMA; (ii) human neutrophils with 1 nM PMA with Heparin (100 IU/mL); (iii) human neutrophils with Heparin (100 IU/mL). The plate was loaded into Cytation 5 plate reader (BioTek-U.S., Winooski, VT, USA), set at 37°C and supplied with 5% CO_2 with a filter setting of 485 nm (excitation) / 527 nm (emission). Kinetic fluorescence intensity was measured every 20 min over 12 hours and analyzed with Gen5 software.

Human corneal epithelial cell culture and wound scratch assay:

SV40-Adeno vector transformed human cornea epithelial cells (HCE-T) (RIKEN Cell Bank RCB2280, Tsukuba, Japan) was used for epithelial wound scratch assay (provided by Deepak Shukla, PhD, University of Illinois at Chicago, Chicago, IL). Cells were grown in DMEM medium (GIBCO) and supplemented with both 10% FBS (Invitrogen) and 1% antibiotic and antimycotic solution, which contains 10,000 units/mL of penicillin, 10,000 μg/mL of streptomycin, and 25 μg/mL of Amphotericin B (Thermo Fisher Scientific). This was then incubated at 37°C in a tissue culture incubator supplied with 5% CO_2. A day before wound scratch, 30,000 cells/well were seeded in a 96-well ImageLock plate (Essen Bioscience) and allowed to grow 18 hours in order to attain monolayer confluence. Wound scratch (700–800 μm wide) was made with an IncuCyte 96-pin wound maker (Essen Bioscience). After scratching, cells were washed twice with 100 μL of phenol red free RPMI-1640 medium and 200 μL conditioned media were added to separate wells. For determining heparin cytotoxicity, wound-scratched HCE-T cells were incubated at 37°C for 30 hours in serum-free RPMI medium with the following: (i) Heparin 100 IU/mL; (ii) Heparin 1,000 IU/mL; and (iii) Heparin 10,000 IU/mL. For determining the effect of NETs on epithelial healing, the following conditions were used: (i) RPMI medium; (ii) 0.5X No NETs (unstimulated neutrophils); (iii) 0.5X NETs (stimulated with 1 nM PMA); and (iv) 0.5X NETs + Heparin (100 IU/mL). Heparin sodium (20,000 IU/mL) was obtained from

Author Manuscript Author Manuscript Author Manuscript Author Manuscript

Sagent pharmaceuticals (NDC #25021–404-01), and diluted with RPMI to the concentrations used. Plates were incubated at 37°C for 30 hours in IncuCyte Zoom live cell analysis system (Essen Bioscience), which captured images every 6 hours. The relative wound density (%) was determined for 30 hours with IncuCyte Zoom software. This metric relies on measuring the spatial cell density in the wound area relative to the spatial cell density outside of the wound area at every time point. It is designed to be 0% at time zero and 100% when the cell density inside the wound is equal to the cell density outside the initial wound. It does not rely on finding cell boundaries. For each condition, six technical replicates were performed in three independent experiments. Cytotoxicity of human corneal epithelial cells was determined by LDH (lactate dehydrogenase) cytotoxicity assay (Thermo Scientific, #88954). Cell culture supernatants were collected from the wound-scratch experiments and 50 μL of supernatant was mixed with 50 μL of reaction mix, according to the manufacturer's instructions, in a 96-well flat bottom plate, and incubated at room temperature for 30 min. The optical density absorbance at wavelengths (490–680 nm) was measured with a Cytation5 plate reader. In parallel experiments, the effect of heparin on cell proliferation in wound scratched human corneal epithelial cells was determined by Celltiter 96 Aqueous one reagent Nonradioactive Cell Proliferation assay kit (Promega, #G3580). The CellTiter 96® AQueous One Solution Reagent contains a tetrazolium compound [3-(4,5-dimethylthiazol-2-yl)-5-(3-carboxymethoxyphenyl)-2-(4-sulfophenyl)-2H-tetrazolium, inner salt; MTS] and an electron coupling reagent (phenazine ethosulfate; PES). After 30 hours incubation of wound-scratched human corneal epithelial cells with different doses of heparin, 20 μL of cell titer reagent was added to each well and incubated at 37°C in a cell culture incubator for 2 hours. The optical density absorbance was read at 490 nm using a Cytation5 plate reader.

Immunofluorescence staining of EMT markers:

HCE-T (50,000 cells/well) were plated in a glass-bottom 24-well plate (Mat Tek, Part #P24G-0–13-F) and allowed to grow for 18 hours at 37°C in a tissue culture incubator. The scratch wound was made with a 1 mL sterile pipette tip. Cells were incubated at 37°C for 30 hours with either No NETs (1X) or NETs 1X. After 30 hours, cells were fixed with ice-cold 100% methanol for 20 min. Cells were washed thrice with 1X PBST (PBS buffer with 0.001% Triton X-100) and blocked with 2.5% donkey serum and 1% BSA diluted in 1X PBS for 2 hours. The following primary antibodies were applied, and incubated overnight at 4°C: (i) mouse alpha-smooth muscle actin (α-SMA; 1:500, Sigma-Aldrich, #A2547); (ii) mouse CTGF (1:50, Santa Cruz Biotechnology, #sc-365970); (iii) rabbit Vimentin (1:500, Abcam, #ab92547); and (iv) rabbit β-Catenin (1:500, Cell Signaling, #C2206). The primary antibodies were removed, and the cells were washed once with a washing buffer. Isotype controls were used as negative controls. Appropriate fluorescence conjugated secondary antibodies were added and incubated for 1 hour at room temperature (Alexa Fluor 488 anti-rabbit, #711–545-152, Alexa Fluor 488 anti-mouse, #115–545-146, Alexa Fluor 594 anti-mouse, #715–585-150 Jackson ImmunoResearch Laboratories, Inc.). Finally, the cells were stained with DAPI for 5 min at room temperature. Images were captured with an LSM 710 Zeiss confocal microscope at 63X magnification.

Author Manuscript Author Manuscript Author Manuscript Author Manuscript

Western blot assay for EMT markers:

HCE-T (200,000 cells/well) were plated in a 4-well chamber slide (Millipore, #PEZGS0416), and incubated for 30 hours at 37°C for the following experimental groups: (i) RPMI; (ii) No NETs; (iii) NETs; and (iv) NETs + Heparin (100 IU/mL). After incubation, the medium was removed and cells were lysed with 100 μL of RIPA-buffer for 5 min on ice, then cells were scraped and collected in an e-tube. The collected supernatant was centrifuged at 5000 rpm for 10 min at 4°C to extract protein from cells. The protein concentration was determined by the Bradford protein assay using the Bio-Rad protein assay kit (Bio-Rad, #5000002). 500 ng of total protein was added per lane and then loaded in ProteinSimple (ProteinSimple, Santa Clare, CA, U.S.A.) The following primary antibodies were used: (i) α-SMA (1:100, Novus, NBP2–33006), (ii) β-Catenin (1:1000, Abcam, ab119801), (iii) CCN2 (1:50, Santa Cruz, sc-365970); (iv) E-Cadherin (5 μg/mL, R&D systems, MAB1838), and (5) Vimentin (1:100, Novus, NBP1–92687). ProteinSimple capillary electrophoresis immunoassay was performed according to the manufacturer's instructions. Data analyses were performed using the Compass software (ProteinSimple) on Wes™.

Human conjunctival fibroblast cell culture and wound scratch assay:

Primary human conjunctival fibroblast cells were obtained from ScienCell Research Laboratories (# 6570) and cultivated in fibroblast medium (ScienCell, # 2301). For all the experiments, cell culture passages 2–7 were used. In a 96-well ImageLock plate, 15,000 cells/well were plated and allowed to grow for 18 hours at 37°C in a tissue culture incubator supplied with 5% CO_2. Wound scratch was made as described previously for epithelial cells, and 200 μL of each of the following conditioned media were added: (i) RPMI medium; (ii) 0.5X NETs; (iii) 0.5X NETs + heparin (100 IU/mL); and (iv) heparin (100 IU/mL) supplemented with 1% FBS in RPMI medium. Images were captured every 6 hours with IncuCyte zoom system. The relative wound density (%) was determined for 30 hours with IncuCyte Zoom software. For each condition, six technical replicates were performed in three independent experiments.

Sircol collagen assay:

Total soluble collagen in cell culture supernatants were measured using a Sircol collagen assay kit (Accurate Chemical Inc., #CLRS1000). Briefly, 100 μL of (i) supernatants collected from human conjunctival fibroblast cell cultures from conditions described above; (ii) blanks; and (iii) standards were each mixed with 1 mL of Sircol collagen dye reagent in a 1.5 mL microcentrifuge tube. The tubes were incubated at room temperature for 30 min, and then centrifuged at 12,000 rpm for 10 min. The supernatant was discarded carefully and the pellet was washed with 750 μL of ice-cold 1X acid-salt wash reagent by centrifugation. The pellet was dissolved in 250 μL of alkali reagent, and 200 μL of the resulting product was transferred to a flat bottom 96-well plate. The absorbance was read at 555 nm with Cytation5 plate reader. The concentration of collagen was calculated using a standard curve.

Author Manuscript Author Manuscript Author Manuscript Author Manuscript

Ki67 staining for cell proliferation:

Cells (80,000 cells/well) were plated in a 4-well chamber glass slide (Millipore, #PEZGS0416), and incubated at 37°C for 30 hours with the following experimental groups: (i) RPMI; (ii) NETs; (iii) NETs+Heparin 100 IU/mL; and (iv) Heparin 100 IU/mL. After incubation, cells were fixed with ice-cold 100% methanol for 20 min. Cells were washed twice with 1X PBST (PBS buffer with 0.001% Triton X-100) and blocked with 2.5% donkey serum and 1% BSA diluted in 1X PBS for 2 hours. Cells were incubated with the primary antibody, Ki67 (1:500, Abcam, #ab16667) for overnight at 4°C. After washing, the secondary antibody, Alexa Fluor 488 anti-rabbit (1:1000, Jackson ImmunoResearch Laboratories, #711–545-152), was added and incubated for 1 hour at room temperature, followed by staining with DAPI. Images were captured with an LSM 710 Zeiss confocal microscope at 63X magnification. Ki67/DAPI ratio data analysis was processed using MetaMorph software (Molecular Devices, Version 7.8.13.0).

Western blot assay for alpha-smooth muscle actin (α-SMA) abundance:

After 30 hours incubation with all experimental conditions as described above, cell lysates of human conjunctival fibroblast cells were prepared. The denatured protein samples, blocking reagent, primary antibody, α-SMA (1:100, Novus, NBP2–33006), HRP-conjugated secondary antibody and chemiluminescent substrate were pipetted into designated wells in an assay plate. ProteinSimple capillary electrophoresis Western immunoassay (ProteinSimple, Santa Clare, CA, U.S.A.) was performed according to the ProteinSimple user manual. Data analyses were performed using the Compass software (ProteinSimple) on Wes™.

Collagen gel contraction assay:

Collagen gels were made using the CytoSelect 24-well cell contraction assay kit (floating matrix model, Cell Biolabs, Inc, #CBA-5020) according to the manufacturer's instruction. Briefly, 2 parts of human conjunctival fibroblast cells were mixed with 8 parts of cold collagen gel working solution. For each replicate, 0.5 mL of cell-collagen mixture was cast into each well, and incubated at 37°C with 5% CO_2 for 1 hour to facilitate collagen polymerization. After collagen polymerization, 1 mL of the following medium were added to the collagen gel lattice: (i) fresh RPMI medium; (ii) 1X NETs; (iii) 1X NETs + heparin (100 IU/mL); and (iv) heparin (100 IU/mL) and further incubated for 24 hours. Gels were imaged immediately at time zero and again after 24 hours. The ability of conjunctival fibroblast cells to contract the floating gels was measured by quantifying the area of gels by ImageJ software. The percent of contraction was calculated by the following formula: contraction % = (Initial surface area of gel – Final surface area of gel / Initial surface area of gel) x 100.

Western blot assay for α-SMA abundance:

After 24 h incubation, the collagen gel lattices were collected and lysed with RIPA buffer. The primary antibody, α-SMA (1:100, Novus, NBP2–33006), was added to the wells. ProteinSimple capillary electrophoresis Western immunoassay (ProteinSimple, Santa Clare,

Author Manuscript Author Manuscript Author Manuscript Author Manuscript

CA, U.S.A.) was performed according to the ProteinSimple user manual. Data analyses were performed using the Compass software (ProteinSimple) on Wes™.

In vivo experiments for corneal epitheliopathy and corneal wound healing

Animals:

All animal experiments were conducted according to the ARVO Statement for the Use of Animals in Ophthalmic and Vision Research. Animal protocol was approved by the Institutional Animal Care and Use Committee (IACUC) of the University of Illinois at Chicago. *Thy1*-YFP (B6.Cg-Tg(*Thy1*-YFP)16Jrs/J) transgenic adult mice at the age of 8–12 weeks were purchased from Jackson Laboratory (Bar Harbor, ME), and all animal experiments were performed based on the protocol. For *in vivo* experiments, mice were anesthetized with intraperitoneal injections of ketamine (90 mg/kg; Phoenix Scientific, St. Joseph, MO) and xylazine (20 mg/kg; Phoenix Scientific). For terminal experiments, mice were sacrificed according to the IACUC protocol. *Thy1*-YFP mice were used so that in addition to corneal epitheliopathy and barrier dysfunction (with fluorescein staining), the effects on corneal nerves and cornea trafficking myeloid cells can be simultaneously observed, as described previously.[71,72] In order to investigate the effects of experimental interventions on corneal nerves and trafficking myeloid cells, sequential *In vivo* Stereofluorescent Microscopy was performed using a fluorescence stereoscope (StereoLumar V.12, Carl Zeiss, GmbH, Hamburg, Germany) equipped with a digital camera (Axiocam MRm) and Axiovision 4.0 software as described previously.[71,72] An anesthetized *Thy1*-YFP mouse was placed on the stereoscope stage. 7 μL of proparacaine (0.5%, Bausch &Lomb, Tampa, FL) was applied to the mouse cornea for 3 min, and the pupil was constricted with 5 μL of 0.01% carbachol (Miostat, Alcon, Fort Worth, TX) for 5 min *in vivo*. Z-stack images were obtained at 5 μm intervals and compacted into one maximum intensity projection image after alignment using Zeiss Axiovision software.

Isolation and induction of mouse NETosis:

Mouse neutrophils were isolated from bone marrow cells. Bone marrow cells were flushed out from femurs and tibiae by a 21-gauge needle fitted to a 1 mL syringe filled with RPMI medium containing 10% FBS. Cells were centrifuged and erythrocytes were eliminated after lysing with erythrocyte lysis buffer. The EasySep mouse neutrophil enrichment kit (STEMCELL Technologies, #19762) was used to isolate the neutrophils from bone marrow cells by negative selection. Non-target cells were removed with biotinylated antibodies, which were directed against non-neutrophils. Remaining cells were labeled with tetrameric antibody complexes and separated using an immuno-magnetic column-free magnet (STEMCELL Technologies, #18000). To induce mouse NETs, 0.5×10^6 neutrophils were plated in 0.5 mL RPMI medium mixed with 50 nM PMA for 5 hours in 24-well plates (Falcon, #353047). The NETs were collected and, using a syringe, filtered through 1 μm PES filters (Whatman, #6780–2510).

Corneal epitheliopathy experiments:

Mice were anesthetized with intraperitoneal injections of ketamine (90 mg/kg; Phoenix Scientific, St. Joseph, MO) and xylazine (20 mg/kg; Phoenix Scientific). 10 μL of

Author Manuscript Author Manuscript Author Manuscript Author Manuscript

conditioned medium were applied on surface of the cornea for 40 min (supplementary figure 1). For determining the effect of NETs, the following groups were used (n=5/group): (i) no NETs; (ii) NETs; and (iii) NETs + Heparin (100 IU/mL). This experiment was performed three times for determining reproducibility. For determining the effect of Oncostatin, the following groups were used (n=6/group): (i) NETs; (ii) NETs + Heparin (100 IU/mL); (iii) NETs + mouse OSM Neutralizing Antibody (NAb) (1 μg/mL, R&D systems #AF-495-NA); (iv) recombinant mouse OSM (5 ng/ mL, R&D systems #495-MO-025); (v) recombinant mouse OSM protein (5 ng/mL) + Heparin (100 IU/mL); and (vi) recombinant mouse OSM protein (5 ng/mL) + mouse OSM NAb (1 μg/mL). This experiment was performed two times for determining reproducibility. In both experiments, after 40 minutes of application, the conditioned medium was removed, and 10 μL of 0.2% fluorescein was applied on the cornea for 1 min and washed two times with 1X PBS. The fluorescein staining was examined and imaged with a slit lamp (Haag Streit, Bern, Switzerland) every day for 6 or 7 days using 40X magnification and cobalt blue light with yellow barrier filter. Fluorescein staining was graded for each replicate from each group, using National Eye Institute (NEI) grading system (Grade 0–3 depending upon density of punctate staining) in four quadrants (nasal, temporal, inferior, superior). Maximum staining equals 12. Mice were sacrificed after day 6 or 7 and corneas were excised from each replicate from each group, lysates were prepared and assayed for IP-10, IL-1β, IL-6 (EMD Millipore) using bead based immunoassays (Luminex). The concentrations of cytokines in pg/mL were normalized to total protein and expressed as pg/μg of protein.

Corneal Epithelial Wound Healing experiments:

Thy1-YFP mice at the age of 10–12 weeks were used for corneal epithelial wound healing experiment using the repetitive injury mouse model as described previously.[73] Mice were anesthetized, the center of the cornea was demarcated by a 2 mm diameter biopsy punch (Kai Industries, Seki, Japan), and corneal epithelium in this area was removed with a rust ring remover (Alger Equipment Co., Inc., Lago Vista, TX) under a ZEISS S5 microscope (Zeiss C, Overckochen, Germany). For repetitive injury, at 24, 48, and 72 hours after the initial wounding, the same 2 mm diameter wound was created centered on the corneal apex. After wounding, the epithelial defect was examined using 10 μL of 0.2% fluorescein and imaged with a slit lamp (Haag Streit) every day for 3 days using 40X magnification and cobalt blue light with yellow barrier filter. After imaging, 10 μL of conditioned media were applied on surface of the cornea for 40 min (supplementary figure 1). For determining the effect of NETs, the following groups were used (n=5/group): (i) RPMI; (ii) No NETs; (iii) NETs; and (iv) NETs + Heparin (100 IU/mL). This experiment was performed two times for determining reproducibility. After 40 minutes, the conditioned medium was removed, and the corneas were covered with Ophthalmic Ointment (Akorn, Lake Forest, IL). The fluorescein stained epithelial wound area was measured in the photographs with AxioVision software (Carl Zeiss). The corneal epithelial defect at each time point was calculated as a percent of the day 0 epithelial defect size.

Meibomian gland epithelial (MGE) cell experiments:

Immortalized human meibomian gland epithelial cells was a generous gift from Dr. David Sullivan (Harvard Medical School, Boston, MA). MG epithelial cells were used for

Author Manuscript Author Manuscript Author Manuscript Author Manuscript

differentiation and proliferation experiments using culture conditions as described previously.[74,75]

MGE cell differentiation experiments:

Cells were plated at 70% confluence (40,000 cells/well) in keratinocyte serum free medium (KSFM; Thermo Fisher, #17005042) in a 4-well glass slide (Millipore, #PEZGS0416), and allowed to grow for 18 hours in a tissue culture incubator at 37°C supplied with 5% CO2. For meibomian gland epithelial cell differentiation experiments, the medium was removed and replaced with Differentiation F12 Medium (DFM) that comprised Dulbecco's Eagle medium and Ham's F12 (GIBCO mix, #11320033) supplemented with 10% fetal bovine serum in 10 ng/mL human EGF (R&D Biosystems, #236-EG). For investigating the effect of NETs on meibomian gland differentiation, cells were incubated with the following conditioned medium for 8 days in a tissue culture incubator at 37°C supplied with 5% CO2: (i) Keratinocyte serum free medium (KSFM); (ii) Differentiation F12 Medium (DFM); (iii) DFM + 10X concentrated NETs+ IgG (5 μg/mL, R&D Biosystems, MAB006); (iv) DFM + 10X concentrated NETs that had been incubated with NGAL antibody (5 μg/mL, R&D Biosystems, #MAB1757) for 1 hour; (v) DFM + 10X NETs that had been incubated with heparin (100 IU/mL) for 1 hour; (vi) DFM + recombinant NGAL (80 ng/mL, R&D Biosystems, #1757-LC); (vii) DFM + recombinant NGAL protein (80 ng/mL) that had been incubated with heparin (100 IU/mL) for 1 hour; and (viii) DFM + recombinant NGAL protein that had been incubated with NGAL antibody 5 μg/mL for 1 hour. Cells were then fixed with 4% PFA for 20 min and washed thrice with 1X PBS. Cells were stained with LipidTOX green neutral lipid stain in 1X PBS (1:800, Thermo Fisher Scientific, # H34475) for 30 min. The nuclei were counterstained with Hoechst 33342 in 1X PBS (1:2000) for 5 min. Images were captured with a Zeiss Axio Vert fluorescence microscope at 40X magnification. The fluorescence intensity was quantified using ImageJ software (http://imagej.nih.gov/ij/).

MG epithelial cell proliferation experiments:

Meibomian Gland (MG) cells were plated at a seeding density of 5,000 cells/well in a 96-well plate (Falcon, #353075), and allowed to grow for 3 days at 37°C in an incubator supplied with 5% CO2 in: (1) KSFM, (2) KSFM with NETs + IgG (5 μg/mL), (3) KSFM with NETs + NGAL neutralizing antibody (NAb) (5 μg/mL), (4) KSFM with NETs + heparin (100 IU/mL), (5) KSFM with recombinant NGAL (80 ng/mL), (6) KSFM with recombinant NGAL (80 ng/mL) + NGAL NAb (5 μg/mL), and (7) KSFM with recombinant NGAL (80 ng/mL) + heparin (100 IU/mL). Cell proliferation was assessed by measuring the cellular DNA content via fluorescent dye binding kit (CyQuant ® NF Cell Proliferation Assay, #C35006, Invitrogen). After 72 hours of incubation, the supernatant was removed with a pipette and 100 μL of 1X CyQuant dye binding solution was added into each well. The plates were then incubated at 37°C for 1 hour. The fluorescence intensity for these samples was measured with excitation wavelength of 485 nm and emission wavelength of 530 nm by Cytation5 plate reader and analyzed by Gen5 software.

Author Manuscript Author Manuscript Author Manuscript Author Manuscript

Mixed lymphocyte reaction (MLR):

The one-way allogeneic MLR procedure has been described previously.[65] Peripheral blood was collected by venipuncture in BD vacutainer sodium heparin tubes from two unrelated healthy subjects. Pan-T cells were isolated by immunomagnetic depletion of non-target cells using MACSxpress beads (MACSxpress Human Pan-T cell isolation kit, Miltenyi Biotech) according to the manufacturer's instruction. The residual erythrocytes were removed using MACSxpress erythrocyte depletion kit (Miltenyi Biotec). Peripheral Blood Mononuclear Cells (PBMCs) were isolated by immunomagnetic depletion of non-target cells using MACSxpress beads (MACSxpress Human PBMC isolation kit, Miltenyi Biotech) according to the manufacturer's instruction. Isolated PBMCs were resuspended in 3 mL of serum free phenol red free RPMI-1640 medium (GIBCO). Non-irradiated T cell (responder cells - R) and irradiated PBMC (stimulator cells - S; irradiation dose: 3000 rad) were suspended in 10% AB (Corning, MT35060CI) prepared in RPMI and plated (1×10^5 cells/well each; 1:1 ratio) in sterile 96-well plates (Corning) for 2 days at 37°C. For determining the effect of NETs on T cell proliferation and MLR, the following groups were used: (i) R, (ii) R + NETs, (iii) R + S (MLR condition), (iv) R + S + NETs, (v) R + S + NETs + Heparin (100 IU/mL); and (vi) R + S + Heparin (100 IU/mL). For determining the effect of LIGHT/TNFSF14 on T cell proliferation and MLR, the following groups were used: (i) R, (ii) R + recombinant LIGHT/TNFSF14 (100 ng/mL, R&D Biosystems), (iii) R + S, (iv) R + S + NETs; and (v) R + S + NETs + LIGHT/TNFSF14 neutralizing antibody (NAb) (10 ng/ml, R&D Biosystems). Cell proliferation was determined using a CyQUANT cell proliferation assay kit (Invitrogen, Carlsbad, CA, USA) according to the manufacturer's protocol. After 48 hours of incubation, the supernatant was removed with a pipette and 100 μL of 1X dye binding solution was added into each well. The plates were then incubated at 37°C for 1 hour. The fluorescence intensity for these samples was measured with excitation wavelength of 485 nm and emission wavelength of 530 nm by Cytation5 plate reader and analyzed by Gen5 software.

Statistical analysis

Based on their subject group as "healthy", "none" oGVHD, and "definite" oGVHD, the clinical measurements (OSDI, Schirmer's I, corneal staining, conjunctival staining, bulbar redness, oGVHD composite score, MMP 9, tear breakup first, tear breakup average, meiboscale, average LLT, and osmolarity) and OSW measurements (eDNA, tear neutrophils, and cytokines) were combined for each group. Using SPSS 24.0 software (IBM, Armonk, NY), a one-way analysis of variance (ANOVA) was performed to determine the statistical difference among "healthy", "none" oGVHD, and "definite" oGVHD for all clinical measurements, as well as eDNA and number of neutrophils in total number of cells. When significant ($p<0.05$) differences were found, post-hoc paired comparisons with Tukey correction were conducted to explore the meaning of such differences by controlling family-wise Type 1 error. The level of significance was set at $\alpha=0.05$ for post-hoc analysis as well. *In vitro* cell culture data and *in vivo* murine experiment data were similarly analyzed. The outliers were excluded before performing statistical significance analysis. The relationship between eDNA and number of neutrophils in total number of cells within the "definite" oGVHD group was investigated through a correlation analysis by computing Pearson's correlation coefficient.

Author Manuscript Author Manuscript Author Manuscript Author Manuscript

RESULTS

Clinical signs and symptoms – Mucocellular Aggregates (MCA).

In order to investigate the role of NETs in pathogenesis of oGVHD, we enrolled age matched patients with definite oGVHD (n=30), none oGVHD (n=18) and healthy subjects (n=20), and performed a detailed clinical ophthalmological examination and laboratory investigation on ocular surface washings. As compared to none oGVHD and healthy subjects, definite oGVHD patients had significantly greater symptoms (OSDI score), lower Schirmer's I value, greater conjunctival and corneal staining and greater bulbar redness, and thus had a significantly higher composite score (Clinical data are shown in Table 1). The presence of mucocellular aggregates (Fig 1, A1, A2) was also significantly greater in definite oGVHD patients (80%) as compared to none oGVHD (16%) and healthy subjects (0%). The mucocellular aggregates (MCA) were present as translucent sheets over the ocular surface or whitish strands in the inferior conjunctival sac or fornix, becoming visible on pulling down the lower eyelid. We collected these MCA using Jewelers forceps and examined them microscopically. Hematoxylin & Eosin staining showed numerous neutrophils, extracellular DNA (eDNA) strands and few epithelial cells (Fig 1, A3). Immunofluorescence staining showed co-localization of neutrophil elastase (Fig 1, B1), CitH3 (Fig 1, B2) and DAPI nuclear staining (Fig 1, B3) in the extracellular strands, thus confirming them to be NETs (Fig 1, B4), as described previously.[76,77] Co-localization of neutrophil elastase (Fig 1, C1), myeloperoxidase (Fig 1, C2) and DAPI nuclear staining (Fig 1, C3) further confirmed that the extracellular strands in MCA are NETs (Fig 1, C4). In an oGVHD patient, MCAs were adhered to the cornea (Fig 1, D1). We applied a filter paper to lift the MCA from the cornea (Fig 1, D2). H&E staining of the filter paper showed presence of neutrophils, eDNA strands and epithelial cells (Fig 1, D3). Immunofluorescence staining showed co-localization of CitH3 (Fig 1, E1), NE (Fig 1, E2) and DAPI nuclear staining (Fig 1, E3) in the extracellular strands, thus confirming that MCAs contain NETs (Fig 1, E4).

Neutrophil Extracellular Traps (NETs) and NET-associated proteins on the ocular surface of oGVHD patients.

Next, we investigated whether NETs are present in the tear film by performing a washing of the ocular surface and examining the ocular surface washings (Fig 2, A1). 50 μL volume of artificial tear was instilled in inferior conjunctival sac and washings collected after one minute (all data shown represents mean ± SEM). The recovered volume was similar in definite oGVHD (34.29 ± 1.14 μL) and none oGVHD (38.00 ± 0.80 μL; $p=0.24$) patients. In healthy subjects recovered volume was significantly greater (43.72 ± 2.05 μL; $p<0.05$). The protein content of ocular surface washings was similar in definite oGVHD (2.24 ± 0.40 mg/mL), none oGVHD (1.85 ± 0.40 mg/mL) and healthy subjects (1.70 ± 0.20 mg/mL; $p=0.53$ between groups). In parallel *in vitro* experiments, we isolated human neutrophils from peripheral venous blood of healthy subjects and stimulated them with PMA to produce NETs (experimental NETosis). We compared the cytology and cytokine profile in ocular surface washings with experimental NETosis to uncover similarities. Cytospin preparations of ocular surface washings showed presence of numerous neutrophils, extracellular DNA and few epithelial cells (Fig 2, A2). The size of neutrophils in ocular surface washings was significantly larger in definite oGVHD patients (13.01 ± 0.05 μm, $p<0.05$) as compared to

Author Manuscript Author Manuscript Author Manuscript Author Manuscript

healthy subjects (11.39 ± 0.21 μm). PMA activated NETosing neutrophils also had significantly increased size (16.46 ± 0.11 μm; $p<0.05$) as compared to naïve peripheral venous blood neutrophils (11.82 ± 0.07 μm) (Fig 2, B2). Sytox Green staining of cytopsin preparations showed numerous extracellular strands in ocular surface washings (Fig 2, A3) that were similar in appearance to Sytox green stained extracellular strands seen in experimental NETosis (Fig 2, B3). Immunofluorescence staining showed co-localization of neutrophil elastase (Fig 2, A4 and B4), MPO (Fig 2, A5 and B5) and DAPI nuclear stain (Fig 2, A6 and B6) in the extracellular strands in ocular surface washings as well as in experimental NETosis (Fig 2, A7 and B7), thus confirming them to be NETs. Extracellular DNA amount was significantly greater in ocular surface washings of definite oGVHD patients (2.37 ± 0.25 μg/mL; $p<0.05$) as compared to none oGVHD (0.83 ± 0.06 μg/mL) and healthy subjects (0.78 ± 0.04 μg/mL) (Fig 2, A8). Similarly, supernatants of PMA stimulated neutrophils had significantly greater eDNA (NETs, 0.38 ± 0.05 μg/mL; $p<0.05$) as compared to unstimulated neutrophils (No NETs, 0.10 ± 0.02 μg/mL) cultured for eight hours and culture media (RPMI, 0.03 ± 0.00 μg/mL) (Fig 2, B8). Although eDNA levels are commonly used as surrogates of NET release, presence of eDNA is not specific for demonstrating NETs because eDNA levels can be raised in necrosis also. Therefore, we used specific methods of NET quantification to definitively demonstrate the presence of NETs.[78,79] MPO-DNA complexes were significantly greater in ocular surface washings of definite oGVHD patients (0.532 ± 0.201; optical density (OD) at 450 nm; $p<0.05$) as compared to none oGVHD (0.063 ± 0.013) and healthy subjects (0.034 ± 0.003) (Fig 2, A9). NE-DNA complexes were also significantly greater in ocular surface washings of definite oGVHD patients (0.554 ± 0.082; $p<0.05$) as compared to none oGVHD (0.084 ± 0.017) and healthy subjects (0.079 ± 0.036) (Fig 2, A10). Similarly, supernatants of PMA stimulated neutrophils had significantly greater MPO-DNA complexes (NETs, 0.208 ± 0.085; $p<0.05$) as compared to unstimulated neutrophils (No NETs, 0.068 ± 0.013) cultured for eight hours and culture media (RPMI, 0.007 ± 0.001) (Fig 2, B9). Supernatants of PMA stimulated neutrophils also had significantly greater NE-DNA (NETs, 0.112 ± 0.019; $p<0.05$) as compared to unstimulated neutrophils (No NETs, 0.002 ± 0.001) cultured for eight hours and culture media (RPMI, 0.031 ± 0.034) (Fig 2, B10). We also determined the DNA fragment size using electropherogram tracings generated with an automated pulsed-field electrophoresis instrument. The DNA fragment size in ocular surface washings of healthy subjects and none oGVHD patients was smaller (approximately 950 bp) as compared to definite oGVHD patients (approximately 6,500 bp) (Fig 2, A11). In addition, definite oGVHD patients had smaller quantities of low (500 bp) and high (80,000 bp) molecular weight fragments. NETs had fragment size of approximately 5,000 bp, which matches DNA fragment size of oGVHD patients (Fig 2, B11).

Ocular surface washings of definite oGVHD patients had significantly higher levels of several cytokines as compared to none oGVHD patients and healthy subjects. These cytokines were: (i) neutrophil elastase (Fig 2, A12); (ii) myeloperoxidase (Fig 2, A13); (iii) IL-8 (Fig 2, A14); (iv) Oncostatin M (Fig 2, A15); (v) LIGHT/TNFSF14 (Fig 2, A16); (vi) TNFα (Fig 2, A17); and (vii) BDNF (data not shown). Similarly, levels of these cytokines (Fig 2, B12-B16), except TNFα (Fig. 2, B17), were significantly higher in supernatants of

Author Manuscript Author Manuscript Author Manuscript Author Manuscript

PMA stimulated neutrophils (NETs) as compared to unstimulated neutrophils (No NETs) and culture media (RPMI).

These complementary experiments demonstrate that NETs and their molecular components are present in ocular surface washings, as evidenced by similar findings generated during experimental NETosis.

Tear fluid neutrophils and severity of ocular surface disease.

The neutrophil numbers in ocular surface washings of definite oGVHD ($2.16\times10^5 \pm 5.48\times10^4$; $p<0.05$) were significantly higher as compared to none oGVHD ($1.10\times10^4 \pm 3.61\times10^3$) and healthy subjects ($6.06\times10^3 \pm 2.35\times10^3$) (Fig 2, C1). In ocular surface washings of definite ocular GVHD patients, we observed a moderately strong correlation (Pearson correlation, $r = 0.797$; $p<0.05$) between neutrophil numbers and amount of eDNA (Fig 2, C2). We divided definite oGVHD patients into two groups based on whether ocular surface washings showed relative excess of epithelial cells (N<E, Fig 2, C3) or excess of neutrophils (N>E, Fig 2, C4), and compared their clinical findings. We found that definite oGVHD patients who had an excess of neutrophils (N>E) in the ocular washings had significantly more severe clinical findings ((higher OSDI score (Fig 2, C5), higher bulbar redness (Fig 2, C6), and higher composite score (Fig 2, C7)) as well as higher eDNA amount (Fig 2, C8) in ocular surface washings as compared to definite oGVHD patients who had an excess of epithelial cells (N<E). In addition to more severe clinical findings, these patients (N>E) also had significantly higher protein (3.17 ± 0.54 mg/mL; $p<0.05$) content in ocular surface washings as compared to N<E patients (0.48 ± 0.22 mg/mL). These findings suggest that N>E eyes are more inflamed as compared to N<E eyes and the higher amount of protein in N>E eyes is likely to be NET-associated proteins given the severely compromised lacrimal gland function in these patients.

Heparin use as a NET-dismantling drug

Having established that NETs are present on the ocular surface of oGVHD patients and are associated with more severe disease in these patients, we performed experiments to determine whether NETs can produce pathological changes that are seen in oGVHD patients and whether dismantling of NETs reduces those pathological changes.

We selected heparin as our target compound to investigate the effect of NETs dismantling because it possesses the highest negative charge density of any known biological macromolecule,[80] thus it can strip positively charged histones from the DNA backbone of NETs to destabilize them. We isolated peripheral blood human neutrophils, cultured them in plate wells (Fig 3, A1) and stimulated them with 1 nM PMA to generate adherent NETs (Fig 3, A2). Incubation of adherent NETs with sub-anticoagulant dose of heparin (100 IU/mL) dismantled NETs as evidenced by the loss of Sytox green stained extracellular DNA strands (Fig 3, A3). Furthermore, the supernatant had increased eDNA after heparin incubation suggesting detachment of adherent NETs (1.96 ± 0.01 μg/mL; $p<0.05$; Fig 3, A4). Next, we detached the adherent NETs by shaking the cultured plates and incubated the non-adherent NETs with either Heparin or RPMI culture and determined the level of NET protein-associated DNA fragments (which represent intact NETs). The levels of histone-associated

Author Manuscript Author Manuscript Author Manuscript Author Manuscript

DNA fragments was significantly decreased after heparin incubation (0.06 ± 0.01; $p<0.05$; Fig 3, A5) as compared to RPMI incubation (0.25 ± 0.03) suggesting dismantling of NETs. Dismantling of NETs was further confirmed using assays to detect MPO-DNA complexes (Fig 3, A6) and NE-DNA complexes (Fig 3, A7). Both, MPO-DNA complexes and NE-DNA complexes (which represent intact NETs) were significantly reduced after heparin incubation. Similarly, we found that heparin 100 IU/mL dose dismantles NETs in MCA collected from oGVHD patients (Fig 3, B1-B4) and reduces histone-associated DNA fragments in supernatant (0.06 ± 0.00; Fig 3, B9). RPMI culture media was unable to dismantle NETs in MCA (Fig 3, B5-B8). To determine whether heparin can dismantle NETs in a clinical setting, we treated a patient who had adherent MCA surrounding the optic of a Boston keratoprosthesis with heparin eye drops (100 IU/mL) three times a day (Fig 3, B10, arrow points to whitish adherent MCA). After 4 weeks of heparin treatment the adherent MCA were much reduced (Fig 3, B11).

We cultured immortalized corneal epithelial cells, created scratch wounds and incubated them in presence of increasing doses of heparin to determine the non-toxic dose (Fig 3, C1-C4). Sub-anticoagulant dose of heparin (100 IU/mL) did not delay epithelial wound closure (Fig 3, C6) whereas anticoagulant doses of heparin (1,000 IU/mL and 10,000 IU/mL) showed significant dose dependent delay in epithelial wound closure (Fig 3, C7 and C8). Relative wound density (RWD, %) after 30 hours incubation was similar in heparin 100 IU/mL (87.21 ± 2.18%; $p=0.99$) and RPMI culture media (88.56 ± 1.57%) (Fig 3, C9 and C10). Compared to RPMI culture media, RWD was significantly lower with heparin 1,000 IU/mL (63.17 ± 3.60%; $p<0.05$) and 10,000 IU/mL (3.72 ± 3.62%; $p<0.05$). In parallel experiments, MTS assay was performed to determine cell proliferation. Heparin (100 IU/mL) increased cell proliferation as compared to RPMI control, whereas Heparin (1,000 IU/mL and 10,000 IU/mL) significantly reduced cell proliferation (Fig 3, C11). LDH assay was performed using supernatant to determine cytotoxicity (Fig 3, C12). Heparin (100 IU/mL) caused no cytotoxicity as compared to RPMI culture media whereas significant cytotoxicity was observed with heparin 1,000 IU/mL and 10,000 IU/mL (Fig 3, C11). In kinetic assay of experimental NETosis (isolated peripheral blood neutrophils stimulated with 1 nM PMA) heparin 100 IU/mL did not affect NETosis (Fig 3, C12). These experiments establish that sub-anticoagulant dose of heparin (100 IU/mL) effectively dismantles NETs without causing toxicity to corneal epithelial cells, thus we used this dose in all subsequent experiments.

NET-induced corneal and conjunctival epitheliopathy.

Since corneal (Fig 4, A1) and conjunctival (Fig 4, A2) epitheliopathy and persistent corneal epithelial defects (Fig 4, A3) are present with significantly greater frequency in definite oGVHD patients as compared to none oGVHD and healthy subjects (Fig 4, A4 and A5), we used *in vitro* and *in vivo* models to determine the effect of NETs on corneal epithelium. We cultured immortalized corneal epithelial cells, created scratch wounds and incubated them in presence of RPMI culture media, unstimulated neutrophils (No NETs), naive NETs and heparinized NETs (Fig 4, B1-B4). As compared to RPMI control (Fig 4, B5) and no NETs (Fig 4, B6) significant delay in epithelial wound closure was seen with naive NETs (Fig 4, B7) but not with heparinized NETs (Fig 4, B8). Relative wound density (%) after 30 hours

Author Manuscript Author Manuscript Author Manuscript Author Manuscript

incubation was similar in RPMI culture media (90.88 ± 1.50%; p>0.05), No NETs (89.48 ± 2.75%), and heparinized NETs (89.24 ± 1.97%). Compared to RPMI culture media, relative wound density was significantly lower with naive NETs (34.96 ± 2.58%; p<0.05) (Fig 4, B9).

In naive NETs group the epithelial cells at the scratch wound margin were elongated spindle shaped resembling fibroblasts (Fig 4, B10 inset). In this group, immunofluorescent staining showed findings that are typically seen in epithelial mesenchymal transition (EMT). These NET-induced EMT changes include: (i) increased expression of alpha smooth muscle actin (Fig 4, C26), CCN2 (Fig 4, C32) and Vimentin (Fig 4, C35), and (ii) nuclear translocation of beta Catenin (Fig 4, C29). Western blot analysis of cell lysates (Fig 4, D1) showed increased abundance of alpha smooth muscle actin (Fig 4, D2), CCN2 (Fig 4, D3), Vimentin (Fig 4, D4) and reduced abundance of E-cadherin protein (Fig 4, D5). Taken together these findings are suggestive of epithelial mesenchymal transition (EMT) induced by NETs.

Next, we performed experiments in a murine model to determine whether NETs can cause corneal epitheliopathy *in vivo* (Fig 10). We applied supernatant from unstimulated neutrophils (No NETs), PMA-stimulated neutrophils (naive NETs) and heparinized NETs to naïve murine corneas for seven consecutive days (40 minutes per topical application per day) (Fig 5, A1-A6). Significantly greater corneal fluorescein staining was observed at Day 7 following application of naive NETs (6.00 ± 0.55; p<0.05; Fig 5, A5) as compared to No NETs (1.80 ± 0.37; Fig 5, A4) and heparinized NETs (1.60 ± 0.24; Fig 5, A6) (Data shown in Fig 5, A7). At Day 7, corneas were excised and abundance of inflammatory cytokines (IP-10 and IL-1β) were determined in lysates. Corneas exposed to naive NETs had significantly higher abundance of IP-10 (Fig 5, A8) and IL-1β (Fig 5, A9) as compared to RPMI culture media, No NETs and heparinized NETs. Next, we performed experiments to determine whether NETs can delay epithelial wound healing *in vivo.* We created an epithelial defect in murine corneas and applied supernatant from unstimulated neutrophils (No NETs), PMA-stimulated neutrophils (naive NETs) and heparinized NETs (Fig 5, B1-B4). The percent epithelial defect area remaining at Day 3 was significantly greater following application of naive NETs (83.02 ± 10.65; p<0.05; Fig 5, B15) as compared to No NETs (23.07 ± 14.49; Fig 5, B14) and heparinized NETs (10.96 ± 6.85; Fig 5, B16) (Data shown in Fig 5, B17).

Next, we investigated the molecular component of NETs that may cause epitheliopathy. Because oncostatin M (OSM) levels were significantly higher in ocular surface washings of definite oGVHD patients (Fig 2, A15) and OSM was present in abundance in experimental NETs (Fig 2, B15), and because OSM is known to cause epithelial barrier dysfunction,[81] we elected to investigate whether this NET component causes corneal epitheliopathy. Immunofluorescent staining showed that OSM was present in abundance in MCA (Fig 6, A1-A5) and ocular surface washings ((1.60±0.24; Fig. 5, A6)) collected from definite oGVHD patients. OSM is a heparin binding protein, therefore incubation with heparin or Neutralizing antibody (NAb) reduced recombinant OSM protein levels (Fig 6, B1). In murine NETs, OSM is present in great abundance (614.67 ± 95.73 pg/mL) and it's levels are significantly reduced in heparinized NETs (19.95 ± 0.00 pg/mL; Fig 5, B2).

Author Manuscript Author Manuscript Author Manuscript Author Manuscript

First, we investigated whether reducing OSM levels in naive NETs using heparin or OSM NAb reduces NETs induced epitheliopathy in murine corneas. We applied naive NETs, heparinized NETs and OSM NAb incubated NETs to naïve murine corneas for five consecutive days (Fig 6, C1-C3). Significantly greater corneal fluorescein staining was observed at Day 5 following application of NETs (7.20 ± 0.97; $p<0.05$; Fig 6, C4) as compared to heparinized NETs (0.80 ± 0.49; Fig 6, C5) and OSM NAb incubated NETs (0.40 ± 0.24; Fig 6, C6) (Data shown in Fig 6, C7). At Day 5, corneas were excised and abundance of inflammatory cytokines (IL-1β, IL-6 and IP-10) were determined in lysates. Corneas exposed to NETs had significantly higher abundance of these inflammatory cytokines as compared to heparinized NETs and OSM NAb incubated NETs (Fig 6, C8-C10).

Second, we investigated whether OSM recombinant protein can produce epitheliopathy similar to NETs and whether reducing OSM levels using heparin or OSM NAb reduces that effect. Significantly greater corneal fluorescein staining was observed at Day 5 following application of OSM (8.75 ± 0.48; $p<0.05$; Fig 6, D4) as compared to OSM incubated with heparin (1.20 ± 0.20; Fig 6, D5) and OSM incubated with OSM NAb (0.80 ± 0.37; Fig 6, D6) (Data shown in Fig 6, D7). Corneas exposed to OSM had significantly higher abundance of inflammatory cytokines (IL-1β, IL-6 and IP-10) as compared to heparinized NETs and OSM NAb incubated NETs (Fig 6, D8-D10).

Taken together these complementary experiments suggest that NETs cause corneal epitheliopathy possibly due to presence of OSM and NET/OSM-induced epitheliopathy can be prevented (or possibly treated) with heparin. Therefore, we treated a patient with “Definite” oGVHD who had corneal and conjunctival epitheliopathy (Fig 6, E1 and E2) with heparin eye drop (100 IU/mL) three times a day for four weeks. We observed a significant reduction in corneal and conjunctival epitheliopathy (Fig 6, E3 and E4).

NET-induced corneal and conjunctival fibrosis.

Conjunctival subepithelial fibrosis (CSEF, Fig 7, A1), fornix foreshortening (Fig 7, A2), and symblepheron formation (Fig 7, A3), are present with significantly greater frequency in definite oGVHD patients. CSEF is present in significantly greater number of oGVHD patients (50.57 ± 5.39%; $p<0.05$) as compared to none oGVHD (7.69 ± 4.32%) and healthy subjects (0.00 ± 0.00%) (Fig 7, A4). Therefore, we used *in vitro* and *in vivo* models to determine the effect of NETs on conjunctival fibroblasts. We cultured primary human conjunctival fibroblasts, created scratch wounds and incubated them in presence of RPMI culture media, naive NETs, heparinized NETs and RPMI culture media with heparin (Fig 7, B1-B4). Heparinized NETs (44.15 ± 2.31%; $p<0.05$; Fig 7, B7) and RPMI culture media with heparin (46.97 ± 1.80%; Fig 7, B8) significantly reduced relative wound density at 24 hours as compared to RPMI (82.70 ± 2.46%; Fig 7, B5) and naive NETs (86.04 ± 2.67%; Fig 7, B6) (Data shown in Fig 7, B9). Collagen I amount was assayed in supernatants. Collagen I amount was significantly less in supernatants of heparinized NETs (49.18 ± 2.85 μg/mL) and RPMI culture media with heparin (9.08 ± 2.11 μg/mL) as compared to naive NETs (65.72 ± 2.86 μg/mL) (Fig 7, B10). Immunofluorescence staining was performed 24 hours after scratch wound to determine the abundance of myofibroblasts. Significantly

Author Manuscript Author Manuscript Author Manuscript Author Manuscript

greater myofibroblasts (positive staining for α-smooth muscle actin) were present in cultures incubated with naive NETs (Fig 7, C4-C6) as compared to heparinized NETs (Fig 7, C7-C9) and RPMI culture media with heparin (Fig 7, C10-C12) (Data shown in Fig 7, C13). Western blot analysis also confirmed increased abundance of α-SMA after incubation with naive NETs (Fig 7, C14 and C15). Ki67 staining showed that fibroblast proliferation was significantly reduced in heparinized NETs (0.71 ± 0.10; Fig 7, D3) and RPMI culture media with heparin (0.36 ± 0.02; Fig 7, D4) as compared to naive NETs (1.01 ± 0.10; $p<0.05$; Fig 7, D3) (Data shown in Fig 7, D5). We also investigated whether NETs can contract collagen matrices loaded with conjunctival fibroblasts (collagen contraction assay). After 24 hours incubation, significantly greater gel contraction was noticed in naive NETs (61.20 ± 3.46%; $p<0.05$; Fig 7, E6) as compared to heparinized NETs (25.44 ± 2.78%; Fig 7, E7) and RPMI culture media with heparin (24.72 ± 2.14%; Fig 7, E8). Western analysis also confirmed significantly increased abundance of α-SMA after incubation of collagen matrices with NETs (Fig 7, E10 and E11).

Taken together, these complementary experiments suggest that NETs cause conjunctival fibroblast proliferation and differentiation and may contribute to conjunctival fibrosis. Heparin inhibits NET-induced profibrotic actions.

NET-induced immunoproliferation.

T cell activation and proliferation are well recognized to play an important role in chronic GVHD pathophysiology. Therefore, we investigated whether NETs can affect proliferation of cultured T cell and proliferation in a mixed lymphocytic reaction (MLR). First, we immunostained MCA with CD3 antibody to demonstrate the presence of T cells. CD3 positive T cells were seen in 42% of 12 MCAs examined (Fig 8, A2-A5). NETs significantly increased proliferation of T cells (Fig 8, B). We performed a MLR using lymphocytes and PBMCs from two different healthy subjects to simulate an alloreaction. NETs significantly increased proliferation in MLR ($6.73\times10^5 \pm 4.99\times10^4$ RFU; $p<0.05$) whereas addition of heparinized NETs resulted in significantly lower MLR proliferation ($5.15\times10^5 \pm 3.72\times10^4$ RFU) (Fig 8, B). Addition of heparin (100 IU/mL) without NETs also resulted in significantly lower proliferation in MLR ($4.17\times10^5 \pm 2.23\times10^4$ RFU; $p<0.05$). Next, we investigated the molecular component of NETs that may have caused MLR proliferation. Because LIGHT/TNFSF14 levels were significantly higher in ocular surface washings of definite oGVHD patients (Fig 2, A16) and LIGHT/TNFSF14 was present in abundance in experimental NETs (Fig 2, B16), and because LIGHT/TNFSF14 is known to cause T cell proliferation[82], we elected to investigate whether this NET-associated protein causes immunoproliferation. First, we immunostained MCA with LIGHT/TNFSF14 antibody and demonstrated the presence of LIGHT/TNFSF14 protein in neutrophil cytoplasm and extracellularly (Fig 8, C2-C5). Next, we investigated the effect of LIGHT/TNFSF14 protein on T cell proliferation. LIGHT/TNFSF14 protein caused significantly increased proliferation of T cells (Fig 8, D). Compared to MLR proliferation induced by NETs only ($6.73\times10^5 \pm 4.99\times10^4$ RFU), when NETs and LIGHT/TNFSF14 NAb were added to MLR, proliferation was significantly reduced ($4.44\times10^5 \pm 5.01\times10^4$ RFU; $p<0.05$) (Fig 8, D). Taken together these data show that NETs increase proliferation of T cells whereas heparin

Author Manuscript Author Manuscript Author Manuscript Author Manuscript

reduces T cell proliferation, and LIGHT/TNFSF14 protein may contribute to NET-induced immunoproliferation.

NET-induced Meibomian gland disease (MGD).

Meibomian gland disease is a conspicuous feature of oGVHD. As compared to normal meibomian gland (Fig 9, A1), patients with oGVHD have extensive atrophy or truncation of meibomian glands (Fig 9, A2). Meiboscale in oGVHD patients is significantly greater (2.07 ± 0.19; $p<0.05$) as compared to healthy subjects or patient with none oGVHD (Fig 9, A3). Because NGAL levels were significantly higher in ocular surface washings of definite oGVHD patients (2212.00 ± 430.71 pg/mL; $p<0.05$) (Fig 9, B1) and NGAL was present in abundance in experimental NETs (9475.34 ± 1052.84 pg/mL; $p<0.05$) (Fig 9, B2), and because NGAL is known to cause sebaceous gland atrophy,[83] we elected to investigate whether this NET-associated protein effects meibomian gland differentiation and proliferation. We immunostained MCA with NGAL antibody and demonstrated the presence of NGAL protein in neutrophil cytoplasm and extracellularly (Fig 9, C2-C5). To determine the effect of NETs on meibomian glands, immortalized meibomian gland epithelial cells were cultured and differentiated. Lipid accumulation was detected using LipidTOX staining. The fluorescence intensity of LipidTox Green neutral lipid stain was significantly higher in differentiation medium (DFM) (24.92 ± 1.21 A.U; $p<0.05$; Fig 9, D2) as compared to Keratinocyte serum free medium (KSFM) (6.93 ± 0.57 A.U; Fig 9, D1). Addition of NETs to DFM medium significantly decreased the accumulation of lipids (7.60 ± 0.85 A.U; $p<0.05$; Fig 9, D3). In contrast, addition of heparinized NETs to DFM medium did not reduce accumulation of lipids (33.98 ± 2.18 A.U; Fig 9, D5). The reduction in lipid accumulation with NETs was reduced with addition of NGAL NAb (21.21 ± 0.83 A.U; Fig 9, D4). Similar to NETs, addition of rNGAL to DFM medium significantly decreased the accumulation of lipids (10.88 ± 0.35 A.U; Fig 9, D6). The reduction of lipid accumulation with rNGAL was reduced with addition of NGAL NAb (17.82 ± 0.43 A.U; Fig 9, D7) and heparin (15.66 ± 1.72 A.U; Fig 9, D8) (Data shown in graph, Fig 9, D9).

Next, we investigated the effect of NGAL on proliferation of human MG cells. As compared to control KSFM medium ($5.52\times10^5 \pm 3.11\times10^4$ RFU), addition of NETs to KSFM medium significantly reduces meibomian gland proliferation ($1.72\times10^5 \pm 1.58\times10^4$ RFU; $p<0.05$) (Fig 9, D10). The reduction of MG cell proliferation with NETs was abrogated with addition of NGAL NAb ($6.98\times10^5 \pm 6.18\times10^4$ RFU) and heparin ($8.25\times10^5 \pm 2.56\times10^4$ RFU). Similar to NETs, addition rNGAL to KSFM medium significantly decreased MG cell proliferation (Fig 9, D6). The reduction of MG cell proliferation with rNGAL was abrogated with addition of NGAL NAb and heparin.

Taken together these data show that NETs or recombinant NGAL significantly reduce MG cell proliferation and differentiation whereas addition of heparin or NGAL NAb abrogates this reduction, suggesting that NGAL (a NET-associated protein) may cause MG cell dysfunction which can be reduced with heparin.

Author Manuscript Author Manuscript Author Manuscript Author Manuscript

Discussion

Using a combination of *in vitro* and *in vivo* model systems and multiple complementary experiments we have profiled the potential of NETs to cause ocular surface pathology in oGVHD patients. We found that NETs are present in abundance in mucocellular aggregates (MCA) and ocular surface washings of oGVHD patients. MCA are generally presumed to be mucoid material, but in fact, they contain neutrophils, NETs, eDNA and exfoliated conjunctival/corneal epithelial cells and are a clinical sign of active inflammation. Ocular surface washings in oGVHD patients have high levels of neutrophil elastase, myeloperoxidase, IL-8, TNFα, BDNF, Oncostatin M, NGAL and LIGHT/TNFSF14. These proteins and cytokines are also secreted by neutrophils during NETosis. NETs and NET-associated proteins contribute to the pathological changes of oGVHD in the following ways: (i) Corneal epitheliopathy. In cultured corneal epithelial cells, NETs delay closure of scratch wounds and induce EMT. In murine corneas, NETs cause epitheliopathy and delay epithelial wound healing. OSM, a molecular component of NETs, contributes to epitheliopathy; (ii) Conjunctival cicatrization. NETs increase proliferation of cultured conjunctival fibroblasts, induce a robust myofibroblast transformation and cause contraction of collagen matrices; (iii) Ocular surface inflammation. Neutrophils and NETs are present in abundance in MCA and ocular surface washings of oGVHD patients. oGVHD patients who have excess of neutrophils relative to epithelial cells in ocular surface washings have greater disease severity. IL-8, a NET-associated protein, may contribute to neutrophil chemotaxis to the ocular surface. NETs also increase proliferation of T cells in an allogenic mixed lymphocytic reaction. LIGHT/TNFSF14, a NET-associated protein, contributes to T cell activation and proliferation over the ocular surface; and (iv) Meibomian gland (MG) disease. NETs significantly reduce MG cell proliferation and differentiation. NGAL, a NET-associated protein, also contributes to Meibomian gland disease.

Taken together these data suggest that NETs contribute to corneal epitheliopathy (via OSM), conjunctival cicatrization, meibomian gland disease (via NGAL) and ocular surface inflammation (via IL-8 and LIGHT/TNFSF14). We also investigated the effect of dismantling NETs on these pathological processes and found that sub-anticoagulant dose of heparin reduces NET-induced epitheliopathy, cicatrization, meibomian gland disease and inflammation. These data point to the therapeutic potential of strategies that dismantle NETs, such as DNase I or sub anticoagulant dose heparin eye drops to treat oGVHD. Specific inhibitors of NET-associated proteins may also have therapeutic potential. Our data also point to the potential clinical utility of NET-associated proteins, particularly eDNA, NGAL, OSM and LIGHT/TNFSF14, as biomarkers that may be useful in discriminating etiology of DED. Our data also shows that eDNA amount and number of cells in ocular surface washings are significantly higher in oGVHD patients. These analyses may also have the potential to serve as biomarkers. Currently, DED clinical tests classify individuals in their correct group (Sjogren's syndrome or oGVHD) in only 40% cases even when all clinical tests are combined.[84]

While we used clinical signs and symptoms to diagnose ocular GVHD using the Chronic Ocular GVHD consensus scoring algorithm, we also investigated emerging in-office diagnostic modalities. Our data shows that bulbar redness, non-invasive tear break up time,

Author Manuscript Author Manuscript Author Manuscript Author Manuscript

meibomian gland dropout and lipid layer thickness measurements are significantly worse in ocular GVHD patients (Table 1). These measurements may have the potential to serve as efficacy end points in clinical trials. We were unable to detect changes in tear fluid osmolarity among oGVHD patients. This may be secondary to insufficient tear fluid sampling due to severe tear deficiency in oGVHD patients. In this study, we applied lissamine green dye to the ocular surface to discriminate between vital (unstained) and irreversibly damaged cells (punctate staining).[85,86] We did not perform fluorescein staining because lissamine green staining gives similar information regarding corneal epitheliopathy as fluorescein staining and it is easier to visualize compared to fluorescein staining, without the need of cobalt blue or yellow barrier filters. Fluorescein staining does give additional information regarding disruption of apical epithelial cell tight junctions. When tight junctions are disrupted, fluorescein enters the intercellular space and the staining spreads beyond the diseased epithelial cell.[87] The practical clinical relevance of knowing epithelial barrier disruption information (provided by fluorescein staining) in addition to corneal epitheliopathy information (provided by lissamine green staining) as it relates to diagnosis and treatment of dry eye is unclear.

We have previously reported the presence of neutrophils, extracellular DNA (eDNA) and NETs on the ocular surface of oGVHD patients as well as increased TLR9 and MyD88 gene expression in the conjunctival exfoliated material from these patients.[39] Since neutrophil recruitment is linked inextricably to TLR9-MyD88 signaling in dead or dying cells,[88,89] we had hypothesized that eDNA may stimulate TLR9-MyD88 signaling in desquamated ocular surface cells to recruit neutrophils to the precorneal tear film of DED patients. Once recruited to the ocular surface, neutrophils can form NETs in the precorneal tear film. Other mechanisms of neutrophil recruitment to the ocular surface likely include complement activation and local autoantibodies. Several lines of evidence supports this autoimmune mechanism. The central role of alternative complement pathway is well established in rheumatoid arthritis, asthma and macular degeneration,[90] and there is evidence that the complement system is involved in dry-eye autoantibody-mediated induction of ocular surface inflammation.[91] Passive transfer of serum from dry-eye mice to nude recipient mice results in neutrophil recruitment to the ocular surface and tissue damage that is dependent on complement activation suggesting that autoantibodies in dry eye disease contribute to neutrophil recruitment to the ocular surface.[92] Data from these adoptive transfer experiments support the hypothesis that autoantibodies present in the dry-eye–specific serum, are sufficient to mediate inflammation-induced dry eye, and demonstrate that recruitment of neutrophils is a prominent feature of dry-eye–specific autoantibody-mediated disease. Additionally, the presence of autoantibodies in the serum of mice with experimental dry eye implicates autoreactive B cells in disease pathologies. Autoreactive B cells are implicated in human autoimmune diseases[92–94] such as, Sjogren's syndrome[95] and chronic GVHD.[96] In chronic GVHD, overexpression of the B-cell activation factor (BAFF) or B-cell receptor (BCR) hyper-responsiveness may account for T-cell– independent activation of autoreactive B cells (without requiring additional antigen stimulation)[97,98] resulting in alloantibodies that develop 4 to 9 months after HSCT.[99] The presence of alloantibodies correlates significantly with clinical chronic GVHD development. The incidence of ocular GVHD also peaks at 9 months after HSCT, therefore, these non-T cell mechanisms may be operational in ocular

Author Manuscript Author Manuscript Author Manuscript Author Manuscript

GVHD as well. B-cell infiltration has been reported in the periductal areas of the lacrimal gland in patients with chronic ocular GVHD.[100] There are two important conclusion from the foregoing data: (i) The possibility that a mechanism exists (alloantibodies from autoreactive B cells) that drives neutrophils to the ocular surface of oGVHD patients, therefore the presence of neutrophils on the ocular surface of oGVHD patients is not just due to inflammation-induced egress from eye vasculature; and (ii) The implication that agents that primarily inhibit T cells (calcineurin inhibitors like cyclosporine) will not abrogate neutrophil trafficking to the ocular surface of oGVHD patients, nor reduce the neutrophil associated tissue damage mechanisms (neutrophil extracellular traps) given the B-cell alloantibody dependent mechanism. Furthermore, in contrast to DED where T cells in regional lymph nodes are activated by antigen presenting cells that migrate from the ocular surface, in chronic GVHD different mechanisms contribute to T cell activation. It has been shown that proinflammatory autoreactive T cells are present in chronic GVHD. It is possible that, as in the skin,[101]there is eye-selective migration of autoreactive T cells induced by interferon (IFN)-γ- inducible chemokines because IFN-γ has been shown to be elevated in tear fluid of oGVHD patients[102] and we have found high levels of CXCL10 in ocular surface washings from these patients (data not shown). The eye-selective effector T cell recruitment in autoreactive GVHD is unlikely to be inhibited by topically applied cyclosporine because it does not inhibit T cell migration. Indeed, the use of cyclosporine 0.05% eye drops has been shown to be ineffective in preventing ocular GVHD in a published prospective randomized clinical trial[103] and in another unpublished clinical trial (ClinicalTrials.gov Identifier:). Therefore, novel strategies that target activation, expansion, survival and antibody production of B-cells, autoreactive T cells or strategies that directly target neutrophils and NETs may have beneficial therapeutic effects in chronic ocular GVHD.[104]

Ocular surface washings of definite oGVHD patients had significantly higher levels of several cytokines (neutrophil elastase, myeloperoxidase, IL-8, TNFα, BDNF, Oncostatin M, NGAL and LIGHT/TNFSF14) as compared to none oGVHD patients and healthy subjects. Similarly, levels of these cytokines were significantly higher in supernatants of PMA stimulated neutrophils (NETs) as compared to unstimulated neutrophils (No NETs). Levels of LIGHT/TNFSF14 found in ocular surface washings and NETosis was comparable at 400 pg/mL and 680 pg/mL respectively. OSM was found at 15 pg/mL from ocular surface washings of individuals with definite oGVHD. This is comparable to the amount of OSM found in NETs (21 pg/mL). These data suggests that NETs may be the source of these cytokines. In contrast, high levels of TNF-α were found in ocular surface washings of individuals with definite oGVHD, but not in NETs. This confirms that neutrophils and NETs are not the source of TNF-α found on the ocular surface. While the presence of some cytokines (neutrophil elastase, myeloperoxidase, IL-8 and TNFα) in the tears has been previously reported,[36,37,105,106] the presence of Oncostatin M, NGAL, BDNF and LIGHT/TNFSF14 is a novel finding and may be clinically relevant as one or more of these NET-associated proteins may serve as a potential biomarker in oGVHD, therefore these will be discussed in more details.

Author Manuscript Author Manuscript Author Manuscript Author Manuscript

Oncostatin M (OSM):

The corneal epithelium serves as the principal barrier to fluid and pathogens, a function performed through production of tight junctions, and constant repopulation through differentiation and maturation of dividing cells in its basal cell layer.[107] Corneal barrier disruption, clinically diagnosed by fluorescein staining of the cornea, develops by protease-mediated lysis of epithelial tight junctions, leading to accelerated cell death; desquamation; an irregular, poorly lubricated cornea surface; and exposure and sensitization of epithelial nociceptors.[108] OSM, a member of the IL-6 family of cytokines, has been shown to play a role in epithelial barrier dysfunction in patients with mucosal diseases.[81,109] Our data showed that OSM levels were significantly higher in ocular surface washings of definite oGVHD patients and OSM was present in abundance in experimental NETs, suggesting that OSM source is neutrophils. This data is in line with previous reports that also show neutrophils to be the major population of cells expressing OSM.[110] Our data showed that OSM caused epitheliopathy in murine corneas as evidenced by increased fluorescein staining. We also showed that OSM-induced epitheliopathy was prevented with heparin. Our data is in line with previous studies in cultured bronchial and nasal epithelium that have demonstrated significant loss of barrier function and disorganization of tight junction structure with OSM stimulation.[81] Taken together, our data suggests that OSM may be mediating corneal epithelial barrier dysfunction, potentially contributing to the chronic inflammatory state of ocular GVHD through increased exposure of the corneal tissue to environmental factors including pathogens, allergens, and pollutants. Since the effects of OSM on epithelial barrier function have been shown to be reversible,[81,109] inhibition of OSM using heparin eye drops may be beneficial to treat loss of barrier function.

Neutrophil gelatinase-associated lipocalin (NGAL):

Our clinical data shows that patients with oGVHD have significant meibomian gland atrophy. This clinical finding is in line with other published reports. Our laboratory data shows that naive NETs inhibit proliferation and differentiation of cultured meibomian gland epithelial cells and that these pathological effects are circumvented with heparinized NETs. We also identified that NETs contain abundant NGAL protein and this protein is present in abundant amounts on the ocular surface of oGVHD patients. NGAL is a multifunctional 25-kDa extracellular protein in the lipocalin superfamily. Like heparin, NGAL neutralizing antibodies also abrogated NET-induced pathological effects on meibomian gland epithelial cells. Recombinant NGAL protein mimicked the pathological effects of NETs on meibomian gland epithelial cells. Given our findings, it is reasonable to posit that NGAL may contribute to meibomian gland disease in oGVHD patients. Several lines of evidence in the published literature also support a pathophysiological role for NGAL in sebaceous/meibomian gland disease.[83] It is known that 13-cis retinoic acid (13-cis RA; also known as isotretinoin) reduces sebaceous lipid production and induces apoptosis in cells cultured from human sebaceous glands.[83] Transcriptional profiling indicates that lipocalin 2 is among the genes most highly upregulated by 13-cis RA. The apoptotic effect of 13-cis RA on the cultured human sebaceous gland cells is mediated, at least in part, by the expression of Lipocalin 2 (Lcn2). Lipocalin 2 (Lcn2) encodes NGAL. Recombinant NGAL also induces apoptosis in sebaceous gland cells.[83] Further evidence of the link between sebaceous gland atrophy and NGAL is provided by the Stearoyl-CoA desaturase (SCD1) null (SCD1−/−)

Author Manuscript Author Manuscript Author Manuscript Author Manuscript

mice. These mice have atrophic sebaceous and meibomian glands.[101] Since there is a robust 27.7-fold elevation of Lcn2 in the skin of mice with skin-specific deletion SCD1, it is possible that the primary disturbance in the skin of SCD1−/− mice is increased expression of Lcn2 leading to sebocyte dysfunction and sebaceous gland hypoplasia.[112] In vitro inhibition of SCD activity with the small molecule A939572 causes a 9-fold upregulation of LCN2 mRNA and protein. Since meibomian glands are a modified type of sebaceous glands,[113] they too are targets of isotretinoin toxicity. Isotretinoin causes meibomian gland disease, characterized by glandular atrophy and reduced secretions.[114] Exposure to 13-cis RA inhibits cell proliferation, increases cell death, and promotes inflammatory mediator and protease expression in cultured meibomian gland epithelial cells.[115] There is a 9-fold increase in NGAL gene expression in 13-cis RA– treated human meibomian gland epithelial cells as compared to vehicle-treated, suggesting a possible role for NGAL in causing meibomian gland disease. These data suggest that NGAL protein component of NETs may play a role in meibomian disease in oGVHD patients. In addition to its potential pathological actions on Meibomian glands, NGAL may also contribute to eyelid margin pathology seen in ocular GVHD. Keratinization of the eyelid margin, squamous metaplasia and lichenoid changes are seen in ocular GVHD patients. Since NGAL has been suggested to play a role in epithelial differentiation pathways and being a marker for dysregulated keratinocyte differentiation in human skin,[116] it is possible that NGAL contributes to keratinization of the eyelid margin and conjunctiva in oGVHD patients.

LIGHT (TNFSF14):

LIGHT/TNFSF14 is a secreted protein of the TNF superfamily. It is also known as tumor necrosis factor superfamily member 14 (TNFSF14) and the acronym ‘LIGHT’ stands for “Homologous to lymphotoxin, exhibits inducible expression and competes with HSV glycoprotein D for binding to herpesvirus entry mediator, a receptor expressed on T lymphocytes”. LIGHT/TNFSF14 is primarily produced by cells with an immunological role, and has been identified as a T cell co-stimulatory cytokine.[82, 117–120] LIGHT/TNFSF14 constitutive expression on T-lymphocytes causes activation and expansion of these cells favoring the development of autoimmune disease.[82,121] Our data shows that LIGHT/TNFSF14 levels are significantly higher in ocular surface washings of definite oGVHD patients and LIGHT/TNFSF14 is present in abundance in experimental NETs, suggesting that LIGHT/TNFSF14 is derived from neutrophils during NETosis in patients with inflammatory ocular surface disease. This is in line with published reports showing expression of LIGHT/TNFSF14 in neutrophils from peripheral blood and bone marrow of patients with inflammatory bone disease.[122] However, to the best of our knowledge, we are the first to show expression of LIGHT/TNFSF14 from neutrophils during NETosis. Our data showed that NETs (which constitutively contain LIGHT/TNFSF14) or recombinant LIGHT/TNFSF14 increase T cell proliferation whereas addition of heparin or LIGHT/TNFSF14 neutralizing antibodies prevents LIGHT/TNFSF14-induced proliferation. Since activation, proliferation and trafficking of donor T cells to target organs and tissues are critical steps in the pathogenesis of GVHD,[123] our data suggests that LIGHT/TNFSF14 may contribute to T cell proliferation over the ocular surface in patients with oGVHD and suppression of this immunoproliferation with heparin eye drops or an antagonist of LIGHT/TNFSF14 may be therapeutically beneficial. It has been previously shown that administration of an antagonist

Author Manuscript Author Manuscript Author Manuscript Author Manuscript

of LIGHT/TNFSF14 interaction with its receptors attenuated the course of graft-versus-host reaction.[124] Blockade of LIGHT/TNFSF14 interaction with its receptors slowed T cell proliferation and decreased the frequency of precursor alloreactive T cells, reducing T cell differentiation toward effector T cells. These results expose the relevance of LIGHT/TNFSF14 for the potential therapeutic control of the allogeneic immune responses mediated by alloreactive T cells.[125,126]

The immunopathophysiology of chronic GVHD involves multiple, distinct interactions among alloreactive T and B cells and innate immune populations including neutrophils that culminate in the initiation and propagation of profibrotic pathways.[2] Fibrosis effects several organs in chronic GVHD, including ocular tissues. Conjunctival subepithelial fibrosis (CSEF), also referred to as subtarsal fibrosis, is present in 50% patients with ocular GVHD but is absent in all none-GVHD moderate or severe dry eye disease patients.[20] Stromal fibroblasts are actively involved in the pathogenic process of chronic ocular GVHD in the lacrimal gland by producing excessive extracellular matrix components. There is an increase in activated stromal fibroblasts (resident host cells or donor bone marrow derived fibrocytes) and excessive fibrosis in the lacrimal glands of patients with chronic GVHD.[100,127] Epithelial mesenchymal transition (EMT) may be partially responsible for the conjunctival and lacrimal gland fibrosis found in patients with chronic GVHD.[128] Our data shows that NETs cause EMT, fibroblast proliferation, myofibroblast transformation and collagen contraction, therefore contributes to ocular cicatricial changes seen in oGVHD. NGAL, a NET-associated protein, is known to promote EMT.[129] The mechanisms involved in the development of subtarsal fibrosis in ocular GVHD have not fully been defined. Because transforming growth factor beta (TGF-β) is known to cause fibrosis, we analyzed the levels TGF-β in ocular surface washings and NETs. TGFB1, TGFB2, TGFB3 were not detected in NETs and their levels were similar in ocular surface washings of healthy subjects and oGVHD patients, therefore we were unable to establish a role for TGF-β in fibrosis in oGVHD patients (data not shown). Several lines of evidence have confirmed profibrotic actions of NETs. NETs induce activation of lung fibroblasts (LFs) and differentiation into myofibroblast (MF) phenotype together with increased connective tissue growth factor expression and collagen production.[130] NETs are present in close proximity to alpha-smooth muscle actin (α-SMA)-expressing fibroblasts in biopsies from patients with fibrotic interstitial lung disease or from skin scar tissue. NET production increases in old age and increased NETs induces cardiac fibrosis.[131, 132] The data suggest that NETs promote age-related organ fibrosis and dysfunction. It is possible that one or more NET-associated proteins may contribute to fibrosis in oGVHD patients. Neutrophil elastase, a NET-associated protein, has been shown to induce fibroblast proliferation and myofibroblast differentiation in a TGF-β-independent fashion.[133] Fibrogenic consequences of neutrophil elastase activity have been reported in the inflamed lung.[134]

Sub-anticoagulant dose of heparin:

Our data shows that sub-anticoagulant dose of heparin (100 IU/ml) dismantles NETs and prevents NET induced epithelial, fibroblast and alloreactive effects. Heparin is a highly sulfated glycosaminoglycan that has the highest negative charge density of any known biological molecule, therefore, a direct interaction with positively charged molecules like

Author Manuscript Author Manuscript Author Manuscript Author Manuscript

histones may be the basis of its biological actions.[135,136] Heparin displaces core histones from chromatin and induces transition of protein-complexed DNA to protein-free DNA[137] leading to destabilization of NETs.[138,139] In addition, heparin-histone interactions partially unfolds the nucleosome, thereby increasing chromatin access for more efficient DNase I digestion,[140,141] thus providing a rationale for using heparin and DNase I as a combination therapy for achieving robust clearance of NETs from the ocular surface. Other proteins that are inhibited due to electrostatic interactions with heparin include neutrophil elastase (NE) and cathepsin G, both highly basic proteins.[142] Extracellular DNA also binds to NE. In oGVHD abundant amounts of eDNA is present on the ocular surface. It has been shown that eDNA outcompetes heparin for binding to NE, rendering nonexistent the inhibitory activity of heparin.[143] DNase degrades DNA into smaller chains liberating bound NE for subsequent inhibition by heparins to yield an anti-inflammatory effect, thus providing another rationale for using heparin and DNase I as a combination therapy.

Our data makes a case for investigating the therapeutic potential of subanticoagulant dose heparin in ocular GVHD. In addition to dismantling NETs, low dose heparin has independent antifibrotic, immunosuppressive and anti-inflammatory actions. Furthermore, sub-anticoagulant dose heparin (100 IU/mL) is non-toxic to the corneal epithelium but anticoagulant doses (1000 IU/mL) exhibit cytotoxicity. Different heparin concentrations affect distinct biological mechanisms,[144] therefore, the beneficial actions that we observed with subanticoagulant dose heparin may not occur with higher doses. The therapeutic window is narrow for sub-anticoagulant heparin's effects on autoimmunity and graft rejection. A doubled dose results in loss of therapeutic benefit.[145] Antifibrotic action of heparin has been investigated on preventing surgical adhesions in two rat models of adhesion formation (cecal abrasion model and avascular mesenteric knot model). For example, sub-anticoagulant doses of heparin (0.02 mg) markedly inhibit adjuvant arthritis whereas higher doses (0.04 mg) have no effect. Antifibrotic and immunomodulating actions of subanticoagulant dose heparin have been described.[146,147] Topical application of tiny doses of heparin (30 IU/ml) in combination with carboxymethylcellulose 4% significantly reduced adhesion formation whereas higher doses of heparin (160 IU/ml) caused increased bleeding. [146] At a dose of 100 IU/ml or more, heparin is profoundly toxic to lymphocytes. At lower concentrations, heparin suppresses lymphocyte transformation in the absence of morphological signs of toxicity.[147] Heparin possibly suppresses antigen detection. Heparin, the most highly negatively charged molecule known, increases the negative charge of already high negative charge of lymphocytes, thus creating an energy barrier that impedes ability of lymphocytes to make contact with alloantigens. Heparin inhibits the proliferation of T-and B-lymphocytes in vitro.[148] Low dose subcutaneous heparin cell mediated immune response and immunosuppressive effects of heparin are unrelated to its anticoagulant activity.[149,150] Oral heparin also prolongs survival of skin allografts. It has also been shown that low dose heparin alters trafficking of T lymphocytes, blocking their expression of heparanase, an enzyme that digests the extracellular matrix.[149,151] Low dose heparin (100 IU/0.1 ml) inhibits neutrophil infiltration in the nasal mucosa in antigen-induced allergic inflammation.[152]

Recent evidence suggests that heparanase is a driver of viral pathogenesis in the cornea and may also play a role in other inflammatory disorders of the cornea.[153,154] Heparin is known

Author Manuscript Author Manuscript Author Manuscript Author Manuscript

to inhibit heparanase,[144,155] therefore, this mechanism may also contribute towards antiinflammatory action of heparin in ocular surface diseases. Other mechanisms that contribute to anti-inflammatory actions of heparin include robust inhibition of alternate complement pathway activity and weaker inhibition of classical pathway.[156] Heparin inhibition of alternate complement pathway is relevant in the context of NETs because several lines of evidence show that NETs activate the alternate complement system, thereby initiating an inflammatory amplification cascade.[157,158] Complement factor B (Bb) and properdin, two important components in the alternative complement pathway, are present on NETs.[157] The concentration of complement cascade terminal products (C3a, C5a and SC5b-9) that are generated by intact NETs are significantly reduced when NETs are degraded by DNase I,[157] suggesting that dismantling of NETs by heparin will also reduce complement system activity.

While there are no published reports on the use of sub-anticoagulant dose of heparin as eye drops, there are several reports of Heparin use clinically in anticoagulant doses (>500 IU/ml) as eye drops. Heparin eye drops have been used to treat patients with ligneous conjunctivitis (5,000 IU/ml 6 times a day for 5 years),[159, 160] paraquat-induced ocular injury,[161] posterior capsular opacification (heparin 5% ~ 5,000 IU/ml tid for 3 months)[162] and amiodarone-induced vortex keratopathy (1,300 IU/mL tid for 3 months).[163] Heparin added into the infusion fluid has been used to reduce postoperative inflammation in patients with Diabetes[164] and in pediatric eyes undergoing cataract surgery with IOL implantation.[165–167] Given that heparin have been used topically and intraocularly in several settings, the use of subanticoagulant dose heparin as eye drops to treat oGVHD is likely to be safe. We have performed a placebo-controlled, randomized clinical trial to compare the safety and efficacy of DNase eye drops 0.1% four times a day for 8 weeks severe tear deficient dry eye patients, including oGVHD patients.[168] DNase eye drops reduced the severity of signs and symptoms in these patients. This clinical trial provides support to our hypothesis that clearing NETs from the ocular surface has beneficial effects. In addition to clearing the NETs (like DNase), heparin has additional antifibrotic and immunosuppressive actions that make it an attractive therapeutic drug. Heparin eye drops may be beneficial in other cicatricial ocular surface diseases, such as Stevens-Johnson syndrome and ocular mucous membrane pemphigoid.

Heparin has the potential to cause corneal stromal hemorrhage as has been reported with subconjunctival injection of low-molecular-weight heparin–taurocholate 7.[169] Although topical heparin is absorbed poorly across healthy tissues with intact barrier function, absorption in inflamed tissues with disrupted barrier function is possible. It has been shown that disruption of the stratum corneum skin barrier dramatically increases transdermal permeability of heparin (~14 folds),[170,171] therefore barrier function perturbation, as occurs in oGVHD, dry eye and other inflammatory ocular surface diseases may allow heparin to permeate to subconjunctival tissues and cause a hemorrhage. This possible risk needs to be evaluated in a controlled clinical trial. Heparin use may be more impactful if started earlier in disease course (prophylactically) and it will likely not regenerate damaged lacrimal and meibomian glands.

In conclusion, our data shows that NETs and NET-associated proteins have the potential to cause ocular surface pathology in oGVHD patients. Our data makes a case for investigating

Author Manuscript Author Manuscript Author Manuscript Author Manuscript

the potential of novel biomarkers (eDNA, OSM, NGAL and LIGHT/TNFSF14) and therapies (DNase I, sub-anticoagulant dose heparin and antagonists of OSM, NGAL and LIGHT/TNFSF14) in managing oGVHD.

Supplementary Material

Refer to Web version on PubMed Central for supplementary material.

Acknowledgement

We acknowledge the help of Grace Dunbar (Department of Ophthalmology, University of Illinois at Chicago) for proof reading the article. We also acknowledge the help of Shivali Shukla (University of Illinois Urbana-Champaign. Urbana, IL), Morgan M. Buwick (University of Illinois College of Medicine. Chicago, IL) and Hirali Shah (Midwestern University Chicago College of Osteopathic Medicine. Downers Grove, IL) for help with search and synthesis of published literature.

Supported by: NEI/NIH grants R01EY024966, P30EY001792, K08EY018874, Research to Prevent Blindness Physician Scientist Award and UIC Chancellor's Innovation Fund Award

REFERENCES

1. Jagasia MH, Greinix HT, Arora M, Williams KM, Wolff D, Cowen EW, Palmer J, Weisdorf D, Treister NS, Cheng GS, Kerr H, Stratton P, Duarte RF, McDonald GB, Inamoto Y, Vigorito A, Arai S, Datiles MB, Jacobsohn D, Heller T, Kitko CL, Mitchell SA, Martin PJ, Shulman H, Wu RS, Cutler CS, Vogelsang GB, Lee SJ, Pavletic SZ, Flowers ME. National Institutes of Health Consensus Development Project on Criteria for Clinical Trials in Chronic Graft-versus-Host Disease: I. The 2014 Diagnosis and Staging Working Group report. Biol Blood Marrow Transplant 2015 3;21(3):389–401.e1. [PubMed: 25529383]
2. Cooke KR, Luznik L, Sarantopoulos S, Hakim FT, Jagasia M, Fowler DH, van den Brink MRM, Hansen JA, Parkman R, Miklos DB, Martin PJ, Paczesny S, Vogelsang G, Pavletic S, Ritz J, Schultz KR, Blazar BR. The Biology of Chronic Graft-versus-Host Disease: A Task Force Report from the National Institutes of Health Consensus Development Project on Criteria for Clinical Trials in Chronic Graft-versus-Host Disease. Biol Blood Marrow Transplant 2017 2;23(2):211–234. [PubMed: 27713092]
3. Shulman HM, Cardona DM, Greenson JK, Hingorani S, Horn T, Huber E, Kreft A, Longerich T, Morton T, Myerson D, Prieto VG, Rosenberg A, Treister N, Washington K, Ziemer M, Pavletic SZ, Lee SJ, Flowers ME, Schultz KR, Jagasia M, Martin PJ, Vogelsang GB, Kleiner DE. NIH Consensus development project on criteria for clinical trials in chronic graft-versus-host disease: II. The 2014 Pathology Working Group Report. Biol Blood Marrow Transplant 2015 4;21(4):589–603. [PubMed: 25639770]
4. Shikari H, Antin JH, Dana R. Ocular graft-versus-host disease: a review. Surv Ophthalmol 2013 May-Jun;58(3):233–51. [PubMed: 23541042]
5. Sun YC, Chai X, Inamoto Y, Pidala J, Martin PJ, Flowers ME, Shen TT, Lee SJ, Jagasia M. Impact of Ocular Chronic Graft-versus-Host Disease on Quality of Life. Biol Blood Marrow Transplant 2015 9;21(9):1687–91. [PubMed: 26033283]
6. Na KS, Yoo YS, Mok JW, Lee JW, Joo CK. Incidence and risk factors for ocular GVHD after allogeneic hematopoietic stem cell transplantation. Bone Marrow Transplant 2015 11;50(11):1459–64. [PubMed: 26301966]
7. Rapoport Y, Freeman T, Koyama T, Engelhardt BG, Jagasia M, Savani BN, Tran U, Kassim AA. Validation of International Chronic Ocular Graft-Versus-Host Disease (GVHD) Group Diagnostic Criteria as a Chronic Ocular GVHD-Specific Metric. Cornea 2017 2;36(2):258–263. [PubMed: 28060078]
8. Khan R, Nair S, Seth T, Mishra P, Mahapatra M, Agarwal T, Tandon R, Vanathi M. Ocular graft versus host disease in allogenic haematopoetic stem cell transplantation in a tertiary care centre in India. Indian J Med Res 2015 11;142(5):543–8. [PubMed: 26658588]

Author Manuscript Author Manuscript Author Manuscript Author Manuscript

9. Shikari H, Amparo F, Saboo U, Dana R. Onset of ocular graft-versus-host disease symptoms after allogeneic hematopoietic stem cell transplantation. Cornea 2015 3;34(3):243–7. [PubMed: 25603230]
10. Ogawa Y Sjögren's Syndrome, Non-Sjögren's Syndrome, and Graft-Versus-Host Disease Related Dry Eye. Invest Ophthalmol Vis Sci 2018 11 1;59(14):DES71–DES79. [PubMed: 30481809]
11. Nassiri N, Eslani M, Panahi N, Mehravaran S, Ziaei A, Djalilian AR. Ocular graft versus host disease following allogeneic stem cell transplantation: a review of current knowledge and recommendations. J Ophthalmic Vis Res 2013 10;8(4):351–8. [PubMed: 24653823]
12. Kosrirukvongs P, Chirapapaisan N, Visuthisakchai S, Issaragrisil S, Gonggetyai V. Sjögren-like syndrome after bone marrow transplantation. J Med Assoc Thai 2008;91:1739–47. [PubMed: 19127798]
13. Mencucci R, Rossi Ferrini C, Bosi A, Volpe R, Guidi S, Salvi G. Ophthalmological aspects in allogenic bone marrow transplantation: Sjögren-like syndrome in graft-versus-host disease. Eur J Ophthalmol 1997;7:13–8. [PubMed: 9101189]
14. Saboo US, Amparo F, Abud TB, Schaumberg DA, Dana R. Vision-Related Quality of Life in Patients with Ocular Graft-versus-Host Disease. Ophthalmology 2015 8;122(8):1669–74. [PubMed: 26001816]
15. Pezzotta S, Rossi GC, Scudeller L, Antoniazzi E, Bianchi PE, Perotti C, Del Fante C. A cross-sectional study on vision-related quality of life in patients with ocular GvHD. Bone Marrow Transplant 2015 9;50(9):1224–6. [PubMed: 26052912]
16. Que L, Zhang X, Li M. Single-Center Retrospective Study on Meibomian Gland Loss in Patients With Ocular Chronic Graft-Versus-Host Disease. Eye Contact Lens 2018 11;44 Suppl 2:S169–S175. [PubMed: 29140823]
17. Kusne Y, Temkit M, Khera N, Patel DR, Shen JF. Conjunctival subepithelial fibrosis and meibomian gland atrophy in ocular graft-versus-host disease. Ocul Surf 2017 10;15(4):784–788. [PubMed: 28789979]
18. Kim S, Yoo YS, Kim HS, Joo CK, Na KS. Changes of meibomian glands in the early stage of post hematopoietic stem cell transplantation. Exp Eye Res 2017 10;163:85–90. [PubMed: 28739099]
19. Engel LA, Wittig S, Bock F, Sauerbier L, Scheid C, Holtick U, Chemnitz JM, Hallek M, Cursiefen C, Steven P. Meibography and meibomian gland measurements in ocular graft-versus-host disease. Bone Marrow Transplant 2015 7;50(7):961–7. [PubMed: 25893453]
20. Kheirkhah A, Coco G, Satitpitakul V, Dana R. Subtarsal Fibrosis Is Associated With Ocular Surface Epitheliopathy in Graft-Versus-Host Disease. Am J Ophthalmol 2018 5;189:102–110. [PubMed: 29505774]
21. Kusne Y, Temkit M, Khera N, Patel DR, Shen JF. Conjunctival subepithelial fibrosis and meibomian gland atrophy in ocular graft-versus-host disease. Ocul Surf 2017 10;15(4):784–788. [PubMed: 28789979]
22. Sivaraman KR, Jivrajka RV, Soin K, Bouchard CS, Movahedan A, Shorter E, Jain S, Jacobs DS, Djalilian AR. Superior Limbic Keratoconjunctivitis-like Inflammation in Patients with Chronic Graft-Versus-Host Disease. Ocul Surf 2016 7;14(3):393–400. [PubMed: 27179980]
23. Jacobs R, Tran U, Chen H, Kassim A, Engelhardt BG, Greer JP, Goodman SG, Clifton C, Lucid C, Vaughan LA, Savani BN, Jagasia M. Prevalence and risk factors associated with development of ocular GVHD defined by NIH consensus criteria. Bone Marrow Transplant 2012 11;47(11):1470–3. [PubMed: 22484321]
24. Ogawa Y, Kim SK, Dana R, Clayton J, Jain S, Rosenblatt MI, Perez VL, Shikari H, Riemens A, Tsubota K. International Chronic Ocular Graft-vs-Host-Disease (GVHD) Consensus Group: proposed diagnostic criteria for chronic GVHD (Part I). Sci Rep 2013 12 5;3:3419. [PubMed: 24305504]
25. Rapoport Y, Freeman T, Koyama T, Engelhardt BG, Jagasia M, Savani BN, Tran U, Kassim AA.Validation of International Chronic Ocular Graft-Versus-Host Disease (GVHD) Group Diagnostic Criteria as a Chronic Ocular GVHD-Specific Metric. Cornea 2017 2;36(2):258–263. [PubMed: 28060078]
26. Herretes S, Ross DB, Duffort S, Barreras H, Yaohong T, Saeed AM, Murillo JC, Komanduri KV, Levy RB, Perez VL. Recruitment of Donor T Cells to the Eyes During Ocular GVHD in

Author Manuscript Author Manuscript Author Manuscript Author Manuscript

Recipients of MHC-Matched Allogeneic Hematopoietic Stem Cell Transplants. Invest Ophthalmol Vis Sci 2015 4;56(4):2348–57. [PubMed: 25655798]

27. Kolaczkowska E, Kubes P. Neutrophil recruitment and function in health and inflammation. Nat Rev Immunol 2013 3;13(3):159–75. [PubMed: 23435331]
28. Yang F, Feng C, Zhang X, Lu J, Zhao Y. The Diverse Biological Functions of Neutrophils, Beyond the Defense Against Infections. Inflammation 2017 2;40(1):311–323. [PubMed: 27817110]
29. Smith CK, Kaplan MJ. The role of neutrophils in the pathogenesis of systemic lupus erythematosus. Curr Opin Rheumatol 2015 9;27(5):448–53. [PubMed: 26125102]
30. Carmona-Rivera C, Carlucci PM, Moore E, Lingampalli N, Uchtenhagen H, James E, Liu Y, Bicker KL, Wahamaa H, Hoffmann V, Catrina AI, Thompson P, Buckner JH, Robinson WH, Fox DA, Kaplan MJ. Synovial fibroblast-neutrophil interactions promote pathogenic adaptive immunity in rheumatoid arthritis. Sci Immunol 2017 4;2(10). pii: eaag3358. [PubMed: 28649674]
31. Khawaja AA, Pericleous C, Ripoll VM, Porter JC, Giles IP. Autoimmune rheumatic disease IgG has differential effects upon neutrophil integrin activation that is modulated by the endothelium. Sci Rep 2019 2 4;9(1):1283. [PubMed: 30718722]
32. Schwab L, Goroncy L, Palaniyandi S, Gautam S, Triantafyllopoulou A, Mocsai A, Reichardt W, Karlsson FJ, Radhakrishnan SV, Hanke K, Schmitt-Graeff A, Freudenberg M, von Loewenich FD, Wolf P, Leonhardt F, Baxan N, Pfeifer D, Schmah O, Schönle A, Martin SF, Mertelsmann R, Duyster J, Finke J, Prinz M, Henneke P, Häcker H, Hildebrandt GC, Häcker G, Zeiser R. Neutrophil granulocytes recruited upon translocation of intestinal bacteria enhance graft-versus-host disease via tissue damage. Nat Med 2014 6;20(6):648–54. [PubMed: 24836575]
33. Hülsdünker J, Ottmüller KJ, Neeff HP, Koyama M, Gao Z, Thomas OS, Follo M, Al-Ahmad A, Prinz G, Duquesne S, Dierbach H, Kirschnek S, Lämmermann T, Blaser MJ, Fife BT, Blazar BR, Beilhack A, Hill GR, Häcker G, Zeiser R. Neutrophils provide cellular communication between ileum and mesenteric lymph nodes at graft-versus-host disease onset. Blood 2018 4 19;131(16): 1858–1869. [PubMed: 29463561]
34. Martin PJ. Pathogenic neutrophils in acute GVHD. Blood 2018 4 19;131(16):1774–1775. [PubMed: 29674354]
35. Herretes S, Ross DB, Duffort S, Barreras H, Yaohong T, Saeed AM, Murillo JC, Komanduri KV, Levy RB, Perez VL. Recruitment of Donor T Cells to the Eyes During Ocular GVHD in Recipients of MHC-Matched Allogeneic Hematopoietic Stem Cell Transplants. Invest Ophthalmol Vis Sci 2015 4;56(4):2348–57. [PubMed: 25655798]
36. Arafat SN, Robert MC, Abud T, Spurr-Michaud S, Amparo F, Dohlman CH, Dana R, Gipson IK. Elevated Neutrophil Elastase in Tears of Ocular Graft-Versus-Host Disease Patients. Am J Ophthalmol 2017 4;176:46–52. [PubMed: 28073648]
37. Byun YS, Yoo YS, Kang MJ, Whang WJ, Na KS, Mok JW, Joo CK.Marked infiltration of neutrophils at the upper palpebral conjunctiva in patients with chronic graft-versus-host disease. Ocul Surf 2018 12 19 pii: S1542–0124(18)30155–1.
38. Williams GP, Nightingale P, Southworth S, Denniston AK, Tomlins PJ, Turner S, Hamburger J, Bowman SJ, Curnow SJ, Rauz S. Conjunctival Neutrophils Predict Progressive Scarring in Ocular Mucous Membrane Pemphigoid. Invest Ophthalmol Vis Sci 2016 10 1;57(13):5457–5469. [PubMed: 27760272]
39. Sonawane S, Khanolkar V, Namavari A, Chaudhary S, Gandhi S, Tibrewal S, Jassim SH, Shaheen B, Hallak J, Horner JH, Newcomb M, Sarkar J, Jain S. Ocular surface extracellular DNA and nuclease activity imbalance: a new paradigm for inflammation in dry eye disease. Invest Ophthalmol Vis Sci 2012;53:8253–63. [PubMed: 23169882]
40. McDermott AM. New insight into dry eye inflammation. Invest Ophthalmol Vis Sci 2012;53:8264. [PubMed: 23248237]
41. Brinkmann V, Reichard U, Goosmann C, Fauler B, Uhlemann Y, Weiss DS, Weinrauch Y, Zychlinsky A. Neutrophil extracellular traps kill bacteria. Science 2004;303:1532–35. [PubMed: 15001782]
42. Boeltz S, Amini P, Anders HJ, Andrade F, Bilyy R, Chatfield S, Cichon I, Clancy DM, Desai J, Dumych T, Dwivedi N, Gordon RA, Hahn J, Hidalgo A, Hoffmann MH, Kaplan MJ, Knight JS, Kolaczkowska E, Kubes P, Leppkes M, Manfredi AA, Martin SJ, Maueröder C, Maugeri N,

Author Manuscript Author Manuscript Author Manuscript Author Manuscript

Mitroulis I, Munoz LE, Nakazawa D, Neeli I, Nizet V, Pieterse E, Radic MZ, Reinwald C, Ritis K, Rovere-Querini P, Santocki M, Schauer C, Schett G, Shlomchik MJ, Simon HU, Skendros P, Stojkov D, Vandenabeele P, Berghe TV, van der Vlag J, Vitkov L, von Köckritz-Blickwede M, Yousefi S, Zarbock A, Herrmann M. To NET or not to NET:current opinions and state of the science regarding the formation of neutrophil extracellular traps. Cell Death Differ 2019 1 8. doi: 10.1038/s41418-018-0261-x. [Epub ahead of print]

43. Tibrewal S, Ivanir Y, Sarkar J, Nayeb-Hashemi N, Bouchard CS, Kim E, Jain S. Hyperosmolar stress induces neutrophil extracellular trap formation: implications for dry eye disease. Invest Ophthalmol Vis Sci 2014 11 18;55(12):7961–9. [PubMed: 25406284]
44. Zhang S, Shu X, Tian X, Chen F, Lu X, Wang G. Enhanced formation and impaired degradation of neutrophil extracellular traps in dermatomyositis and polymyositis: a potential contributor to interstitial lung disease complications. Clin Exp Immunol 2014;177:134–41. [PubMed: 24611519]
45. Bonaventura A, Liberale L, Carbone F, Vecchié A, Diaz-Cañestro C, Camici GG, Montecucco F, Dallegri F. The Pathophysiological Role of Neutrophil Extracellular Traps in Inflammatory Diseases. Thromb Haemost 2018 1;118(1):6–27. [PubMed: 29304522]
46. Lee KH, Kronbichler A, Park DD, Park Y, Moon H, Kim H, Choi JH, Choi Y, Shim S, Lyu IS, Yun BH, Han Y, Lee D, Lee SY, Yoo BH, Lee KH, Kim TL, Kim H, Shim JS, Nam W, So H, Choi S, Lee S, Shin JI. Neutrophil extracellular traps (NETs) in autoimmune diseases: A comprehensive review. Autoimmun Rev 2017 11;16(11):1160–1173. [PubMed: 28899799]
47. Schiffman RM, Christianson MD, Jacobsen G, Hirsch JD, Reis BL. Reliability and validity of the Ocular Surface Disease Index. Arch Ophthalmol 2000;118:615–21. [PubMed: 10815152]
48. Hallak JA, Jassim S, Khanolkar V, Jain S. Symptom burden of patients with dry eye disease: a four domain analysis. PLOS One 2013;8:e82805. [PubMed: 24349365]
49. Miller KL, Walt JG, Mink DR, Satram-Hoang S, Wilson SE, Perry HD, Asbell PA, Pflugfelder SC. Minimal clinically important difference for the ocular surface disease index. Arch Ophthalmol 2010 1;128(1):94–101. [PubMed: 20065224]
50. Lemp MA. Report of the National Eye Institute/Industry workshop on Clinical Trials in Dry Eyes. CLAO J 1995 10;21(4):221–32. [PubMed: 8565190]
51. Schulze MM, Jones DA, Simpson TL. The development of validated bulbar redness grading scales. Optom Vis Sci 2007;84:976–83. [PubMed: 18049363]
52. Xie W, Zhang X, Xu Y, Yao YF. Assessment of Tear Film and Bulbar Redness by Keratograph 5M in Pediatric Patients After Orthokeratology. Eye Contact Lens 2018 11;44 Suppl 2:S382–S386. [PubMed: 29554029]
53. Wu S, Hong J, Tian L, Cui X, Sun X, Xu J. Assessment of Bulbar Redness with a Newly Developed Keratograph. Optom Vis Sci 2015 8;92(8):892–9. [PubMed: 26099055]
54. Pult H, Riede-Pult B. Comparison of subjective grading and objective assessment in meibography. Cont Lens Anterior Eye 2013 2;36(1):22–7. [PubMed: 23108007]
55. Yeotikar NS, Zhu H, Markoulli M, Nichols KK, Naduvilath T, Papas EB. Functional and Morphologic Changes of Meibomian Glands in an Asymptomatic Adult Population. Invest Ophthalmol Vis Sci 2016 8 1;57(10):3996–4007. [PubMed: 27490319]
56. Ralfkiaer E, Pulford KA, Lauritzen AF, Avnstrøm S, Guldhammer B, Mason DY. Diagnosis of acute myeloid leukaemia with the use of monoclonal anti-neutrophil elastase (NP57) reactive with routinely processed biopsy samples. Histopathology 1989 6;14(6):637–43. [PubMed: 2759560]
57. Pulford KA, Erber WN, Crick JA, Olsson I, Micklem KJ, Gatter KC, Mason DY. Use of monoclonal antibody against human neutrophil elastase in normal and leukaemic myeloid cells. J Clin Pathol 1988 8;41(8):853–60. [PubMed: 2844860]
58. Hirose T, Hamaguchi S, Matsumoto N, Irisawa T, Seki M, Tasaki O, Hosotsubo H, Yamamoto N, Yamamoto K, Akeda Y, Oishi K, Tomono K, Shimazu T. Presence of neutrophil extracellular traps and citrullinated histone H3 in the bloodstream of critically ill patients. PLoS One 2014 11 13;9(11):e111755. [PubMed: 25392950]
59. Neeli I, Radic M. Opposition between PKC isoforms regulates histone deimination and neutrophil extracellular chromatin release. Front Immunol 2013 2 20;4:38. [PubMed: 23430963]
60. Welm AL, Kim S, Welm BE, Bishop JM. MET and MYC cooperate in mammary tumorigenesis. Proc Natl Acad Sci U S A 2005 3 22;102(12):4324–9. [PubMed: 15738393]

Author Manuscript Author Manuscript Author Manuscript Author Manuscript

61. Goreczny GJ, Ouderkirk-Pecone JL, Olson EC, Krendel M, Turner CE. Hic-5 remodeling of the stromal matrix promotes breast tumor progression. Oncogene 2017 5 11;36(19):2693–2703. [PubMed: 27893716]
62. Dyugovskaya L, Berger S, Polyakov A, Lavie L. The development of giant phagocytes in long-term neutrophil cultures. J Leukoc Biol 2014 10;96(4):511–21. [PubMed: 24577569]
63. Ranguelova K, Rice AB, Lardinois OM, Triquigneaux M, Steinckwich N, Deterding LJ, Garantziotis S, Mason RP. Sulfite-mediated oxidation of myeloperoxidase to a free radical: immuno-spin trapping detection in human neutrophils. Free Radic Biol Med 2013 7;60:98–106. [PubMed: 23376232]
64. Gibbs A, Hirbod T, Li Q, Bohman K, Ball TB, Plummer FA, Kaul R, Kimani J, Broliden K, Tjernlund A. Presence of CD8+ T cells in the ectocervical mucosa correlates with genital viral shedding in HIV-infected women despite a low prevalence of HIV RNA-expressing cells in the tissue. J Immunol 2014 4 15;192(8):3947–57. [PubMed: 24639358]
65. Planagumà J, Leypoldt F, Mannara F, Gutiérrez-Cuesta J, Martín-García E, Aguilar E, Titulaer MJ, Petit-Pedrol M, Jain A, Balice-Gordon R, Lakadamyali M, Graus F, Maldonado R, Dalmau J. Human N-methyl D-aspartate receptor antibodies alter memory and behaviour in mice. Brain 2015 1;138(Pt 1):94–109. [PubMed: 25392198]
66. Sun B, Guo W, Hu S, Yao F, Yu K, Xing J, Wang R, Song H, Liao Y, Wang T, Jiang P, Han B, Deng J. Gprc5a-knockout mouse lung epithelial cells predicts ceruloplasmin, lipocalin 2 and periostin as potential biomarkers at early stages of lung tumorigenesis. Oncotarget 2017 2 21;8(8): 13532–13544. [PubMed: 28088789]
67. Furukawa T, Shimoyama S, Miki Y, Nikaido Y, Koga K, Nakamura K, Wakabayashi K, Ueno S. Chronic diazepam administration increases the expression of Lcn2 in the CNS. Pharmacol Res Perspect 2017 1 31;5(1):e00283. [PubMed: 28596835]
68. Dicker AJ, Crichton ML, Pumphrey EG, Cassidy AJ, Suarez-Cuartin G, Sibila O, Furrie E, Fong CJ, Ibrahim W, Brady G, Einarsson GG, Elborn JS, Schembri S, Marshall SE, Palmer CNA, Chalmers JD. Neutrophil extracellular traps are associated with disease severity and microbiota diversity in patients with chronic obstructive pulmonary disease. J Allergy Clin Immunol 2018 1;141(1):117–127. [PubMed: 28506850]
69. Azzouz D, Khan MA, Sweezey N, Palaniyar N. Two-in-one: UV radiation simultaneously induces apoptosis and NETosis. Cell Death Discov 2018 4 27;4:51.
70. Khan MA, Palaniyar N. Transcriptional firing helps to drive NETosis. Sci Rep 2017 2 8;7:41749. [PubMed: 28176807]
71. Sarkar J, Chaudhary S, Jassim SH, Ozturk O, Chamon W, Ganesh B, Tibrewal S, Gandhi S, Byun YS, Hallak J, Mahmud DL, Mahmud N, Rondelli D, Jain S. CD11b+GR1+ myeloid cells secrete NGF and promote trigeminal ganglion neurite growth: implications for corneal nerve regeneration. Invest Ophthalmol Vis Sci 2013 9 3;54(9):5920–36. [PubMed: 23942970]
72. Namavari A, Chaudhary S, Ozturk O, Chang JH, Yco L, Sonawane S, Katam N, Khanolkar V, Hallak J, Sarkar J, Jain S. Semaphorin 7a links nerve regeneration and inflammation in the cornea. Invest Ophthalmol Vis Sci 2012 7 9;53(8):4575–85. [PubMed: 22700709]
73. Zhang Y, Kobayashi T, Hayashi Y, Yoshioka R, Shiraishi A, Shirasawa S, Higashiyama S, Ohashi Y. Important role of epiregulin in inflammatory responses during corneal epithelial wound healing. Invest Ophthalmol Vis Sci 2012 4 30;53(4):2414–23. [PubMed: 22427548]
74. Liu S, Hatton MP, Khandelwal P, Sullivan DA. Culture, immortalization, and characterization of human meibomian gland epithelial cells. Invest Ophthalmol Vis Sci 2010 8;51(8):3993–4005. [PubMed: 20335607]
75. Liu Y, Kam WR, Fernandes P, Sullivan DA. The Effect of Solithromycin, a Cationic Amphiphilic Drug, on the Proliferation and Differentiation of Human Meibomian Gland Epithelial Cells. Curr Eye Res 2018 6;43(6):683–688. [PubMed: 29283676]
76. Hirose T, Hamaguchi S, Matsumoto N, Irisawa T, Seki M, Tasaki O, Hosotsubo H, Yamamoto N, Yamamoto K, Akeda Y, Oishi K, Tomono K, Shimazu T. Presence of neutrophil extracellular traps and citrullinated histone H3 in the bloodstream of critically ill patients. PLoS One 2014 11 13;9(11):e111755. [PubMed: 25392950]

Author Manuscript Author Manuscript Author Manuscript Author Manuscript

77. Lewis HD, Liddle J, Coote JE, Atkinson SJ, Barker MD, Bax BD, Bicker KL, Bingham RP, Campbell M, Chen YH, Chung CW, Craggs PD, Davis RP, Eberhard D, Joberty G, Lind KE, Locke K, Maller C, Martinod K, Patten C, Polyakova O, Rise CE, Rüdiger M, Sheppard RJ, Slade DJ, Thomas P, Thorpe J, Yao G, Drewes G, Wagner DD, Thompson PR, Prinjha RK, Wilson DM. Inhibition of PAD4 activity is sufficient to disrupt mouse and human NET formation. Nat Chem Biol 2015 3;11(3):189–91. [PubMed: 25622091]

78. Yoo DG, Floyd M, Winn M, Moskowitz SM, Rada B. NET formation induced by Pseudomonas aeruginosa cystic fibrosis isolates measured as release of myeloperoxidase-DNA and neutrophil elastase-DNA complexes. Immunol Lett 2014 8;160(2):186–94. [PubMed: 24670966]

79. Kessenbrock K, Krumbholz M, Schönermarck U, Back W, Gross WL, Werb Z, Gröne HJ, Brinkmann V, Jenne DE. Netting neutrophils in autoimmune small-vessel vasculitis. Nat Med 2009 6;15(6):623–5. [PubMed: 19448636]

80. Shriver Z, Capila I, Venkataraman G, Sasisekharan R. Heparin and heparan sulfate: analyzing structure and microheterogeneity. Handb Exp Pharmacol 2012;(207):159–76. [PubMed: 22566225]

81. Pothoven KL, Norton JE, Hulse KE, Suh LA, Carter RG, Rocci E, Harris KE, Shintani-Smith S, Conley DB, Chandra RK, Liu MC, Kato A, Gonsalves N, Grammer LC 3rd, Peters AT, Kern RC, Bryce PJ, Tan BK, Schleimer RP. Oncostatin M promotes mucosal epithelial barrier dysfunction, and its expression is increased in patients with eosinophilic mucosal disease. J Allergy Clin Immunol 2015 9;136(3):737–746. [PubMed: 25840724]

82. Shaikh RB, Santee S, Granger SW, Butrovich K, Cheung T, Kronenberg M, Cheroutre H, Ware CF. Constitutive expression of LIGHT on T cells leads to lymphocyte activation, inflammation, and tissue destruction. J Immunol 2001 12 1;167(11):6330–7. [PubMed: 11714797]

83. Nelson AM, Zhao W, Gilliland KL, Zaenglein AL, Liu W, Thiboutot DM. Neutrophil gelatinase-associated lipocalin mediates 13-cis retinoic acid-induced apoptosis of human sebaceous gland cells. J Clin Invest 2008 4;118(4):1468–78. [PubMed: 18317594]

84. Garcia DM, Reis de Oliveira F, Módulo CM, Faustino J, Barbosa AP, Alves M, Rocha EM. Is Sjögren's syndrome dry eye similar to dry eye caused by other etiologies? Discriminating different diseases by dry eye tests. PLoS One 2018 12 3;13(12):e0208420. [PubMed: 30507949]

85. Lawrence MS, Miller JW. Ocular tissue permeabilities. Int Ophthalmol Clin 2004 Summer;44(3): 53–61. [PubMed: 15211177]

86. Goldacre RJ, Sylven B. A rapid method for studying tumour blood supply using systemic dyes. Nature 1959 7 4;184:63–4. [PubMed: 13850569]

87. Bron AJ, Argüeso P, Irkec M, Bright FV. Clinical staining of the ocular surface: mechanisms and interpretations. Prog Retin Eye Res 2015 1;44:36–61. [PubMed: 25461622]

88. Nance SC, Yi AK, Re FC, Fitzpatrick EA. MyD88 is necessary for neutrophil recruitment in hypersensitivity pneumonitis. J Leukoc Biol 2008 5;83(5):1207–17. [PubMed: 18285403]

89. Krysko DV, Kaczmarek A, Krysko O, Heyndrickx L, Woznicki J, Bogaert P, Cauwels A, Takahashi N, Magez S, Bachert C, Vandenabeele P. TLR-2 and TLR-9 are sensors of apoptosis in a mouse model of doxorubicin-induced acute inflammation. Cell Death Differ 2011 8;18(8):1316–25. [PubMed: 21311566]

90. Thurman JM, Holers VM. The central role of the alternative complement pathway in human disease. J Immunol 2006 2 1;176(3):1305–10. [PubMed: 16424154]

91. Stern ME, Schaumburg CS, Siemasko KF, Gao J, Wheeler LA, Grupe DA, De Paiva CS, Calder VL, Calonge M, Niederkorn JY, Pflugfelder SC. Autoantibodies contribute to the immunopathogenesis of experimental dry eye disease. Invest Ophthalmol Vis Sci 2012 4 24;53(4): 2062–75. [PubMed: 22395876]

92. Stern ME, Schaumburg CS, Siemasko KF, Gao J, Wheeler LA, Grupe DA, De Paiva CS, Calder VL, Calonge M, Niederkorn JY, Pflugfelder SC. Autoantibodies contribute to the immunopathogenesis of experimental dry eye disease. Invest Ophthalmol Vis Sci 2012 4 24;53(4): 2062–75. [PubMed: 22395876]

93. Leadbetter EA, Rifkin IR, Marshak-Rothstein A. Toll-like receptors and activation of autoreactive B cells. Curr Dir Autoimmun 2003;6:105–22. [PubMed: 12408049]

Author Manuscript Author Manuscript Author Manuscript Author Manuscript

94. Groom J, Mackay F. B cells flying solo. Immunol Cell Biol 2008 1;86(1):40–6. [PubMed: 18172443]

95. Nocturne G, Mariette X. B cells in the pathogenesis of primary Sjögren syndrome. Nat Rev Rheumatol 2018 3;14(3):133–145. [PubMed: 29416129]

96. Sarantopoulos S, Stevenson KE, Kim HT, Bhuiya NS, Cutler CS, Soiffer RJ, Antin JH, Ritz J. High levels of B-cell activating factor in patients with active chronic graft-versus-host disease. Clin Cancer Res 2007 10 15;13(20):6107–14. [PubMed: 17947475]

97. Sarantopoulos S, Stevenson KE, Kim HT, Cutler CS, Bhuiya NS, Schowalter M, Ho VT, Alyea EP, Koreth J, Blazar BR, Soiffer RJ, Antin JH, Ritz J. Altered B-cell homeostasis and excess BAFF in human chronic graft-versus-host disease. Blood 2009 4 16;113(16):3865–74. [PubMed: 19168788]

98. Allen JL, Tata PV, Fore MS, Wooten J, Rudra S, Deal AM, Sharf A, Hoffert T, Roehrs PA, Shea TC, Serody JS, Richards KL, Jagasia M, Lee SJ, Rizzieri D, Horwitz ME, Chao NJ, Sarantopoulos S. Increased BCR responsiveness in B cells from patients with chronic GVHD. Blood 2014 3 27;123(13):2108–15. [PubMed: 24532806]

99. Miklos DB, Kim HT, Miller KH, Guo L, Zorn E, Lee SJ, Hochberg EP, Wu CJ, Alyea EP, Cutler C, Ho V, Soiffer RJ, Antin JH, Ritz J. Antibody responses to H-Y minor histocompatibility antigens correlate with chronic graft-versus-host disease and disease remission. Blood 2005 4 1;105(7): 2973–8. [PubMed: 15613541]

100. Sale GE, Shulman HM, Schubert MM, Sullivan KM, Kopecky KJ, Hackman RC, Morton TH, Storb R, Thomas ED. Oral and ophthalmic pathology of graft versus host disease in man: predictive value of the lip biopsy. Hum Pathol 1981 11;12(11):1022–30. [PubMed: 7033104]

101. Villarroel VA, Okiyama N, Tsuji G, Linton JT, Katz SI. CXCR3-mediated skin homing of autoreactive CD8 T cells is a key determinant in murine graft-versus-host disease. J Invest Dermatol 2014 6;134(6):1552–1560. [PubMed: 24390137]

102. Jung JW, Han SJ, Song MK, Kim TI, Kim EK, Min YH, Cheong JW, Seo KY. Tear Cytokines as Biomarkers for Chronic Graft-versus-Host Disease. Biol Blood Marrow Transplant 2015 12;21(12):2079–2085. [PubMed: 26303101]

103. Boynton GE, Raoof D, Niziol LM, Hussain M, Mian SI. Prospective Randomized Trial Comparing Efficacy of Topical Loteprednol Etabonate 0.5% Versus Cyclosporine-A 0.05% for Treatment of Dry Eye Syndrome Following Hematopoietic Stem Cell Transplantation. Cornea 2015 7;34(7):725–32. [PubMed: 25850708]

104. Zeiser R, Sarantopoulos S, Blazar BR. B-cell targeting in chronic graft-versus-host disease. Blood 2018 3 29;131(13):1399–1405. [PubMed: 29437591]

105. Nair S, Vanathi M, Mahapatra M, Seth T, Kaur J, Velpandian T, Ravi A, Titiyal JS, Tandon R. Tear inflammatory mediators and protein in eyes of post allogenic hematopoeitic stem cell transplant patients. Ocul Surf 2018 7;16(3):352–367. [PubMed: 29723628]

106. Cocho L, Fernández I, Calonge M, Martínez V, González-García MJ, Caballero D, López-Corral L, García-Vázquez C, Vázquez L, Stern ME, Enríquez-de-Salamanca A. Biomarkers in Ocular Chronic Graft Versus Host Disease: Tear Cytokine- and Chemokine-Based Predictive Model. Invest Ophthalmol Vis Sci 2016 2;57(2):746–58. [PubMed: 26927568]

107. Eghrari AO, Riazuddin SA, Gottsch JD. Overview of the Cornea: Structure, Function, and Development. Prog Mol Biol Transl Sci 2015;134:7–23. [PubMed: 26310146]

108. Pflugfelder SC, de Paiva CS. The Pathophysiology of Dry Eye Disease: What We Know and Future Directions for Research. Ophthalmology 2017 11;124(11S):S4–S13. [PubMed: 29055361]

109. Pothoven KL, Schleimer RP. The barrier hypothesis and Oncostatin M: Restoration of epithelial barrier function as a novel therapeutic strategy for the treatment of type 2 inflammatory disease. Tissue Barriers 2017 7 3;5(3):e1341367. [PubMed: 28665760]

110. Pothoven KL, Norton JE, Suh LA, Carter RG, Harris KE, Biyasheva A, Welch K, Shintani-Smith S, Conley DB, Liu MC, Kato A, Avila PC, Hamid Q, Grammer LC 3rd, Peters AT, Kern RC, Tan BK, Schleimer RP. Neutrophils are a major source of the epithelial barrier disrupting cytokine oncostatin M in patients with mucosal airways disease. J Allergy Clin Immunol 2017 6;139(6): 1966–1978.e9. [PubMed: 27993536]

Author Manuscript Author Manuscript Author Manuscript Author Manuscript

111. Miyazaki M, Man WC, Ntambi JM. Targeted disruption of stearoyl-CoA desaturase1 gene in mice causes atrophy of sebaceous and meibomian glands and depletion of wax esters in the eyelid. J Nutr 2001 9;131(9):2260–8. [PubMed: 11533264]

112. Flowers MT, Paton CM, O'Byrne SM, Schiesser K, Dawson JA, Blaner WS, Kendziorski C, Ntambi JM. Metabolic changes in skin caused by Scd1 deficiency: a focus on retinol metabolism. PLoS One 2011 5 9;6(5):e19734. [PubMed: 21573029]

113. Rötzer V, Egu D, Waschke J. Meibomian gland cells display a differentiation-dependent composition of desmosomes. Histochem Cell Biol 2016 12;146(6):685–694. [PubMed: 27539078]

114. Moy A, McNamara NA, Lin MC. Effects of Isotretinoin on Meibomian Glands. Optom Vis Sci 2015 9;92(9):925–30. [PubMed: 26154692]

115. Ding J, Kam WR, Dieckow J, Sullivan DA. The influence of 13-cis retinoic acid on human meibomian gland epithelial cells. Invest Ophthalmol Vis Sci 2013 6 26;54(6):4341–50. [PubMed: 23722388]

116. Mallbris L, O'Brien KP, Hulthén A, Sandstedt B, Cowland JB, Borregaard N, Ståhle-Bäckdahl M. Neutrophil gelatinase-associated lipocalin is a marker for dysregulated keratinocyte differentiation in human skin. Exp Dermatol 2002 12;11(6):584–91. [PubMed: 12473066]

117. Mauri DN, Ebner R, Montgomery RI, Kochel KD, Cheung TC, Yu GL, Ruben S, Murphy M, Eisenberg RJ, Cohen GH, Spear PG, Ware CF. LIGHT, a new member of the TNF superfamily, and lymphotoxin alpha are ligands for herpesvirus entry mediator. Immunity 1998 1;8(1):21–30. [PubMed: 9462508]

118. Harrop JA, Reddy M, Dede K, Brigham-Burke M, Lyn S, Tan KB, Silverman C, Eichman C, DiPrinzio R, Spampanato J, Porter T, Holmes S, Young PR, Truneh A. Antibodies to TR2 (herpesvirus entry mediator), a new member of the TNF receptor superfamily, block T cell proliferation, expression of activation markers, and production of cytokines. J Immunol 1998 8 15;161(4):1786–94. [PubMed: 9712045]

119. Granger SW, Rickert S. LIGHT-HVEM signaling and the regulation of T cell-mediated immunity. Cytokine Growth Factor Rev 2003 Jun-Aug;14(3–4):289–96. [PubMed: 12787566]

120. Tamada K, Shimozaki K, Chapoval AI, Zhu G, Sica G, Flies D, Boone T, Hsu H, Fu YX, Nagata S, Ni J, Chen L. Modulation of T-cell-mediated immunity in tumor and graft-versus-host disease models through the LIGHT co-stimulatory pathway. Nat Med 2000 3;6(3):283–9. [PubMed: 10700230]

121. Wang J, Lo JC, Foster A, Yu P, Chen HM, Wang Y, Tamada K, Chen L, Fu YX.The regulation of T cell homeostasis and autoimmunity by T cell-derived LIGHT. J Clin Invest 2001 12;108(12): 1771–80. [PubMed: 11748260]

122. Brunetti G, Rizzi R, Oranger A, Gigante I, Mori G, Taurino G, Mongelli T, Colaianni G, Di Benedetto A, Tamma R, Ingravallo G, Napoli A, Faienza MF, Mestice A, Curci P, Specchia G, Colucci S, Grano M. LIGHT/TNFSF14 increases osteoclastogenesis and decreases osteoblastogenesis in multiple myeloma-bone disease. Oncotarget 2014 12 30;5(24):12950–67. [PubMed: 25460501]

123. Kumar S, Leigh ND, Cao X. The Role of Co-stimulatory/Co-inhibitory Signals in Graft-vs.-Host Disease. Front Immunol 2018 12 21;9:3003.. [PubMed: 30627129]

124. Tamada K, Tamura H, Flies D, Fu YX, Celis E, Pease LR, Blazar BR, Chen L. Blockade of LIGHT/LTbeta and CD40 signaling induces allospecific T cell anergy, preventing graft-versus-host disease. J Clin Invest 2002 2;109(4):549–57. [PubMed: 11854328]

125. del Rio ML, Fernandez-Renedo C, Chaloin O, Scheu S, Pfeffer K, Shintani Y, Perez-Simon JA, Schneider P, Rodriguez-Barbosa JI. Immunotherapeutic targeting of LIGHT/LTβR/HVEM pathway fully recapitulates the reduced cytotoxic phenotype of LIGHT-deficient T cells. MAbs 2016;8(3):478–90. [PubMed: 26752542]

126. del Rio ML, Schneider P, Fernandez-Renedo C, Perez-Simon JA, Rodriguez-Barbosa JI. LIGHT/HVEM/LTβR interaction as a target for the modulation of the allogeneic immune response in transplantation. Am J Transplant 2013 3;13(3):541–51 [PubMed: 23356438]

127. Ogawa Y, Yamazaki K, Kuwana M, Mashima Y, Nakamura Y, Ishida S, Toda I, Oguchi Y, Tsubota K, Okamoto S, Kawakami Y. A significant role of stromal fibroblasts in rapidly

Author Manuscript Author Manuscript Author Manuscript Author Manuscript

progressive dry eye in patients with chronic GVHD. Invest Ophthalmol Vis Sci 2001 1;42(1): 111–9. [PubMed: 11133855]

128. Ogawa Y, Shimmura S, Kawakita T, Yoshida S, Kawakami Y, Tsubota K. Epithelial mesenchymal transition in human ocular chronic graft-versus-host disease. Am J Pathol 2009 12;175(6):2372–81. [PubMed: 19893038]
129. Li T, Yu L, Wen J, Liao Q, Liu Z. An early-screening biomarker of endometrial carcinoma: NGAL is associated with epithelio-mesenchymal transition. Oncotarget 2016 12 27;7(52):86064–86074. [PubMed: 27863382]
130. Chrysanthopoulou A, Mitroulis I, Apostolidou E, Arelaki S, Mikroulis D, Konstantinidis T, Sivridis E, Koffa M, Giatromanolaki A, Boumpas DT, Ritis K, Kambas K. Neutrophil extracellular traps promote differentiation and function of fibroblasts. J Pathol 2014 7;233(3): 294–307. [PubMed: 24740698]
131. Martinod K, Witsch T, Erpenbeck L, Savchenko A, Hayashi H, Cherpokova D, Gallant M, Mauler M, Cifuni SM, Wagner DD. Peptidylarginine deiminase 4 promotes age-related organ fibrosis. J Exp Med 2017 2;214(2):439–458. [PubMed: 28031479]
132. Dimmeler S, Zeiher AM. Netting Insights into Fibrosis. N Engl J Med 2017 4 13;376(15):1475–1477. [PubMed: 28402777]
133. Gregory AD, Kliment CR, Metz HE, Kim KH, Kargl J, Agostini BA, Crum LT, Oczypok EA, Oury TA, Houghton AM. Neutrophil elastase promotes myofibroblast differentiation in lung fibrosis. J Leukoc Biol 2015 8;98(2):143–52. [PubMed: 25743626]
134. Chua F, Dunsmore SE, Clingen PH, Mutsaers SE, Shapiro SD, Segal AW, Roes J, Laurent GJ. Mice lacking neutrophil elastase are resistant to bleomycin-induced pulmonary fibrosis. Am J Pathol 2007 1;170(1):65–74. [PubMed: 17200183]
135. Hildebrand CE, Gurley LR, Tobey RA, Walters RA. Action of heparin on mammalian nuclei. I. Differential extraction of histone H1 and cooperative removal of histones from chromatin. Biochim Biophys Acta 1977 8 2;477(3):295–311. [PubMed: 884118]
136. Cassinelli G, Naggi A. Old and new applications of non-anticoagulant heparin. Int J Cardiol 2016 6;212 Suppl 1:S14–21. [PubMed: 27264866]
137. Napirei M, Ludwig S, Mezrhab J, Klöckl T, Mannherz HG. Murine serum nucleases--contrasting effects of plasmin and heparin on the activities of DNase1 and DNase1-like 3 (DNase1l3). FEBS J 2009 2;276(4):1059–73. [PubMed: 19154352]
138. Fuchs TA, Brill A, Duerschmied D, Schatzberg D, Monestier M, Myers DD Jr, Wrobleski SK, Wakefield TW, Hartwig JH, Wagner DD. Extracellular DNA traps promote thrombosis. Proc Natl Acad Sci U S A 2010 9 7;107(36):15880–5. [PubMed: 20798043]
139. Napirei M, Ludwig S, Mezrhab J, Klöckl T, Mannherz HG. Murine serum nucleases--contrasting effects of plasmin and heparin on the activities of DNase1 and DNase1-like 3 (DNase1l3). FEBS J 2009 2;276(4):1059–73. [PubMed: 19154352]
140. Villeponteau B Heparin increases chromatin accessibility by binding the trypsin-sensitive basic residues in histones. Biochem J 1992 12 15;288 (Pt 3):953–8. [PubMed: 1281984]
141. Napirei M, Ludwig S, Mezrhab J, Klöckl T, Mannherz HG. Murine serum nucleases--contrasting effects of plasmin and heparin on the activities of DNase1 and DNase1-like 3 (DNase1l3). FEBS J 2009 2;276(4):1059–73. [PubMed: 19154352]
142. Redini F, Tixier JM, Petitou M, Choay J, Robert L, Hornebeck W. Inhibition of leucocyte elastase by heparin and its derivatives. Biochem J 1988 6 1;252(2):515–9. [PubMed: 3415672]
143. Kummarapurugu AB, Afosah DK, Sankaranarayanan NV, Navaz Gangji R, Zheng S, Kennedy T, Rubin BK, Voynow JA, Desai UR. Molecular principles for heparin oligosaccharide-based inhibition of neutrophil elastase in cystic fibrosis. J Biol Chem 2018 8 10;293(32):12480–12490. [PubMed: 29903912]
144. Barbosa GO, Bruni-Cardoso A, da Silva Pinhal MA, Augusto TM, Carvalho HF. Heparanase-1 activity and the early postnatal prostate development. Dev Dyn 2019 1 17. doi: 10.1002/dvdy.12. [Epub ahead of print].
145. Vlodavsky I, Eldor A, Naparstek Y, Cohen I. Method for inhibiting heparanase activity (1993) US Patent Number US5206223A Retrieved from https://patents.google.com/patent/US5206223A/en?oq=5%2c206%2c223+ on 02/11/2019.

Author Manuscript Author Manuscript Author Manuscript Author Manuscript

146. Docherty JR, McCormick PA. A carboxymethylcellulose-heparin combination for the prevention of surgical adhesions. J Surg Res 2017 6 1;213:228–233. [PubMed: 28601319]

147. Currie GA. Effect of heparin on mixed lymphocyte cultures. Nature 1967 7 8;215(5097):164–5. [PubMed: 6049105]

148. Górski A, Wasik M, Nowaczyk M, Korczak-Kowalska G. Immunomodulating activity of heparin. FASEB J 1991 6;5(9):2287–91. [PubMed: 1860620]

149. Górski A, Lagodziński Z. Oral heparin prolongs survival of skin allografts. Arch Immunol Ther Exp (Warsz) 1991;39(5–6):557–62. [PubMed: 1841553]

150. Lagodzinski Z, Górski A, Wasik M. Immunosuppressive action of low-dose heparin. Effect on skin allograft survival. Transplantation 1990 10;50(4):714–5. [PubMed: 2219298]

151. Lider O, Mekori YA, Miller T, Bar-Tana R, Vlodavsky I, Baharav E, Cohen IR, Naparstek Y. Inhibition of T lymphocyte heparanase by heparin prevents T cell migration and T cell-mediated immunity. Eur J Immunol 1990 3;20(3):493–9. [PubMed: 2318247]

152. Ogawa T, Shimizu S, Shimizu T. The effect of heparin on antigen-induced mucus hypersecretion in the nasal epithelium of sensitized rats. Allergol Int 2013 3;62(1):77–83. [PubMed: 23000727]

153. Hadigal SR, Agelidis AM, Karasneh GA, Antoine TE, Yakoub AM, Ramani VC, Djalilian AR, Sanderson RD, Shukla D. Heparanase is a host enzyme required for herpes simplex virus-1 release from cells. Nat Commun 2015 4 27;6:6985. [PubMed: 25912399]

154. Agelidis AM, Hadigal SR, Jaishankar D, Shukla D. Viral Activation of Heparanase Drives Pathogenesis of Herpes Simplex Virus-1. Cell Rep 2017 7 11;20(2):439–450. [PubMed: 28700944]

155. Loka RS, Sletten ET, Barash U, Vlodavsky I, Nguyen HM. Specific Inhibition of Heparanase by Glycopolymer with Well-Defined Sulfation Pattern Prevents Breast Cancer Metastasis in Mice. ACS Appl Mater Interfaces 2018 12 13. doi: 10.1021/acsami.8b17625. [Epub ahead of print].

156. Weiler JM, Linhardt RJ. Comparison of the activity of polyanions and polycations on the classical and alternative pathways of complement. Immunopharmacology 1989 Mar-Apr;17(2):65–72. [PubMed: 2722479]

157. Wang H, Wang C, Zhao MH, Chen M. Neutrophil extracellular traps can activate alternative complement pathways. Clin Exp Immunol 2015 9;181(3):518–27. [PubMed: 25963026]

158. Yuen J, Pluthero FG, Douda DN, Riedl M, Cherry A, Ulanova M, Kahr WH, Palaniyar N, Licht C. NETosing Neutrophils Activate Complement Both on Their Own NETs and Bacteria via Alternative and Non-alternative Pathways. Front Immunol 2016 4 14;7:137. [PubMed: 27148258]

159. Hiremath M, Elder J, Newall F, Mitchell S, Dyas R, Monagle P. Heparin in the long-term management of ligneous conjunctivitis: a case report and review of literature. Blood Coagul Fibrinolysis 2011 10;22(7):606–9. [PubMed: 21885957]

160. De Cock R, Ficker LA, Dart JG, Garner A, Wright P. Topical heparin in the treatment of ligneous conjunctivitis. Ophthalmology 1995 11;102(11):1654–9. [PubMed: 9098258]

161. Jian-Wei L, Xiu-Yun L, Ai-Jun D. Effectiveness of heparin eye drops in paraquat-induced ocular injury. Cutan Ocul Toxicol 2017 12;36(4):377–380. [PubMed: 28279080]

162. Mastropasqua L, Lobefalo L, Ciancaglini M, Ballone E, Gallenga PE. Heparin eyedrops to prevent posterior capsule opacification. J Cataract Refract Surg 1997 4;23(3):440–6. [PubMed: 9159691]

163. Frings A, Schargus M. Recovery From Amiodarone-Induced Cornea Verticillata by Application of Topical Heparin. Cornea 2017 11;36(11):1419–1422. [PubMed: 28834813]

164. Ilhan O, Ilhan N, Coşkun M, Dağlioğlu MC, Ayhan Tuzcu E, Ayintap E, Keskın U, Oksüz H. The effect of enoxaparin-containing irrigation fluid used during cataract surgery on postoperative inflammation in patients with diabetes. Am J Ophthalmol 2013 12;156(6):1120–1124.e3. [PubMed: 24075427]

165. Vasavada VA, Praveen MR, Shah SK, Trivedi RH, Vasavada AR. Anti-inflammatory effect of low-molecular-weight heparin in pediatric cataract surgery: a randomized clinical trial. Am J Ophthalmol 2012 8;154(2):252–258.e4. [PubMed: 22541652]

Author Manuscript Author Manuscript Author Manuscript Author Manuscript

166. Rumelt S, Stolovich C, Segal ZI, Rehany U. Intraoperative enoxaparin minimizes inflammatory reaction after pediatric cataract surgery. Am J Ophthalmol 2006 3;141(3):433–7. [PubMed: 16490487]

167. Rumelt S, Stolovich C, Segal ZI, Rehany U. Intraoperative enoxaparin minimizes inflammatory reaction after pediatric cataract surgery. Am J Ophthalmol 2006 3;141(3):433–7. [PubMed: 16490487]

168. Mun C, Gulati S, Tibrewal S, Chen YF, An S, Surenkhuu B, Raju I, Buwick M, Ahn A, Kwon JE, Atassi N, Pradeep A, Rondelli D, Jain S. A Phase I/II Placebo-Controlled Randomized Pilot Clinical Trial of Recombinant Deoxyribonuclease (DNase) Eye Drops Use in Patients with Dry Eye Disease. Transl Vis Sci Technol 2019;(Accepted for publication).

169. Yoon SY, Kim JY, Kim ES, Kim SY, Kim MJ, Tchah H. Subconjunctival injection of low-molecular-weight heparin-taurocholate 7 inhibits corneal neovascularization. Cornea 2013 11;32(11):1488–92. [PubMed: 24055905]

170. Lanke SS, Kolli CS, Strom JG, Banga AK. Enhanced transdermal delivery of low molecular weight heparin by barrier perturbation. Int J Pharm 2009 1 5;365(1–2):26–33. [PubMed: 18801420]

171. Farkouh A, Frigo P, Czejka M. Systemic side effects of eye drops: a pharmacokinetic perspective. Clin Ophthalmol 2016 12 7;10:2433–2441. eCollection 2016. [PubMed: 27994437]

Author Manuscript Author Manuscript Author Manuscript Author Manuscript

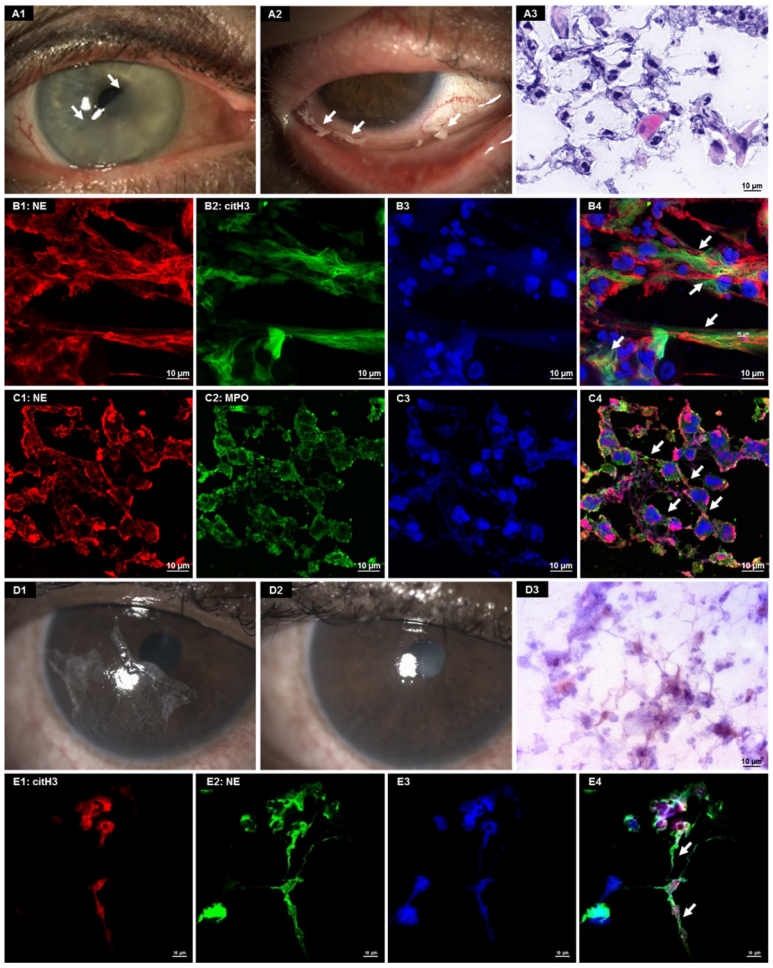

Figure 1. Immunofluorescent staining of mucocellular aggregates (MCA) in oGVHD patients to demonstrate the presence of NETs.

(**A1 & A2**) Clinical photographs of oGVHD patients showing translucent and whitish MCAs on the ocular surface (arrows). (**A3**) Hematoxylin and Eosin (H&E) staining of MCA shows numerous neutrophils, surface epithelial cells and extracellular DNA strands. (**B1-B4**) Confocal immunofluorescent staining of MCA showing co-localization of neutrophil elastase (NE) (**B1**, red), Citrulline H3 (**B2**, citH3, green) and DAPI nuclear staining (**B3**, blue) in extracellular strands **(B4**, arrows) confirming that these extracellular strands are NETs. Confocal immunofluorescent staining of MCA showing co-localization of NE (**C1**, red), myeloperoxidase (**C2**, green) and DAPI nuclear stain (**C3**, blue) in extracellular strands (**C4**, white arrows) further confirming that these extracellular strands are NETs. (**D1-E4**): Analysis of a MCA adhered to the cornea of an oGVHD patient. (**D1**) Clinical photograph of an oGVHD patient showing MCAs adhered to the cornea. (**D2**) Clinical photograph of the same patient after application of a filter paper to the cornea to lift the MCA. (**D3**) H&E staining of the filter paper shows that MCA comprises of neutrophils, surface epithelial cells and extracellular DNA strands. (**E1-E4**) Confocal immunofluorescent staining of the MCA shows co-localization of citH3 (**E1**, red), NE (**E2**, green) and DAPI nuclear staining (**E3**, blue) in extracellular strands (**E4**, white arrows) confirming that these extracellular strands within the MCA are NETs.

Author Manuscript Author Manuscript Author Manuscript Author Manuscript

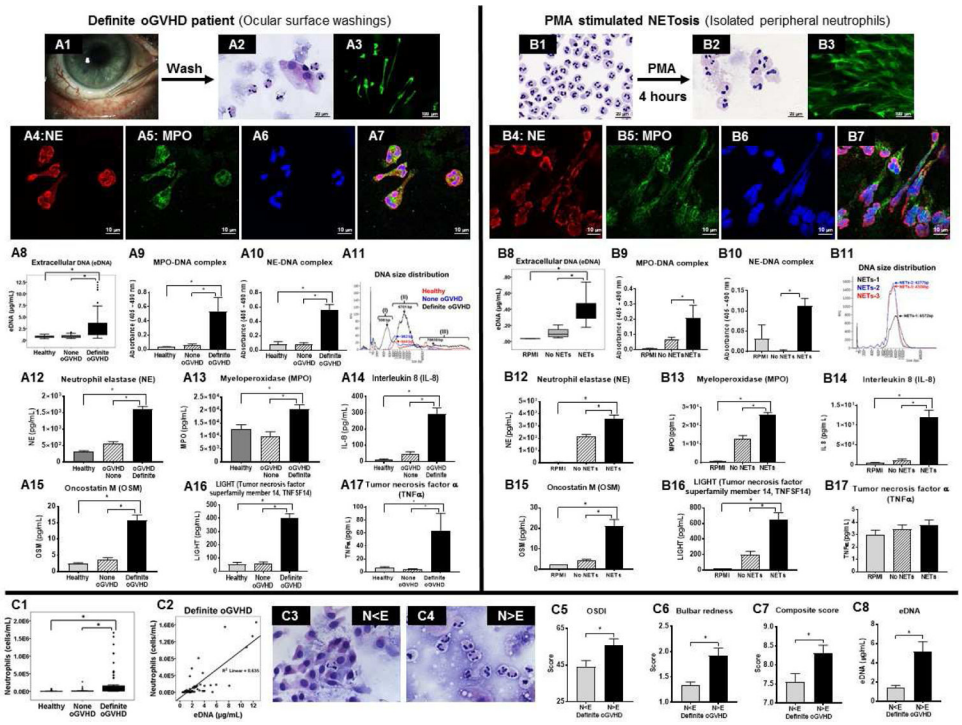

Figure 2. Presence of NETs and their molecular components in ocular surface washings of oGVHD patients and comparison with experimentally induced NETs.

(A1): Clinical photograph showing ocular surface of an oGVHD patient. **(A2):** H&E staining shows numerous enlarged neutrophils and surface epithelial cells from ocular surface washings of an oGVHD patient. **(A3):** Sytox Green staining shows extracellular strands in ocular surface washings of a definite oGVHD patient. Confocal immunofluorescent staining of ocular surface washings of an oGVHD patient shows co-localization of NE (**A4**, red), MPO (**A5**, green) and DAPI nuclear stain (**A6**, blue) in extracellular strands (**A7**, merged image) confirming presence of NETs. **(A8):** Boxplot shows level of eDNA from healthy subjects (n=40 eyes), none oGVHD (n=35 eyes) and definite oGVHD patients (n=55 eyes). **(A9 & A10):** Graphs showing the level of MPO-DNA complex (**A9**) and NE-DNA complex (**A10**) measured by ELISA from ocular surface washings of healthy subjects (n=10 eyes), none oGVHD (n=10 eyes) and definite oGVHD (n=10 eyes) patients. **(A11):** Representative FEMTO pulse capillary electrophoresis data showing the size of eDNA from ocular surface washings of healthy subjects, none oGVHD and definite oGVHD patients. **A12-A17:** Graphs showing the amount of NE (**A12**), MPO (**A13**), IL-8 (**A14**), OSM (**A15**), LIGHT (**A16**) and TNFa (**A17**) measured by Luminex from ocular surface washings of healthy subjects, none oGVHD, and definite oGVHD patients. **(B1):** H&E staining shows multi-lobed nucleus of intact isolated human neutrophils from peripheral venous blood. **(B2):** H&E staining shows enlarged neutrophils from human peripheral blood after stimulation with 1 nM PMA. **(B3)**: Sytox Green staining shows extracellular DNA strands from human peripheral neutrophils stimulated with 1 nM PMA. **(B4-B7):** Confocal immunofluorescent staining of PMA activated human neutrophils from peripheral venous blood shows co-localization of NE (**B4**, red), MPO (**B5**, green) and DAPI (**B6**, blue) in extracellular strands (**B7**, merged image) confirming them to be NETs. **(B8):**

Author Manuscript Author Manuscript Author Manuscript Author Manuscript

Boxplot shows level of eDNA in supernatant from RPMI culture media alone (n=9), unstimulated neutrophils (no NETs, n=10) and neutrophils stimulated with PMA to induce NETosis (NETs, n=11). **(B9 & B10):** Graphs showing the level of MPO-DNA complex (**B9**) and NE-DNA complex (**B10**) measured by ELISA from RPMI medium (n=3) alone and supernatants of unstimulated neutrophils (no NETs, n=15) and PMA stimulated neutrophils (NETs, n=15). **(B11):** FEMTO pulse capillary electrophoresis data showing the size of eDNA from PMA stimulated human neutrophils (NETs). **(B12-B17):** Graph showing the amount of NE (**B12**), MPO (**B13**), IL-8 (**B14**), OSM (**B15**), LIGHT (**B16**) and TNFa (**B17**) measured by Luminex from RPMI medium alone and supernatants of unstimulated neutrophils (no NETs) and PMA stimulated neutrophils. **(C1):** Boxplot shows the number of neutrophils in ocular surface washings of healthy subjects (n=40 eyes), none oGVHD (n=35 eyes) and definite oGVHD (n=55 eyes) patients. **(C2):** Scatter plot showing correlation of eDNA (n=53 eyes) and number of neutrophils (n=53 eyes) for definite oGVHD patients. **(C3):** Representative H&E staining of ocular surface wash in definite oGVHD patients shows numerous epithelial cells and few neutrophils (N<E group). **(C4):** Representative H&E staining of ocular surface wash in definite oGVHD patients shows numerous neutrophils and few epithelial cells (N>E group). **(C5-C8):** Graphs comparing signs and symptoms between N<E and N>E groups in definite oGVHD patients. **(C5):** OSDI score between N<E group (n=19 eyes) and N>E group (n=36 eyes). **(C6)** Bulbar redness score between N<E group (n=18 eyes) and N>E group (n=32 eyes). **(C7)** Composite score for definite oGVHD patients between N<E group (n=18 eyes) and N>E group (n=36 eyes). **(C8)** eDNA amount in ocular surface wash between N<E group (n=19 eyes) and N>E group (n=30 eyes).

Author Manuscript Author Manuscript Author Manuscript Author Manuscript

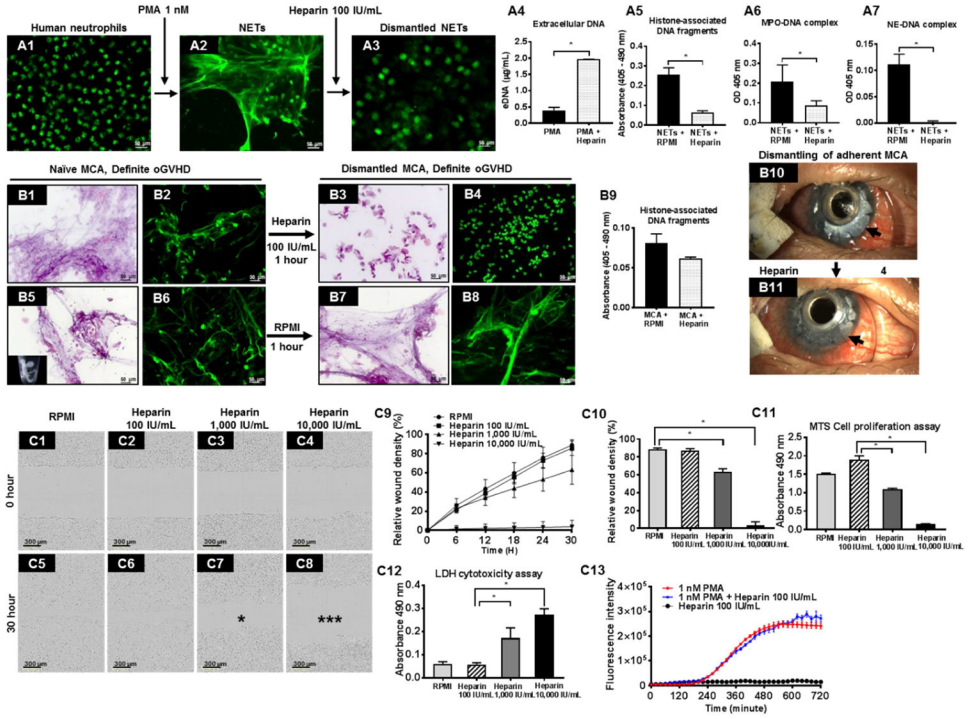

Figure 3. Effect of heparin on NETs in oGVHD patients.

(A1-A3): Representative images of Sytox Green staining showing dismantling of NETs with Heparin after experimental NETosis. **(A1):** naïve neutrophils; **(A2):** PMA stimulated human neutrophils showing abundant NETs; **(A3):** Sub-anticoagulant dose of heparin (100 IU/mL) for 1 h dismantles the NETs. **(A4-A7):** Graphs showing protein-associated DNA fragments in supernatants to confirm dismantling of NETs by Heparin. **(A4):** eDNA amount from supernatants of naïve adherent NETs (n=4) and Heparin dismantled NETs (n=4); **(A5):** Histone-associated DNA fragments measured in supernatants of naïve adherent NETs (n=15) and Heparin dismantled NETs (n=13). **(A6):** MPO-associated DNA fragment measured in supernatants of naïve adherent NETs (n=15) and Heparin dismantled NETs (n=15). **(A7):** NE-associated DNA fragment measured in supernatants of naïve adherent NETs (n=15) and Heparin dismantled NETs (n=15). **(B1-B8):** Dismantling of NETs in MCAs by Heparin. **(B1, B2, B5, B6):** Naïve MCAs are collected from the ocular surface and stained with H&E (**B1, B5**) and Sytox Green (**B2, B6**) to show the presence of NETs. The physical appearance of isolated MCA is shown as an inset in B5. **(B3, B4, B7, B8):** Naïve MCAs are incubated with Heparin 100 IU/mL (**B3, B4**) or RPMI as control (**B7, B8**). H&E staining (**B3, B7**) and Sytox Green staining (**B4, B8**) show dismantling of NETs in MCA with Heparin (**B3, B4**) but not with RPMI control (**B7, B8**). (**B9**): Graph showing amount of Histone-associated DNA fragments in the supernatant of MCAs incubated in the presence (n=5) or absence of Heparin (n=6). **(B10 & B11):** Representative clinical images of an oGVHD patient who had adherent MCA over a keratoprosthesis (**B10**) and treated with heparin (100 IU/mL) eye drops three times a day for 4 weeks (**B11**). Adherent MCA were much reduced after heparin eye drop use. **(C1-C8):** Representative images showing scratch wound assay in immortalized human corneal epithelial cells that are incubated with various doses of Heparin. Representative kinetic curve over 30 hours (**C9**) and graph at 30 hour time

Author Manuscript Author Manuscript Author Manuscript Author Manuscript

point (**C10**) showing relative wound density with various doses of Heparin after epithelial wound scratch. **(C11):** Graph showing the cell proliferation (MTS assay) of various doses of heparin after epithelial scratch wound. **(C12):** Graph showing cytotoxicity for various doses of heparin in epithelial scratch wounds as measured by LDH assay (n=6/group, 3 separate experiments). **(C13):** Representative kinetic assay showing effect of Heparin on NETosis. Sytox Green fluorescence intensity in supernatants from neutrophils stimulated with 1 nM PMA (naïve NETs), 1 nM PMA with heparin (dismantled NETs) and heparin alone (no NETs, control).

Author Manuscript Author Manuscript Author Manuscript Author Manuscript

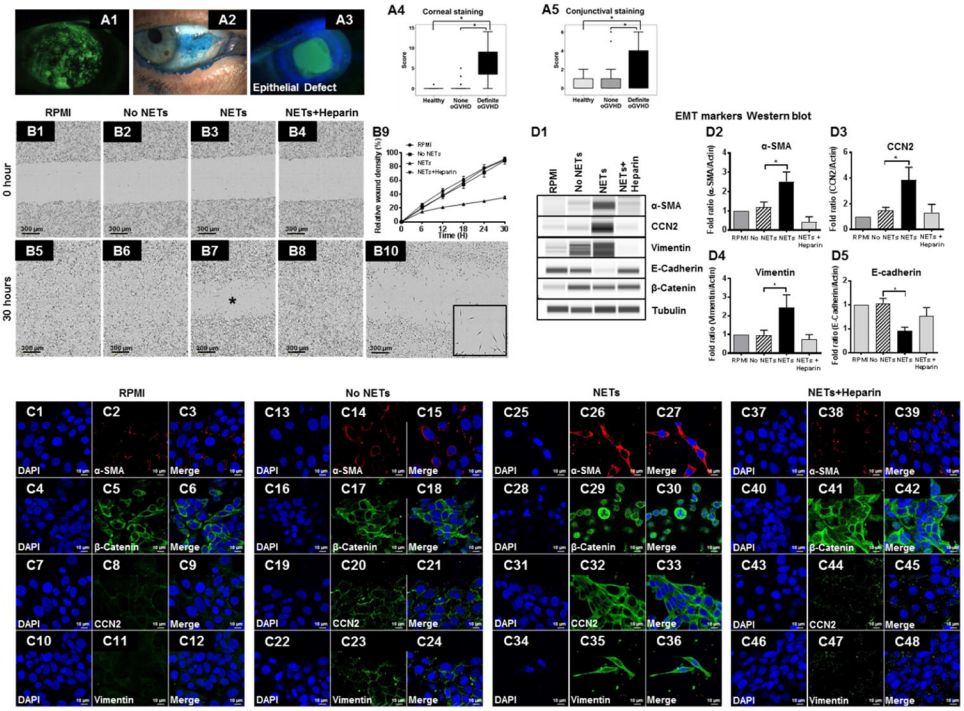

Figure 4. Pathological effects of NETs on corneal epithelial cells.

(A1-A3): Representative clinical images of an ocular GVHD patient showing corneal disease. **(A1)** corneal fluorescein staining showing superficial punctate keratopathy; **(A2)** conjunctival lissamine green staining showing punctate epitheliopathy; **(A3)** fluorescein staining showing corneal epithelial defect. **(A4, A5):** Boxplot showing lissamine green staining scores in healthy subjects (n=40 eyes), none oGVHD (n=35 eyes) and definite oGVHD patients (n=48 eyes); **(A4)** corneal staining score; **(A5)** conjunctival staining score. **(B1-B8):** Representative image showing scratch wound assay in immortalized human corneal epithelial cells incubated with RPMI culture medium, unstimulated neutrophils (no NETs), PMA-stimulated neutrophils (naive NETs) and heparinized NETs. **(B9):** Kinetic curve showing the relative wound density at different time points. **(B10):** Higher magnification image showing scratch wound assay in immortalized human corneal epithelial cells incubated with naive NETs for 30 hours. The inset shows elongated spindle shaped cells resembling fibroblasts. **(C1-C48):** Representative confocal immunofluorescent staining images of scratch wounds in corneal epithelial cells to show evidence for epithelial mesenchymal transition (EMT). Epithelial cells were incubated with RPMI culture medium **(C1-C12)**, unstimulated neutrophils (no NETs, **C13-C24**), PMA-stimulated neutrophils (naive NETs, **C25–36**) and heparinized NETs (**C37–48**). **(D1):** Representative Western blots probed with antibodies for mesenchymal markers. **(D2-D5):** Quantitative data from Western blots showing the fold change in EMT markers (three independent experiments); **(D2)** alpha-smooth muscle actin; **(D3)** CCN2; **(D4)** vimentin; **(D5)** E-cadherin.

Author Manuscript Author Manuscript Author Manuscript Author Manuscript

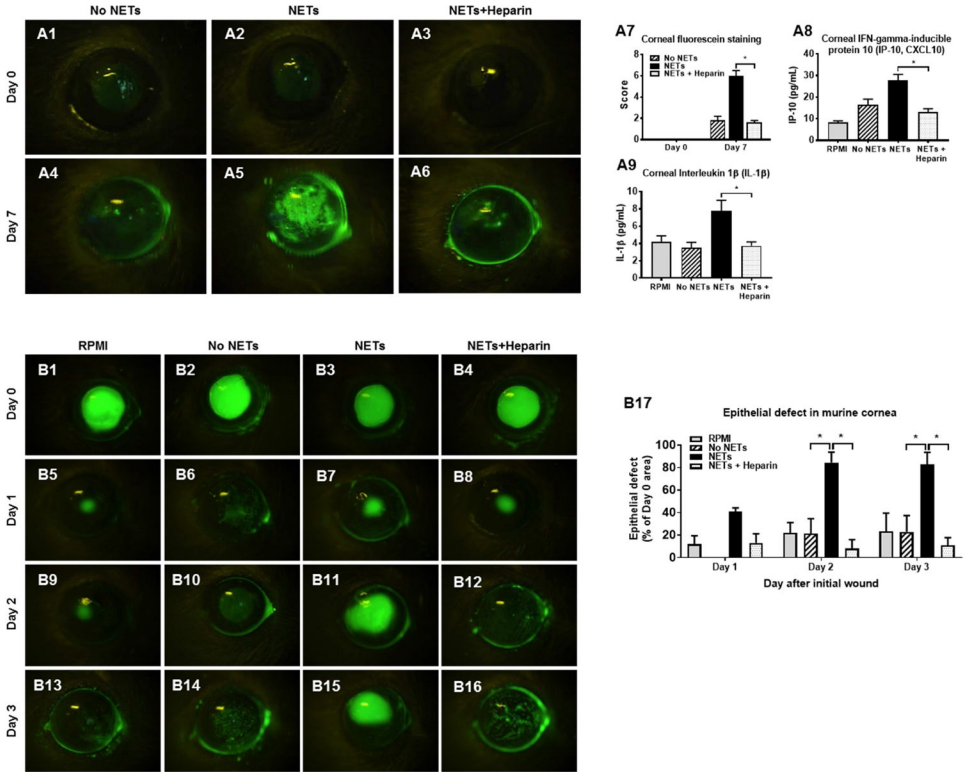

Figure 5. Pathological effects of NETs on murine ocular surface.

(A1-A6): Representative images of murine corneas (n=5/group) showing fluorescein staining after topical application of unstimulated murine neutrophils supernatant (no NETs), PMA stimulated murine neutrophils (naive NETs), and heparinized murine NETs (dismantled NETs). **(A7):** Graph comparing fluorescein staining data between groups at Day 0 and Day 7. **(A8):** Graph showing amount of IP-10 in corneal lysates prepared after 7 days of topical application of RPMI (n=12 corneas), no NETs (n=12 corneas), NETs (n=12 corneas), and heparinized NETs (n=27 corneas). **(A9):** Graph showing amount of IL-1β in corneal lysates prepared after 7 days of topical application of RPMI (n=12 corneas), no NETs (n=12 corneas), NETs (n=24 corneas) and heparinized NETs (n=15 corneas). **(B1-B16):** Representative images of murine corneas showing fluorescein staining after epithelial scratch and application of RPMI culture medium, unstimulated murine neutrophils supernatant (no NETs), PMA-stimulated murine neutrophils (naïve NETs), and heparinized murine NETs (dismantled NETs). **(B17):** Graph comparing the epithelial defect area between groups at Day 1 to Day 3 (n=5/group).

Author Manuscript Author Manuscript Author Manuscript Author Manuscript

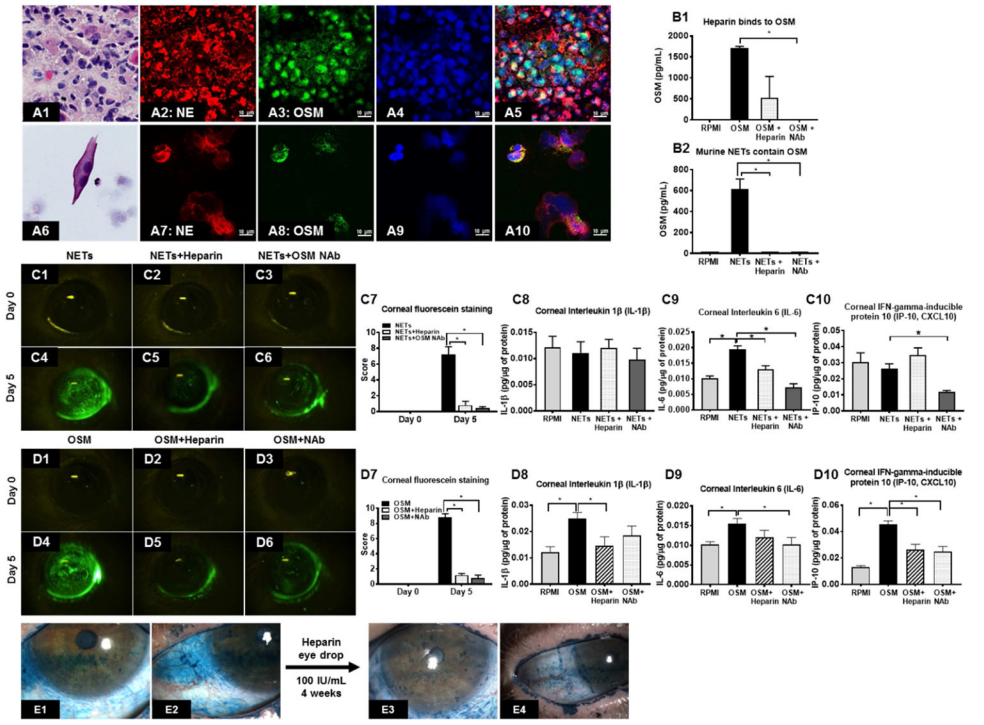

Figure 6. Pathological effect of oncostatin M (OSM) on ocular surface.

(A1-A5): H&E and confocal immunofluorescent images of mucocellular aggregates (MCA) collected from ocular surface of a definite oGVHD patient; (**A1**) H&E staining; (**A2**) neutrophil elastase (NE, red); (**A3**) OSM (green); (**A4**) DAPI nuclear stain (blue); (**A5**) Merged image showing co-localization of NE and OSM. **(A6-A10):** H&E and cytospin preparations of ocular surface washings from a definite oGVHD patient; (**A6**) H&E staining; (**A7**) neutrophil elastase (NE, red); (**A8**) OSM (green); (**A9**) DAPI nuclear stain (blue); (**A10**) Merged image showing co-localization of NE and OSM. **(B1):** Graph showing data demonstrating OSM (10 ng/mL) and heparin (100 IU/mL) binding. **(B2):** Graph showing data demonstrating OSM presence in murine NETs. **(C1-C6):** Representative fluorescein stained images of murine corneas showing pathological effect of naïve NETs, heparinized NETs and NETs with OSM neutralizing antibodies that were topically applied to murine corneas for five days. **(C1-C3):** At Day 0, corneas in all groups do not show fluorescein staining. **(C4-C6):** At day 5, significant corneal fluorescein staining is seen with naïve NETs (**C4**) but not with heparinized NETs (**C5**) or NETs incubated with OSM neutralizing antibody (**C6**). **(C7):** Graph showing data comparing corneal fluorescein staining between groups. **(C8-C10):** Graph showing amount of IL-1β (**C8**), IL-6 (**C9**) and IP-10 (**C10**) in corneal lysates (n=5/group) prepared after 5 days of topical application. **(D1-D6):** Representative fluorescein stained images of murine corneas showing pathological effect of recombinant mouse OSM protein, recombinant mouse OSM protein + heparin, recombinant mouse OSM protein +OSM neutralizing antibody that were topically applied to murine corneas for five days. **(D1-D3):** At Day 0, corneas in all groups do not show fluorescein staining. **(D4-D6):** At day 5, significant corneal fluorescein staining is seen with recombinant OSM protein (**D4**) but not with recombinant OSM protein + heparin (**D5**) or recombinant OSM protein + OSM neutralizing antibody (**D6**). **(D7):** Graph showing data

Author Manuscript Author Manuscript Author Manuscript Author Manuscript

comparing corneal fluorescein staining between groups. **(D8-D10):** Graph showing amount of IL-1β (**D8**), IL-6 (**D9**) and IP-10 (**D10**) in corneal lysates (n=5/group) prepared after 5 days of topical application. (**E1-E4):** Treatment of an oGVHD patient with severe ocular surface disease with Heparin 100IU/mL eye drops twice a day for 4 weeks. Lissamine green staining showed severe corneal (**E1**) and conjunctival (**E2**) epitheliopathy prior to treatment with Heparin eye drops. After 4 weeks of treatment, corneal (**E3**) and conjunctival (**E4**) staining was significantly reduced.

Author Manuscript Author Manuscript Author Manuscript Author Manuscript

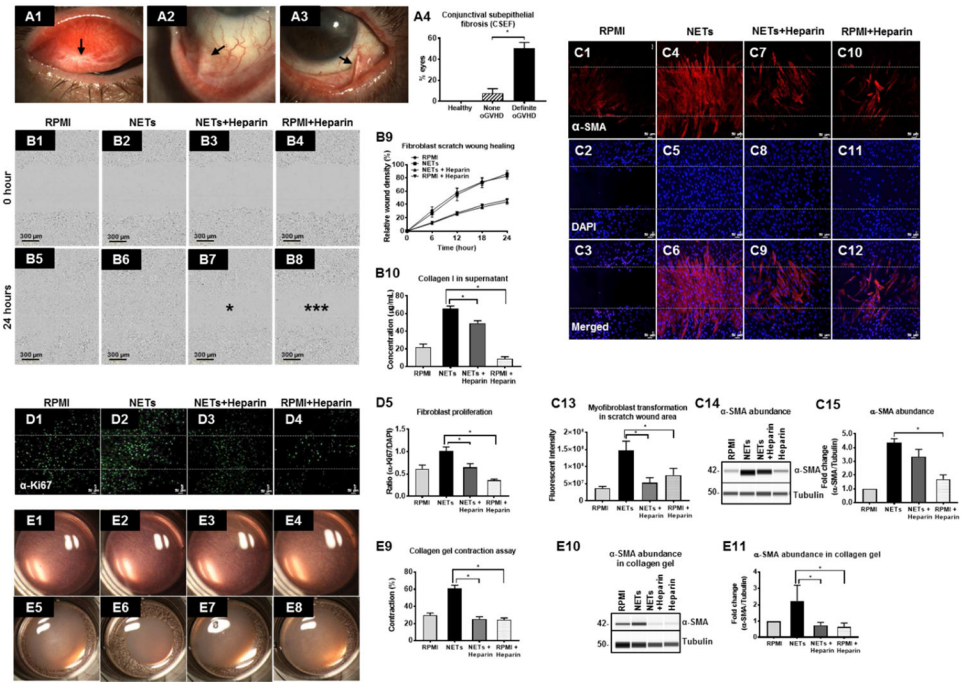

Figure 7. Pathological effects of NETs on conjunctival fibroblasts.

(A1-A3): Representative clinical images of an ocular GVHD patient showing conjunctival cicatricial disease; **(A1)** Conjunctival subepithelial fibrosis (CSEF) under upper lid palpebral conjunctiva; **(A2)** conjunctival fornix foreshortening; **(A3)** symblepheron formation. **(A4):** Graph showing data comparing presence of CSEF (% eyes) between healthy subjects (n=15 eyes), none oGVHD (n=39 eyes) and definite oGVHD (n=87 eyes) patients. **(B1-B8):** Representative image showing scratch wound assay in primary human conjunctival fibroblast cells incubated with RPMI culture medium, PMA-stimulated neutrophils (naive NETs), heparinized NETs, and heparin alone. **(B9):** Kinetic curve showing the relative wound density at different time points. **(B10):** Graph showing data comparing collagen concentration measured from the supernatants of conjunctival fibroblast scratch wound assays (RPMI n=12; NETs n=15; heparinized NETs n=15; heparin alone n=5). **(C1-C12):** Representative confocal immunofluorescent staining images of scratch wounds in conjunctival fibroblasts to show the evidence of myofibroblast transformation. Conjunctival fibroblasts were incubated with RPMI culture medium **(C1-C3)**, PMA-stimulated neutrophils (naive NETs, **C4-C6**), heparinized NETs (**C7-C9**) and heparin alone (**C10-C12**). **(C13):** Graph showing data comparing myofibroblast transformation (fluorescent intensity in immunofluorescent staining images) between conjunctival fibroblasts incubated with RPMI (n=6); NETs (n=4); heparinized NETs (n=5) or heparin alone (n=5). **(C14, C15):** Representative Western blot image (**C14**) and graph (**C15**) to compare α-SMA abundance between conjunctival fibroblasts incubated with RPMI; NETs; heparinized NETs or heparin alone. Tubulin was shown as the loading control. **(D1-D4):** Representative confocal immunofluorescent staining images of scratch wounds in conjunctival fibroblasts to show the evidence of fibroblast proliferation using α-Ki67 antibody. Conjunctival fibroblasts were incubated with RPMI (**D1**); NETs (**D2**); heparinized NETs (**D3**) or heparin alone (**D4**). **(D5):** Graph showing data comparing fibroblast proliferation (fluorescent intensity of α-

Author Manuscript Author Manuscript Author Manuscript Author Manuscript

Ki67 positive cells in immunofluorescent staining images) between conjunctival fibroblasts incubated with RPMI (n=6); NETs (n=4); heparinized NETs (n=9) or heparin alone (n=7). **(E1-E8):** Representative images from a collagen gel contraction assay. Conjunctival fibroblasts were seeded in collagen matrices and incubated with RPMI (**E1, E5**; n=9); NETs (**E2, E6**; n=9); heparinized NETs (**E3, E7**; n=9) and heparin alone (**E4, E8**; n=9). Collagen gel images were obtained at baseline (**E1-E4**) and after 24 hours incubation (**E5-E8**). **(E9):** Graph showing data comparing collagen gel contraction (%) between collagen matrices incubated with RPMI (n=9); NETs (n=9); heparinized NETs (n=9); heparin alone (n=9). **(E10, E11):** Representative Western blot image (**E10**) and graph (**E15**) to compare α-SMA abundance between collagen matrices incubated with RPMI; NETs; heparinized NETs or heparin alone. Tubulin blot is shown as the loading control.

Author Manuscript Author Manuscript Author Manuscript Author Manuscript

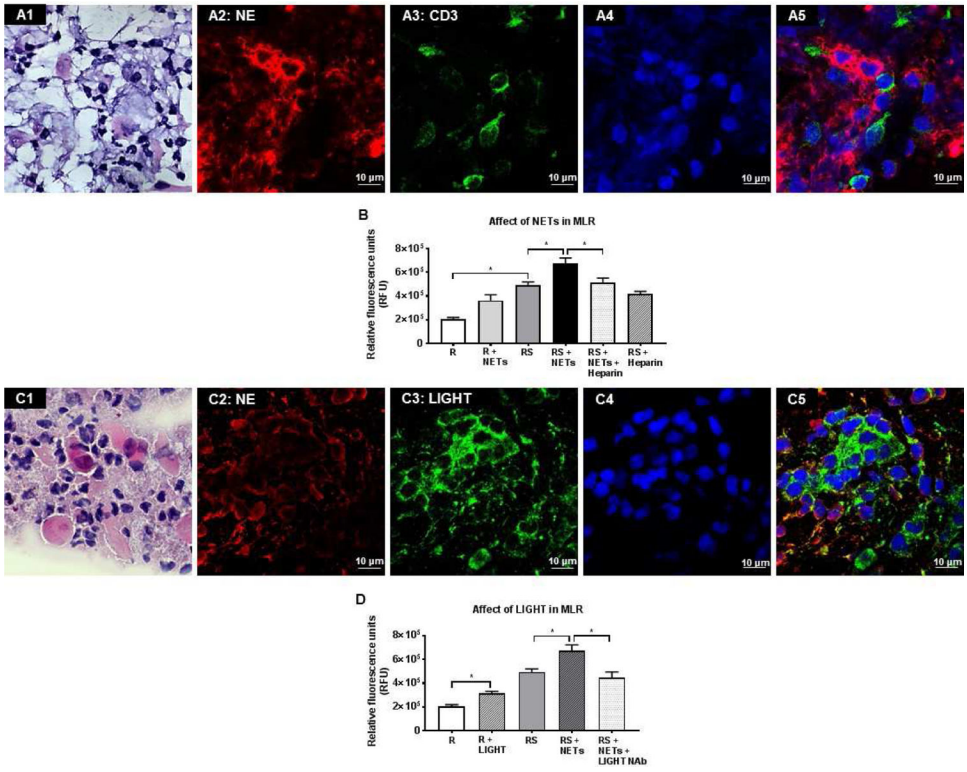

Figure 8. Pathological effect of NETs on immune cell proliferation.

(A1): H&E staining of mucocellular aggregates (MCA) showed numerous neutrophils, surface epithelial cells and mononuclear cells. **(A2-A5):** Confocal immunofluorescent staining images of MCA showing the presence of neutrophil elastase (NE) (**A2**, red), CD3 positive T cells (**A3**, green), DAPI nuclear staining (**A4**, blue) and merged image (**A5**). **(B):** Graph shows NET-induced T cell proliferation in mixed lymphocyte reaction (MLR). NETs promote proliferation of MLR. Heparin inhibits MLR proliferation. **(C1):** H&E staining of mucocellular aggregates (MCA) showed numerous neutrophils, surface epithelial cells and mononuclear cells. **(C2-C5):** Confocal immunofluorescent staining images of MCA showing the presence of neutrophil elastase (NE) (**C2**, red), LIGHT protein (**C3**, green), DAPI nuclear staining (**C4**, blue) and merged image (**C5**). **(D):** Graph shows effect of human recombinant LIGHT/TNFSF14 protein induced on T cell proliferation and in MLR. LIGHT/TNFSF14 induces T cell proliferation. LIGHT/TNFSF14 neutralizing antibodies inhibit NET-induced MLR proliferation.

Author Manuscript Author Manuscript Author Manuscript Author Manuscript

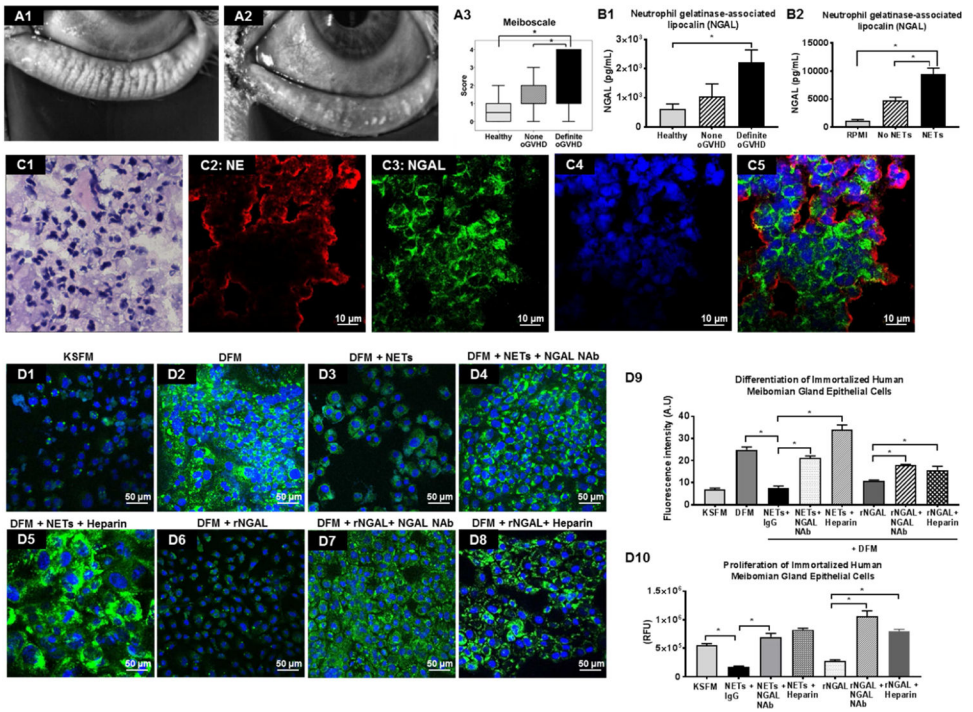

Figure 9. Pathological effect of NETs on Meibomian glands.

Representative infrared images of the lower lid showing the presence of normal meibomian glands in healthy subjects (**A1**) and severe Meibomian gland atrophy in a patient with definite oGVHD (**A2**). **(A3):** Graph showing data comparing meiboscale (score 0–4 based on severity of meibomian gland atrophy) between healthy subjects (n=40 eyes), none oGVHD (n=35 eyes) and definite oGVHD (n=54 eyes) patients. **(B1):** Graph showing data comparing amount of NGAL in conjunctival washings between healthy subjects, none oGVHD and definite oGVHD. **(B2):** Graph showing data comparing amount of NGAL in RPMI, unstimulated human neutrophils (no NETS) and PMA stimulated neutrophils (NETs). **(C1):** H&E staining of mucocellular aggregates (MCA) showed numerous neutrophils, surface epithelial cells and mononuclear cells. **(C2-C5):** Confocal immunofluorescent staining images of MCA showing the presence of neutrophil elastase (NE) (**C2**, red), NGAL protein (**C3**, green), DAPI nuclear staining (**C4**, blue) and merged image (**C5**). **(D1-D8):** Effect of NETs and NGAL on immortalized Meibomian gland (MG) epithelial cell differentiation. Lipid accumulation was detected using LipidTOX staining (green). **(D1):** Keratinocyte serum free medium (KSFM) only; (**D2**): differentiation medium (DFM) only; (**D3**): DFM + NETs; (**D4**) DFM + NETs + NGAL neutralizing antibody (NAb); (**D5**) DFM + NETs + heparin 100 IU/mL; (**D6**) DFM + human recombinant NGAL protein (rNGAL); (**D7**): DFM + rNGAL + NGAL Nab; (**D8**) DFM + rNGAL + heparin. **(D9):** Graph showing data comparing LipidTox staining (fluorescence intensity) under various differentiation culture conditions. **(D10):** Graph showing data comparing MG cell proliferation that was determined by measuring the cellular DNA content (fluorescence intensity) using a commercially available dye binding kit under various culture conditions.

Author Manuscript Author Manuscript Author Manuscript Author Manuscript

Table 1:

Descriptive statistics comparing clinical signs and symptoms between healthy subjects, none oGVHD patients and definite oGVHD patients.

	Healthy (n=20 patients)	oGVHD None (n=18 patients)	oGVHD Definite (n=30 patients)	*p*-value (Healthy vs oGVHD Definite)	*p*-value (oGVHD None vs oGVHD Definite)
Age (years)	49.90±6.88	49.27±14.72	51.86±15.67	0.868	0.795
Tear Protein (mg/mL)	1.70±1.24	1.85±2.37	2.24±2.95	0.528	0.737
eDNA (μg/mL)	0.78±0.23	0.83±0.30	2.36±1.72	<0.001	<0.001
Neutrophils number in OSW	$1.62\times10^{3}\pm 2.78\times10^{3}$	$2.32\times10^{4}\pm 1.15\times10^{4}$	$5.83\times10^{4}\pm 7.66\times10^{4}$	<0.001	<0.001
OSDI (scale 0–100)	0.48±0.95	17.12 ±15.17	50.27±17.64	<0.001	<0.001
NITBUT-first (seconds)	7.82±4.41	6.62±3.72	4.02±1.47	<0.001	0.002
NITBUT- average (seconds)	11.12±5.21	10.42±5.11	5.95±2.60	<0.001	<0.001
Stare Time (seconds)	15.31±6.60	15.05±6.98	7.61±3.36	<0.001	<0.001
Bulbar Redness (scale 0.0–4.0)	1.12±0.35	1.09±0.50	1.76±0.75	<0.001	<0.001
Osmolarity (mOsm/L)	299.76±9.99	300.81±14.43	297.81±15.13	0.847	0.689
Average LLT (nm)	82.48±13.94	79.22±19.68	62.26±24.49	<0.001	0.003
Meiboscale (scale 0–4)	0.55±0.60	1.26±0.78	2.07±1.39	<0.001	0.001
Schirmer I (mm/5 min)	21.38±11.76	14.34±10.36	0.07±0.25	<0.001	<0.001
MMP-9 (scale 0–3)	0.65±0.66	1.23±0.87	2.57±0.66	<0.001	<0.001
Corneal Stain (scale 0–15)	0.05±0.22	0.07±0.25	5.56±3.77	<0.001	<0.001
Conjunctival Stain (scale 0–6)	0.43±0.71	0.36±0.60	2.08±1.97	<0.001	<0.001
Total Score (scale 0–11)	0.83±1.13	2.60±1.63	8.09±1.23	<0.001	<0.001

Data is shown as sample mean and standard deviation, $(\bar{x} \pm \sigma)$. *p*-values are for pair-wise comparisons of the means between the oGVHD definite group and the others computed by using Tukey post-hoc tests. The outliers were excluded before performing statistical significance analysis. eDNA, extracellular DNA; OSW, ocular surface washings; OSDI, ocular surface disease index; NITBUT, non-invasive tear film break-up time; LLT, lipid layer thickness; MMP-9, matrix metallopeptidase 9.